Development of a compact, passive helium purification system for the advanced high temperature reactor

Steyn B.S.

orcid.org 0000-0003-1408-0083

Dissertation accepted in partial fulfilment of the requirements for the degree *Master of Engineering in* Nuclear Engineering at the Potchefstroom Campus of the North-West University

Supervisor: Dr AC Cilliers

Graduation: July 2020

Student number: 22210105

Acknowledgements

First and foremost, I would like to thank my amazing wife, Marcé, for listening to every story with patience (more than 10 times in some cases), for motivating me when I couldn't continue working, for reminding me that I could have a much harder subject, and keeping my feet on the ground when I received good feedback. I love you to the moon and back.

Secondly, my father without whose support my undergrad and this work would never have happened. Thank you for providing useful feedback and finances where I had none of my own. I know its been a long road but you helped me walk it without unnecessary concerns.

Thank you mom. I know we only saw each other a handful of times but you made a tremendous amount of effort to make each one special. Everyone else in my family, thank you for listening to me drone on about nuclear safety and the case for nuclear power. I know it sounds like loads of gibberish but you always listened and took each story with a willing ear.

Next, I would like to thank my study leader Dr. Anthonie Cilliers. You helped me by giving me hints but also pushing me to do the work on my own and present results. Thank you for listening to each "long story" and having patience when I couldn't explain myself in 3 words or less. I appreciate the opportunity afforded to me to work on this project and the experience and knowledge I gain will stay with me for the rest of my life.

Finally, I would like to thank Bo Chen and his colleagues for the provision of the Memcal software. I know you gave it freely, with no intention to claim any copy right but I really appreciate the unnecessary effort this software saved me and I look forward to working with you in future.

Abstract

In this study the possibility of a compact, passive membrane system to separate helium from the impurities that may be present in the AHTR primary system was investigated. The current helium purification systems that are used in the HTTR, HTR-10, and the old PBMR system are discussed and a more efficient alternative is sought in membrane technology. The Memcal software was identified and is validated as an accurate method of designing preliminary systems to prove the idea. Five different designs were decided upon each with their own specific setup and reasoning. Design 1 features as many membranes as possible and a stage cut of 90%. Design 2 features a changing stage cut and a minimum limit of what the retentate flow can be for each last membrane in a row. Design 3 was similar to design 1 in that it had a set stage cut at 90% but it also had a minimum limit for permeate and retentate flows. Design 4 featured a different transmembrane pressure, 5 bar, which allowed separation of certain species to happen much faster. Design 5 is just a shortened version of design 1, such that it has the same membrane system as design 4 and so that they can be compared. The designs are simulated and the results compared with each other, as each has a different setup and configuration, in an attempt to find the best solution. With the results for each of the different designs, displayed in **Table 0-1**, it is shown that a passive helium purification system, while compact, may be designed successfully through the use of gas separation membranes.

Table 0-1: Compilation of results from this study

Characteristic	Design 1	Design 2	Design 3	Design 4	Design 5
Total He recovery	98.74%	84.27%	89.43%	98.21%	98.21%
Total impurities removed	28.97%	60.64%	47.43%	31.83%	23.07%
Number of membranes	91	60	60	54	54
Total area of membranes (m^2)	4345	4192	4685	2983	3608

Keywords: helium, helium purification system, membrane, gas separation, PBMR, AHTR.

Table of Contents

List of figures

List of tables

List of equations

Nomenclature

List of commonly used definitions

Permeate: The stream that leaves a membrane unit after passing through the separation surface

Retentate: The stream that leaves a membrane unit without passing through the separation surface

Zeolite: A type of microporous aluminosilicate mineral

Glassy polymer: A type of polymer which structure is rigid or crystalline as long as the temperature is kept below its glass transition temperature

Polyimide: A type of rigid resin polymer made of imide monomers

Passive system: A term commonly used in nuclear engineering to refer to a system that has no moving parts

Membrane row: An arbitrary notation used to indicate in which position the membrane unit is, in the rows the retentate flows from the first membrane to the next

Membrane column: An arbitrary notation used to indicate in which position the membrane unit is, in the columns the permeate from the first membrane flows to the next

Membrane position: An arbitrary notation formed by noting the row and column of the membrane with the first membrane being in row 1 and column 1 as membrane 1,1. The orientation is set up as “row, column” with 1,1 being the first membrane at the bottom left of any simulation and working upwards and to the right side. The retentate from membrane 1,1 will flow to membrane 1,2 and the permeate to membrane 2,1.

List of acronyms

AHTR: Advanced high temprature reactor

Barrer: Arbitrary gas permeability unit = $1x10^{-10}$ cm^3(STP).cm/cm^2.s.cmHg

EOS: Equations of state

GFR: Gas-cooled fast reactor

GPU: Arbitrary gas permeance unit = $1x10^{-6}$(STP)/cm^2.s.cmHg = 1 Barrer/1 μm membrane thickness

HPC: High pressure compressor

HPS: Helium purification system

HTR: High temperature reactor

HTTR: High temperature testing reactor

ICS: Inventory control system

IPC: Intermediate pressure compressor

LPC: Low pressure compressor

LTA: Low temperature absorber

Memcal: Membrane calculation software (Chen *et al.*, 2016)

MPS: Main power system

PBMR: Pebble bed modular reactor

ODE: Ordinary differential equation

PCU: Power conversion unit

ppm: Parts per million (concentration)

ppb: Parts per billion (concentration)

STP: Standard temperature and pressure; 24 ^oC and 1 Atm

VHTR: Very high temperature reactor

List of units (Metric units to be used, SI units listed first)

Length:	Metre (m) = 100 centimetre (cm) = 10^3 millimetre (mm) = 10^6 micrometre (µm)
Mass:	Kilogram (kg) = 1000 gram (g)
Area:	Square metre (m^2) = 10^4 square centimetre (cm^2)
Volume:	Cubic metre (m^3) = 10^6 cubic centimetre (cm^3)
Temperature:	Degree Celsius (^oC)
Molecular amount:	Mole (mol) = 1/1000 kilomole (kmol)
Time:	Second (s)
Speed:	Metre per second (m/s)
Density:	Kilogram per cubic metre (kg/m^3)
Pressure:	Pascal ($kg/m.s^2$) = 1/1000 kilopascal (kPa) = 0.00075 centimetres of mercury (cmHg) = 10^{-5} bar (Bar) = 1/101325 atmospheres (Atm)
Permeability:	Barrer ($1x10^{-10}$ cm^3(STP).cm/cm^2.s.cmHg)
Permeance:	GPU ($1x10^{-6}$(STP)/cm^2.s.cmHg) = 1 Barrer/1 µm membrane thickness

List of symbols

i: The component being inspected at any one time

j_i: The volume flux (cm^3 (STP) /cm^2.s) of component i through the membrane

p_{ii}: The partial pressure of i at the inlet of the membrane

p_{io}: The partial pressure of i at the outlet of the membrane

D_i: The diffusion coefficient of i as the permeate

L: The thickness of the membrane

K_i: The sorption coefficient (cm^3 (STP) /cm^3 of polymer pressure) of component i

P_i: The permeability of component i in the membrane

α_{ij}: The selectivity of the membrane to permeate component i rather than j

Å: An ångström or $1x10^{-10}$ m

(It should be noted that where the symbols for a specific set of equations are needed, they are explained after the equations. This is to save confusion as some symbols are used more than once but with different meanings.)

Chapter 1: Introduction

1.1: Background

From as early as the 1950s High Temperature Reactors (HTR) have been in development and have, since then, seen a great deal of variations and innovation. Abram & Ion (2008) are of the opinion that HTRs could be a possible solution to the slow evolution of the nuclear technology sector as they are seen as one of the Generation IV types of reactors that will replace the Generation III and Generation III+ reactors. Currently, most HTRs utilize helium as the reactor coolant gas, which either heats water to steam, or is used directly to produce electricity in the turbine (Yan, et al., 2003, Yao. et al., 2002, Berka, et al., 2012., Sakaba, et al., 2004).

The design of the Advanced High Temperature Reactor (AHTR) was commissioned as part of Eskom's plan to secure the future of South Africa's power grid and was restarted from the old Pebble Bed Modular Reactor (PBMR) project (Nicholls *et al.*, 2017). It will include an improved and more thoroughly tested fuel pebble, that can withstand higher temperatures and emit fewer unwanted particles into the primary helium loop. The new design has been calculated to reach efficiencies of up to 60% (Nicholls *et al.*, 2017). A table of the properties which are being worked towards is shown in **Table 1-1**.

Table 1-1: AHTR basic design properties

Property	Value
Heat generation in the reactor	100MW
Helium temperature at reactor inlet	400^{o}C
Helium temperature at reactor outlet	1200^{o}C
Maximum pressure	9000kPa
Pressure loss in the reactor	~80kPa
Helium flow	~33kg/s
Helium total inventory	~2000kg

A helium purification system (HPS) must be included as part of this project to prevent corrosion from the various chemical, and occasionally radioactive, contaminants in the rest of the primary system.The type of corrosion or damage that is most likely to become problematic is the damage to the turbine blades due to impurities seeping into the blades

and causing cracks, however, other parts may also be damaged by contaminants. The HPS for the AHTR could differ from the PBMR HPS, as new technologies may prove to be more efficient in solving the problem of removing contaminants in the primary system.

The primary cycle in the proposed AHTR differs from the PBMR system in that it includes three heat exchangers and three compressors to remove the excess heat from the helium after the turbine, illustrated in **Figure 1-1**. This excess heat is transferred to either a secondary heat storage, or a steam driven electricity generation cycle. The system will also feature a power conversion unit (PCU) that is displayed and labeled in **Figure 1-2**. This PCU is completely “plug and play,” meaning it can be replaced by simply removing it and placing a new PCU in its position.

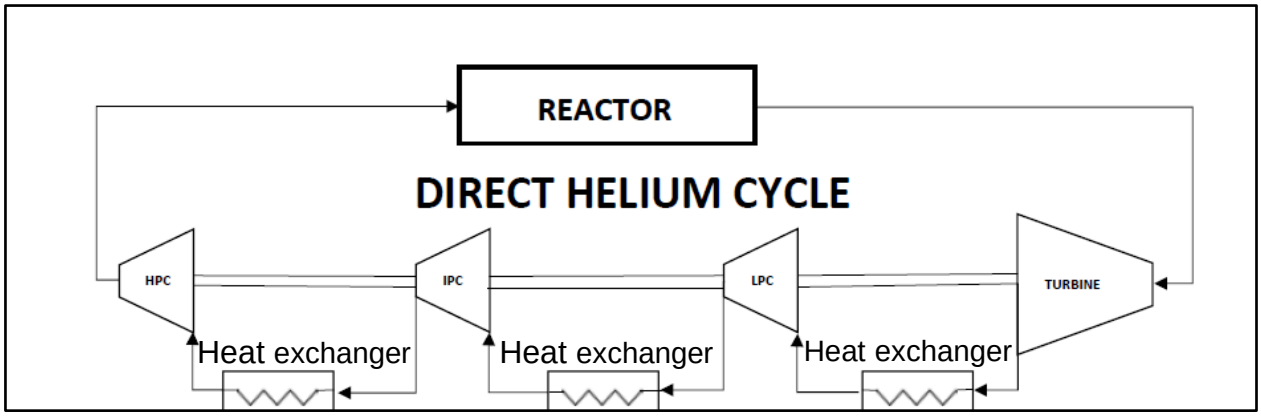

Figure 1-1: AHTR primary power generation circuit

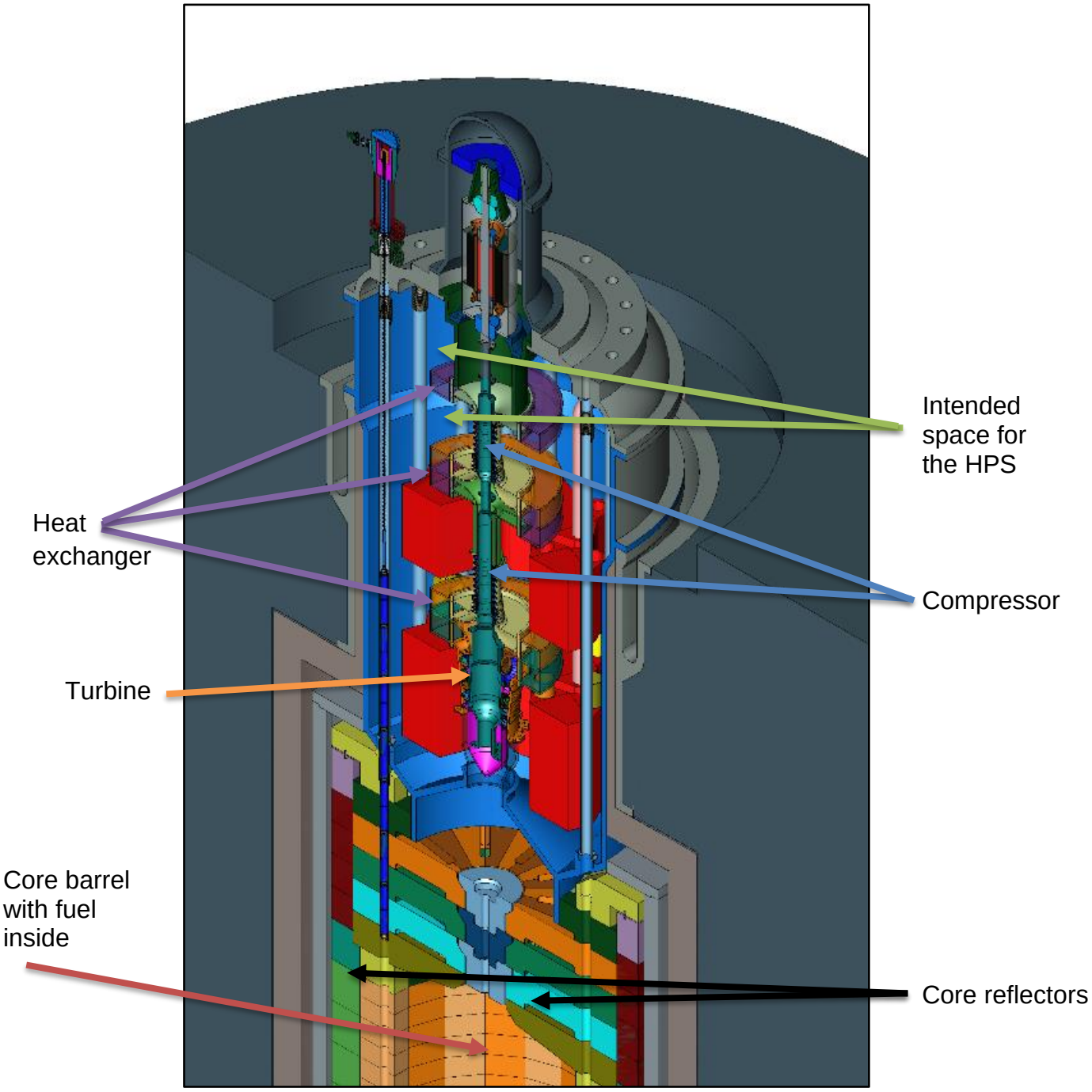

Figure 1-2: Diagram of a possible power conversion unit for the AHTR system

1.2: New Developments and Objectives

When the PBMR project was restarted several improvements were made in order to ensure that problems that occurred in the previous project did not resurface in the AHTR (Nicholls *et al.*, 2017). The fuel was tested with a new coating design intended to prevent any materials from escaping the pebbles unless an incident occurred that would cause damage

to the fuel. However, this does not eliminate the possibility of radionuclides and chemical contaminants being released into the helium flow, and thus these must still be removed. This study will attempt to provide a better solution for the necessary purification; focusing on the removal of gaseous chemical contaminants such as nitrogen, methane, carbon dioxide, and hydrogen. The gases used in this study are not a concrete representation of the gases that will be found in the reactor, but will provide results that may be used analogously for any gases of similar sizes or properties.

Nicholls *et al.* (2017) explain the importance of further design changes as it would remove the possibility of steam or any form of water interacting with the primary power generation system. As a result, the possibility of steam being found in the primary loop may be discounted, and thus the purification system will not have to remove steam or any other molecules that may be formed because of its presence. The specific design changes are, however, proprietary information and may thus not be disclosed freely.

1.3: Problem statement and goal to be achieved

Eskom is in the process of designing the AHTR for electric power generation, which will require the process gas (helium) to be purified in order to avoid corrosion from chemical contaminants or radionuclides. Previous designs as well as work done by other companies have included systems where, among other materials, steam, carbon dioxide, and nitrogen are present. This study, and subsequent theoretical designs, will attempt to prove that a more compact, passive system can be designed and implemented. This design would fit inside the PCU illustrated in **Figure 1-2**, and, once implemented, could carry out the same purification as the old system, if not more efficiently. As there are no empirical values for which molecules will be detected in the AHTR primary system, the values used in this study will focus on the chemical components that may be anticipated, and, in part, specified by the PBMR HPS design (PBMR Pty Ltd., 2010).

1.4: Research process

To accomplish the goals set for this study, an established research process will be useful to ensure focus remains on the important aspects, and a solution is found. This approach is shown in **Figure 1-3**. This study will also include a thorough literature review as part of the

solution seeking process. In terms of the hypothetical solution, this study will consider more than one, and the method for creating this hypothesis will be qualified before it can be completed and tested. If the hypothesis satisfies the problem statement, it will be considered a theory, and because of the nature of this study, there will be more than one theory that will be compared with each other. After this process, the objectives set for this project will be completed, and further research can be conducted as specified in the conclusions and/or recommendations.

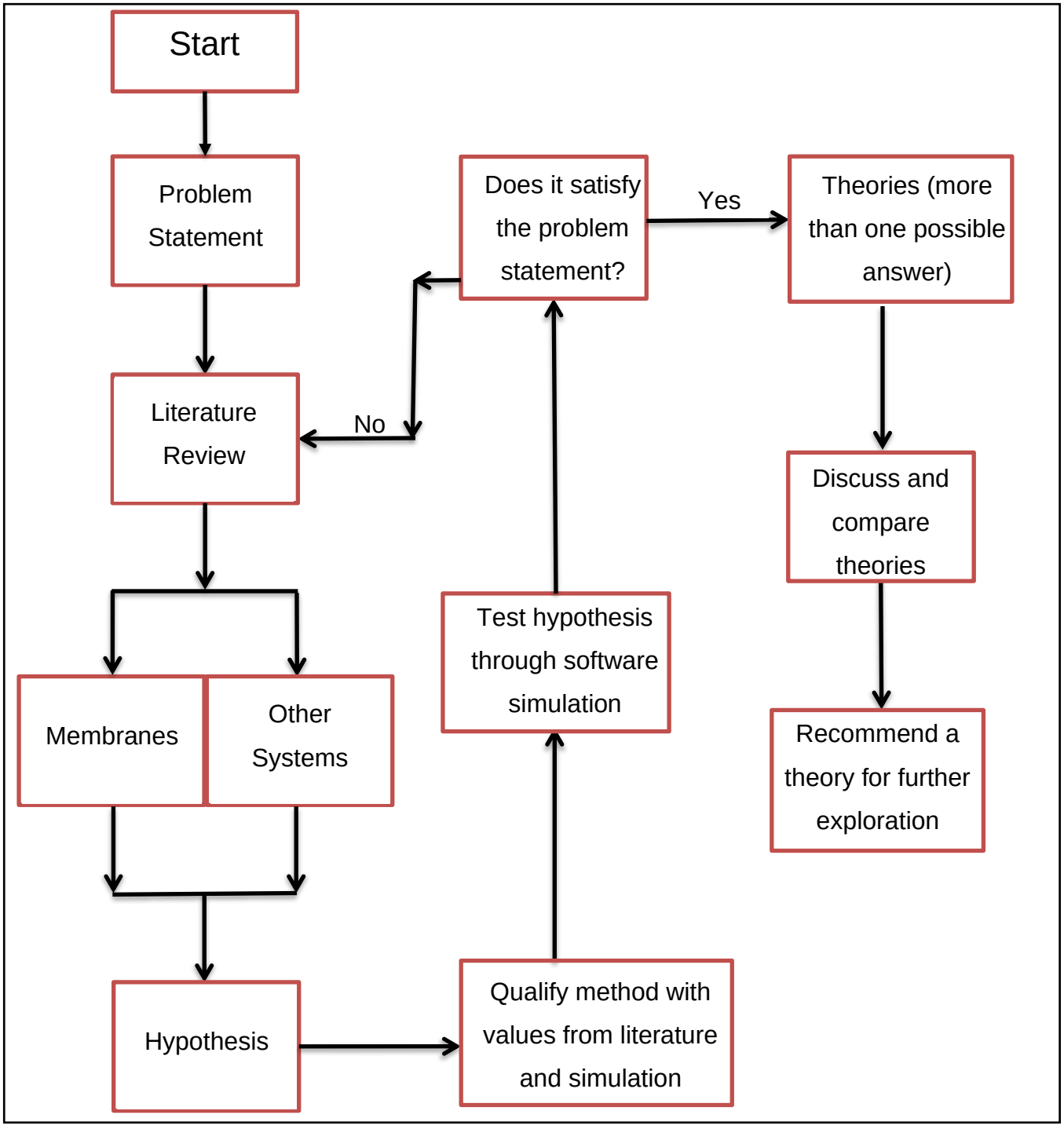

Figure 1-3: Illustration of research process

Chapter 2:Literature Review

2.1: Other Helium Purification Systems for High Temperature Reactors

2.1.1 – The PBMR system

The helium purification system (HPS) in the PBMR demonstration reactor system (PBMR Pty Ltd., 2010) is in many ways similar to many other HTR helium purification systems (Yao *et al.*, 2002, Sakaba *et al.* 2004, Berka *et al*. 2015). The main components are displayed in a process flow diagram, exemplified by **Figure 2-1**. The main source of the contaminants in this system were either from leaks out of the fuel pebbles or from gases left over from the start-up procedures; the contaminants in the AHTR will be based upon these facts since the fuel used is similar.

The HPS starts with the flow from the high-pressure compressor (HPC, 1), which is equipped with a dust filter to remove any larger solid particles, to provide a constant pressure inlet flow to the system. The flow to the HPC consists of a helium flow from the main power system (MPS, 1) and the helium inventory control system (ICS, 2). The HPS is also equipped with multiple heaters and coolers to control the temperature as per the design.

The first chemical treatment stage is the catalytic oxidizer (3) which changes any hydrocarbons, carbon monoxide molecules, and loose hydrogen molecules into water and carbon dioxide molecules. The water will then be removed in the subsequent cooler and water coalescer (4). After the water has been removed, the carbon dioxide may be removed by the molecular sieves (5).

The final step involves sending either the whole helium flow, or only a portion, through the low temperature absorber (LTA, 6) in an effort to remove excess nitrogen and any other radionuclide particles that may be present in the system. This low temperature absorber was designed, but not installed. The designers did specify that they could not guarantee the removal of radio nuclides or nitrogen for this design.

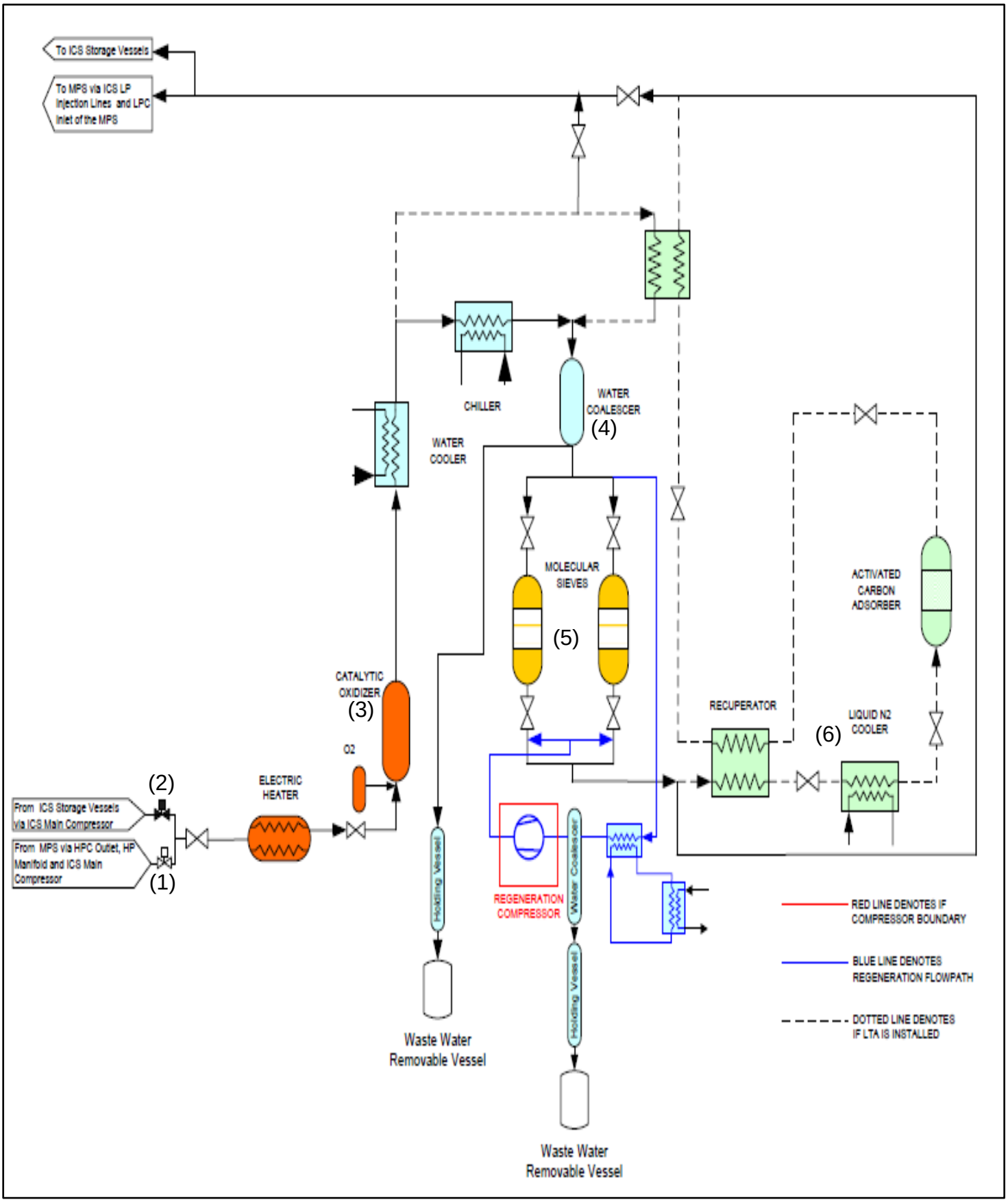

Figure 2-1: PBMR HPS process flow diagram (PBMR Pty. Ltd., 2010)

This system was designed to remove all the chemical contaminants, not only from the main power generation system, but also from the helium inventory control system, whilst remaining within the required parameters as indicated in **Table 2-1** below for a flow of 100 kg/hr:

Table 2-1: Impurity concentration parameters (PBMR Pty. Ltd., 2010)

Type of impurity	Expected range of the impurity at the HPS inlet (ppm)	Specified concentration of the impurity at the HPS outlet (ppm)
Carbon Monoxide (CO)	3.9 – 19.5	3.9
Carbon Dioxide (CO_2)	< 0.1	< 0.1
Hydrogen (H_2)	3.9 – 19.7	3.9
Methane (CH_4)	< 0.5	< 0.1
Nitrogen (N_2)	37-131	126
Oxygen (O_2)	< 0.5	< 0.1
Water (H_2O)	< 0.5	< 0.1

2.1.2 – The Chinese HTR-10 system

The Chinese HTR-10 project was a small 10MW system that served as a tester unit for future development and the helium purification system it used is very similar to that of the PBMR project. Yao *et al.* (2002) explains that the plant consists of a coal filter (1), copper-oxide catalytic bed (2), a molecular sieve absorber (3), a cryogenic absorber (4), and two diaphragm compressors (5) as indicated in **Figure 2-2**. This system was small, relative to the systems that will need to be employed in future HTRs, with a total flow rate of 10.5 kg/hr, which purified roughly 5% of the total helium per hour.

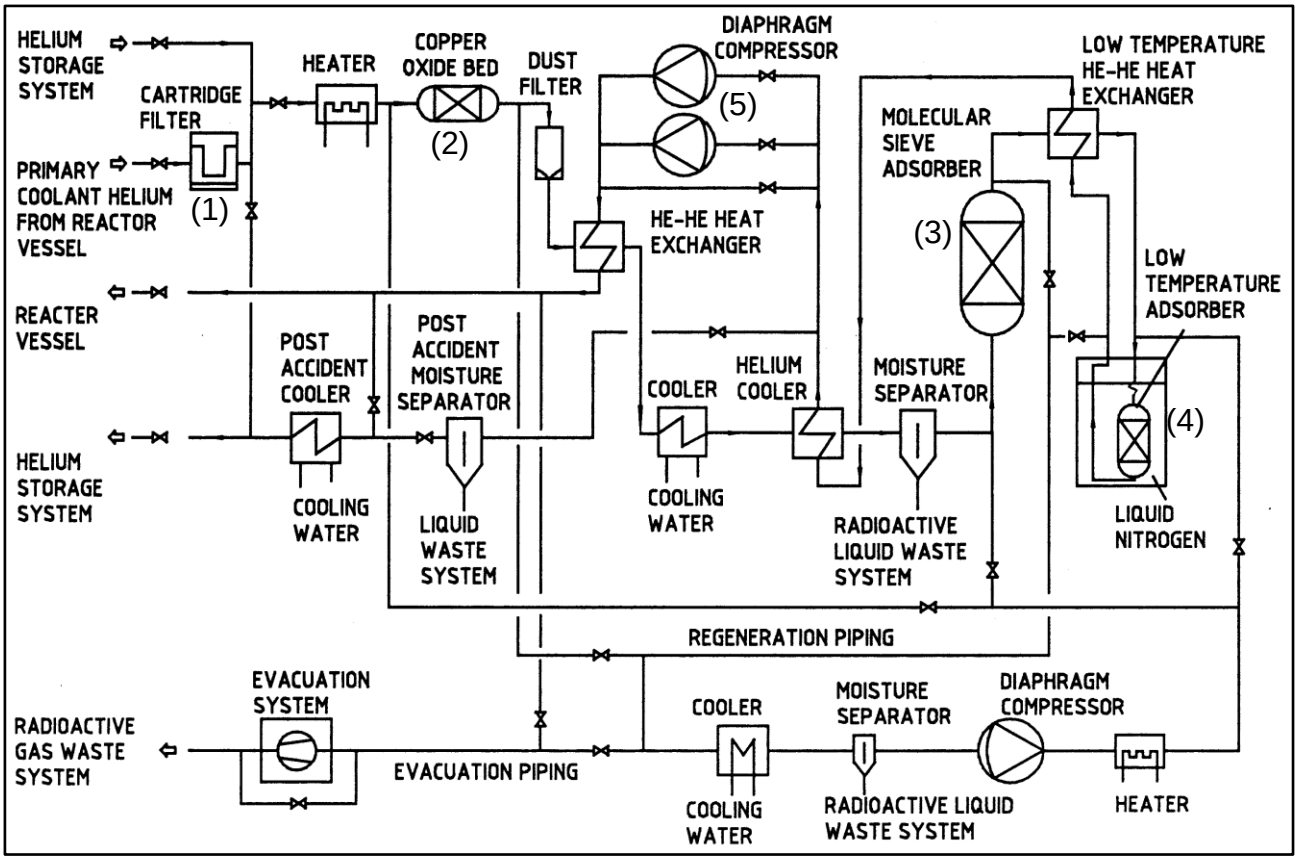

Figure 2-2: Chinese HTR-10 Helium purification system (Yao *et al.*, 2002)

2.1.3 – The Japanese HTTR system

The helium purification system employed by the Japanese on the High Temperature Testing Reactor (HTTR) is very similar to that of the PBMR system. Sakaba *et al.* (2004) explained that this system also started with an activated charcoal filter (1), followed by a copper-oxide catalytic bed (2), a molecular sieve to trap any water or carbon dioxide produced (3), and finally, a cryogenic charcoal trap (4) to remove any remaining contaminants as shown in **Figure 2-3.** This system purified 10% of the helium inventory through the first 3 stages but, only 2.5% in the cryogenic stage.

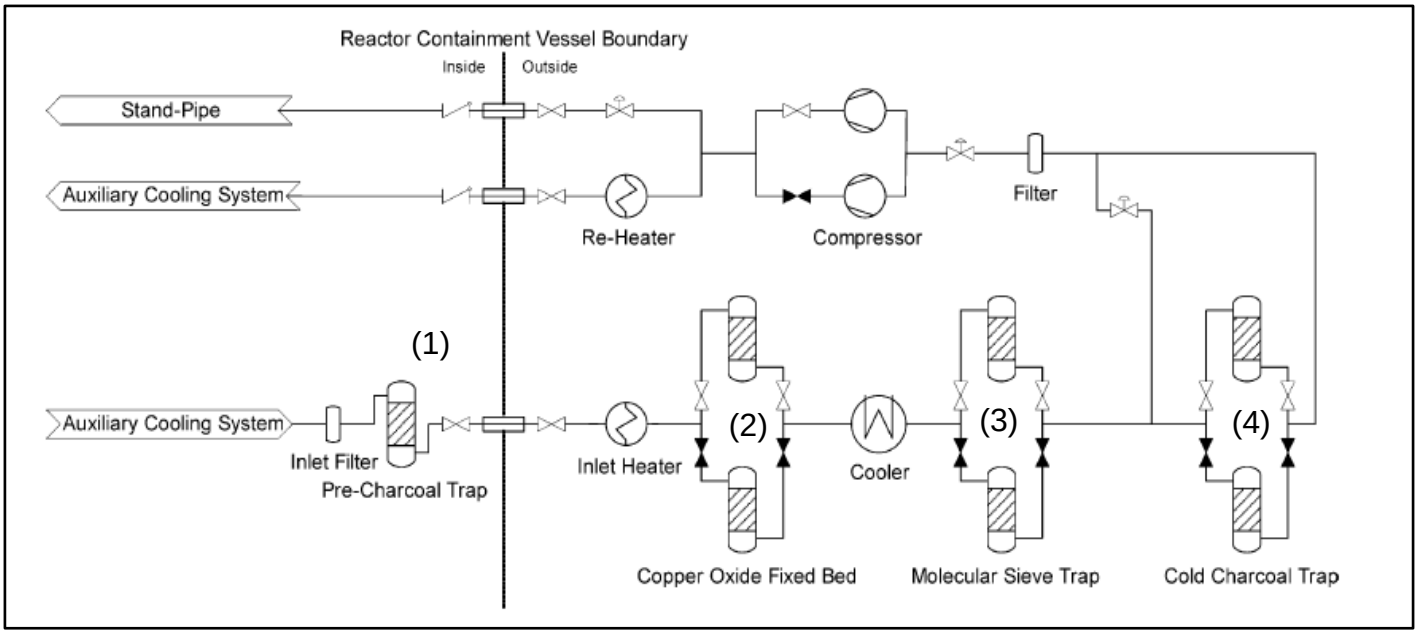

Figure 2-3: Japanese HTTR helium purification system (Sakaba *et al*., 2004)

2.1.4 – The Czech testing system

The system developed by Berka *et al.* (2015) is intended to test different parameters in the helium purification system. These parameters may be used in future on Very High Temperature Reactors (VHTR) or Gas-Cooled Fast Reactors (GFR). It consists of a similar set of parts as the PBMR system with a set of mechanical filters at the start (1), the catalytic oxidizers follow the filters (2), molecular sieves to remove any water or carbon dioxide produced in the oxidizers (3), and a cryogenic absorber (4) at the end to remove any remaining impurities as is illustrated in **Figure 2-4**. This test apparatus is adjustable and as a result, may be used in a variety of different situations, or for completing sensitivity analysis of the system.

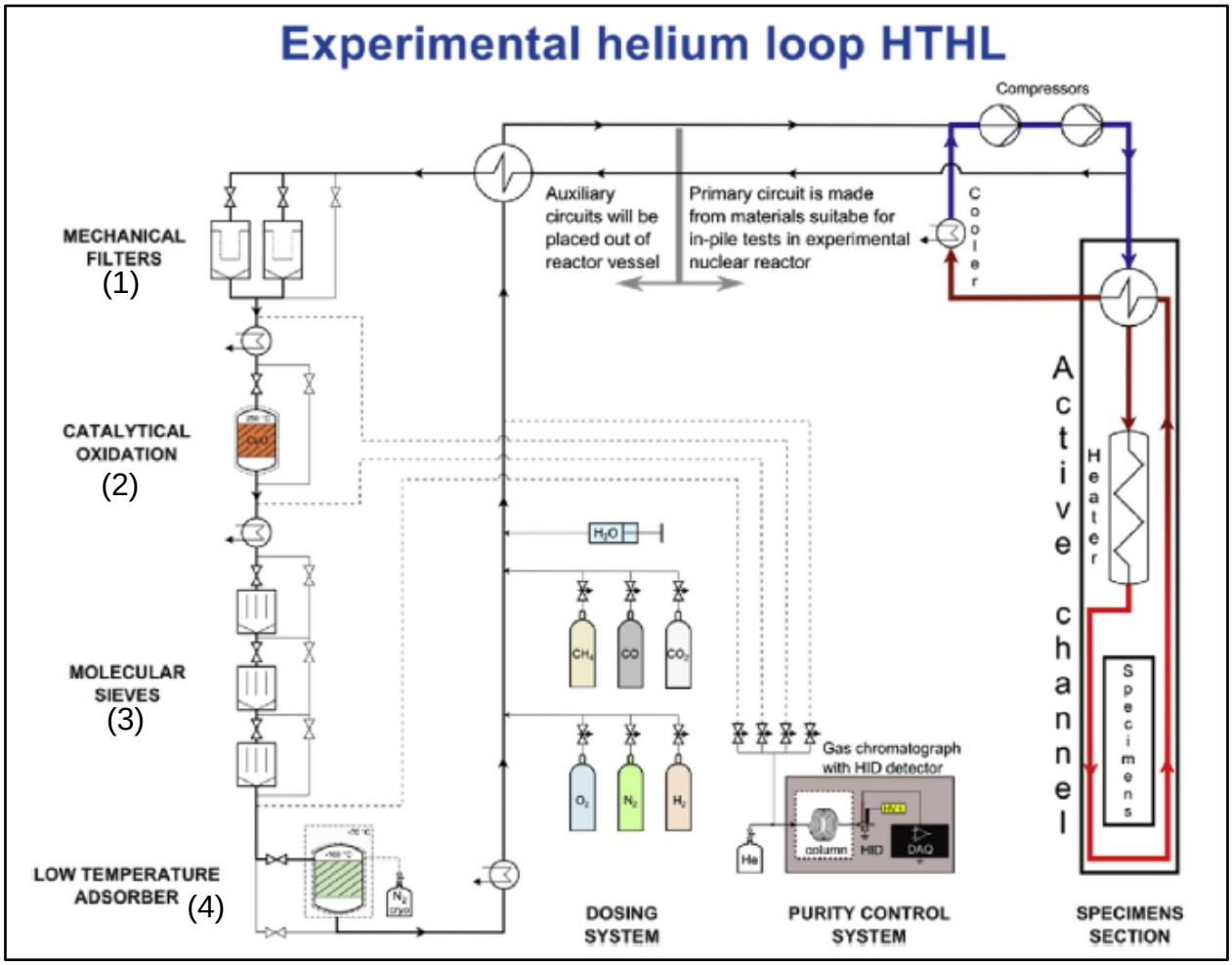

Figure 2-4: Czech helium purification test loop (Berka *et al.*, 2015)

2.2: Membrane technology

As the designs of the previous types of helium purification systems have been researched and developed to a technological plateau, little improvement can be made and an alternative approach must be sought. Membrane technology appears to be the most promising option, in terms of fulfilling the specific needs of a passive and inherently safer system.

2.2.1 – Introduction to membrane gas separation

In membrane separation technology, there are many different types of separations, such as liquid-liquid, solid-liquid, liquid-gas, and gas-gas, where the main difference between the type of membrane used is the pore size (Li et al., 2008). Membrane technology has seen a dramatic increase in research according to Sunarso *et al.* (2017) for reasons such as low cost of maintenance (no moving parts in the membranes), passive separation action (no

chemical reaction takes place), small physical area it occupies, lack of a phase change mechanism in gas separations, and the fact that membranes can be safely tested in experimental setups.

The gas-gas separations of interest for this project are those where one gas is more valuable and must be purified of any contaminants. The maximum pore size for these separations is 100 Å; for reasons being that at pore sizes above this the gases flow through the membrane with more ease and are not separated (Baker, 2012) as is seen in **Figure 2-5**.

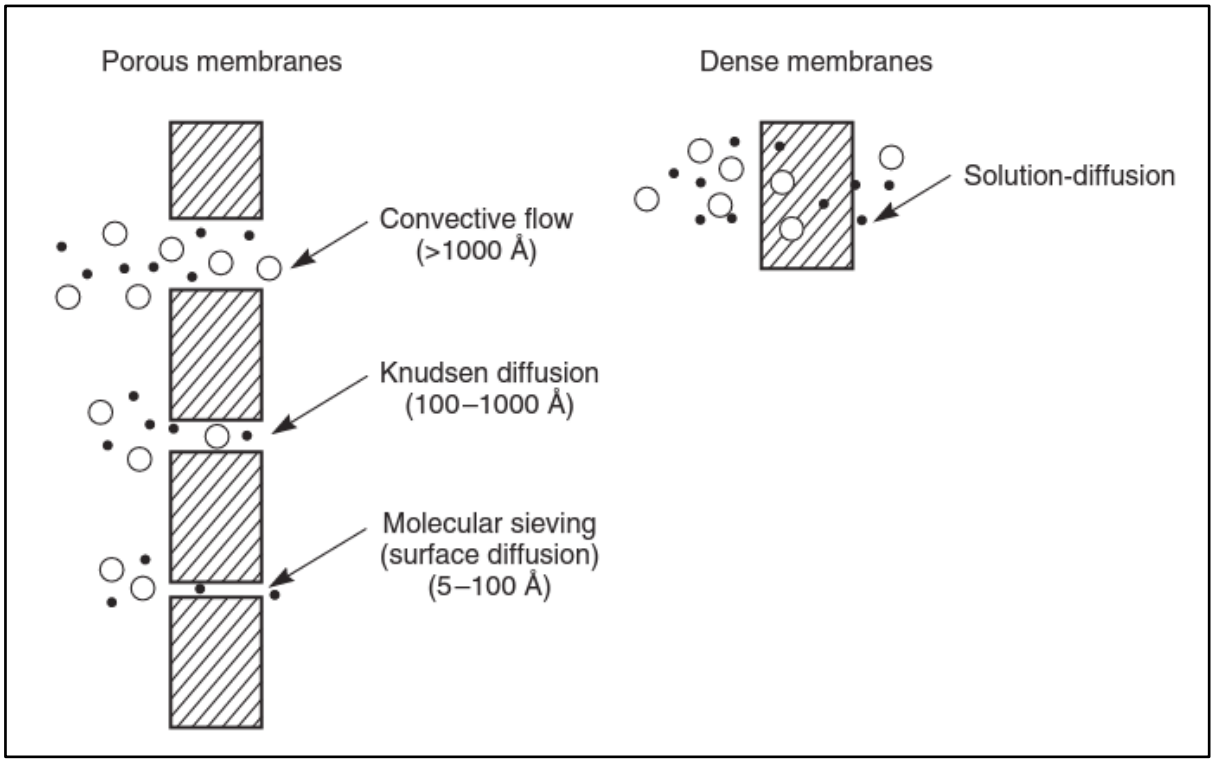

Figure 2-5: Different flow models with specific interest in the dense membranes (Baker, 2012)

The basic concept of molecular diffusion relies not only on the size of the molecule, but also the shape, as that is what determines the kinetic diameter of the molecule. The kinetic diameter is the deciding factor of whether the molecule will diffuse into the next cavity present in the membrane. A practical example of this from Baker (2012) is the difference between methane and oxygen molecules**.** In **Figure 2-6** it is evident, when viewed from above, that methane and oxygen have similar diameters, at 3.72 ångström (Å) and 3.75 Å,

respectively, but the oxygen molecule is oblong where the methane molecule is spherical in shape, and thus the oxygen molecule may rotate to fit into a smaller cavity than the methane molecule.

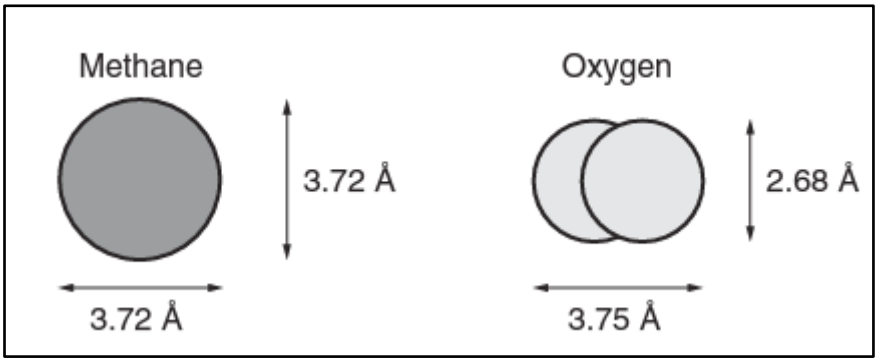

Figure 2-6: Dimensions and orientation of methane and oxygen (Baker, 2012)

Baker (2012) elaborates that the flow of gases through membranes is caused by a higher pressure in the feed side of the membrane, which in turn causes flow through to the lower pressure permeate side of the membrane. The solution-diffusion model most accurately describes the diffusion of gases through dense membranes and is thoroughly explained by Baker (2012). **Equation 1** through **Equation 18** illustrates the solution-diffusion model, while **Table 2-2** provides a legend for the various symbols. The complete explanation of the model is not included here; although it is applicable, the derivation could not be done in a clearer manner than is already present in Baker (2012). It should be noted that wherever the super script G is present it is only for reference to specify the gas phase.

Equation 1 $$J_i = -X_i \frac{d\mu_i}{dx}$$

Equation 2 $$d\mu_i = RTdln(\gamma_i n_i) + v_i dp$$

Equation 3 $$\mu_i = \mu_i^0 + RTln(\gamma_i n_i) + v_i(p - p_{i_{sat}})$$

Equation 4

$$\mu_i = \mu_i^0 + RTln(\gamma_i n_i) + RTln\frac{p}{p_{i_{sat}}}$$

Equation 5

$$c_i = m_i \rho n_i$$

Equation 6

$$p_{i_{sat}} \geq p_{i_o} \geq p_{i_L}$$

Equation 7

$$\mu_i^0 + RTln\left(\gamma_{i_o}^G n_{i_o}\right) + RTln\frac{p_o}{p_{i_{sat}}} =$$

$$\mu_i^0 + RTln\left(\gamma_{i_{o(m)}} n_{i_{o(m)}}\right) + v_i(p_o - p_{i_{sat}})$$

Equation 8

$$c_{i_{o(m)}} = \frac{m_i \rho_m \gamma_{i_o}^G}{\gamma_{i_{o(m)}} p_{i_{sat}}} \cdot p_{i_o} \exp\left[\frac{-v_i\left(p_o - p_{i_{sat}}\right)}{RT}\right]$$

Equation 9

$$K_i^G = \frac{m_i \rho_m \gamma_{i_o}^G}{\gamma_{i_{o(m)}} p_{i_{sat}}}$$

Equation 10

$$c_{i_{o(m)}} = K_i^G \cdot p_{i_o} \exp\left[\frac{-v_i\left(p_o - p_{i_{sat}}\right)}{RT}\right]$$

Equation 11

$$c_{i_{L(m)}} = K_i^G \cdot p_{i_L} \exp\left[\frac{-v_i\left(p_o - p_{i_{sat}}\right)}{RT}\right]$$

Equation 12

$$J_i = \frac{D_i K_i^G \left(p_o - p_{i_L}\right)}{L} \cdot \exp\left[\frac{-v_i\left(p_o - p_{i_{sat}}\right)}{RT}\right]$$

Equation 13

$$J_i = \frac{D_i K_i^G (p_{i_o} - p_{i_L})}{L}$$

Equation 14

$$P_i^G = D_i K_i^G = \frac{D_i m_i \rho_m \gamma_i^G}{\gamma_{i_{(m)}} p_{i_{sat}}}$$

Equation 15

$$j_i = \frac{J_i v_i^G}{m_i}$$

Equation 16

$$P_i^G = \frac{p_i^G v_i^G}{m_i}$$

Equation 17

$$j_i = \frac{P_i^G (p_{i_o} - p_{i_L})}{L}$$

Equation 18

$$\alpha_{ij} = \frac{P_i^G}{P_j^G} = \left(\frac{D_i}{D_j}\right)\left(\frac{K_i^G}{K_j^G}\right)$$

Table 2-2: List of symbols for equations 1 to 18 (Baker, 2012)

Symbol	Explanation	Units
i	Component i	N/A
J_i	Mass flux of component i	g/cm^2 s
μ_i	Chemical potential of component i	J/mol
$d\mu_i/dx$	Gradient of chemical potential of component i	N/A
X_i	Proportional link between flux and chemical potential	N/A
n_i	Mole fraction of component i	mol/mol
γ_i	Link between activity and mole fraction, activity coefficient	mol/mol
p	Pressure	Bar or kPa
v_i	Molar volume of component i	cm^3/mol
μ_i^o	Reference chemical potential at pressure P_i^o	N/A
p_i^o	Reference pressure	bar or kPa
$p_{i\ sat}$	Vapour saturation pressure	bar or kPa
c_i	Concentration of component i	g/cm^3
m_i	Molar weight of component i	g/mol
ρ_i	Molar density of component i	mol/cm^3
μ_i^0	Reference chemical potential in the feed gas	N/A
$p_{i\ L}$	Pressure of component i in the permeate flow	bar or kPa
R	Universal gas constant	J/mol K
T	Temperature	K or ^{o}C
$\gamma_{i\ o}^G$	Activity coefficient of component i in the feed gas phase	mol/mol
$p_{i\ o}$	Vapour pressure of component i in the feed	bar or kPa
$n_{i\ o}$	Mole fraction of component i in the feed	mol/mol
$\gamma_{i\ o(m)}$	Activity coefficient of component i at the feed interface with the membrane	N/A
$n_{i\ o(m)}$	Mole fraction of component i at the feed interface with the membrane	mol/mol
$c_{i\ o(m)}$	Concentration of component i at the feed interface with the membrane	g/cm^3
K_i^G	Sorption coefficient of component i between the membrane and gas phases	cm^3(STP)/cm^3
ρ_m	Molar density of the membrane	mol/cm^3
$c_{i\ L(m)}$	Concentration of component i at the permeate interface with the membrane	g/cm^3
$\gamma_{i\ o(m)}^G$	Activity coefficient of component i at the feed interface with the membrane	mol/mol

$\mathbf{D_i}$	Diffusion coefficient of component i	Many
L	Thickness of the membrane area	cm
$\mathbf{P_i^G}$	Permeability coefficient of component i	GPU
$\mathbf{j_i}$	Molar flux of component i	$cm^3(STP)/cm^2s$
$\mathbf{\alpha_{ij}}$	Selectivity of the membrane for component i over component j	N/A
$\mathbf{P_j^G}$	Permeability coefficient of component j	GPU
$\mathbf{D_j}$	Diffusion coefficient of component j	Many
$\mathbf{K_j^G}$	Sorption coefficient of component j between the membrane and gas phases	N/A

2.2.2 – Types of applicable membranes for gas separations

Baker (2012) explains that for gas separations, the most applicable types of membrane modules are the spiral wound modules or the hollow fibre modules. The spiral wound modules are shown in **Figure 2-7** while the hollow fibre modules are displayed in **Figure 2-8**. Hollow fibre modules are the only option for this separation design because of the key points below.

- The footprint of the system must be minimized.
- The pressure in the system is too high for spiral wound modules.
- The large separation area required will be impractical for spiral wound modules.
- The difficulty of separation, because of the small size of the molecules that need to be recovered, could provide problems for the spiral wound modules.

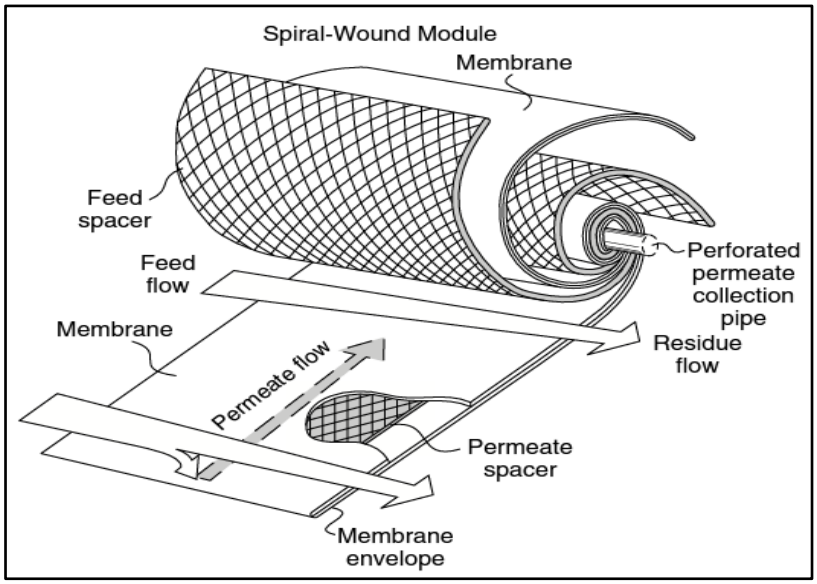

Figure 2-7: Spiral-wound module (Baker, 2012)

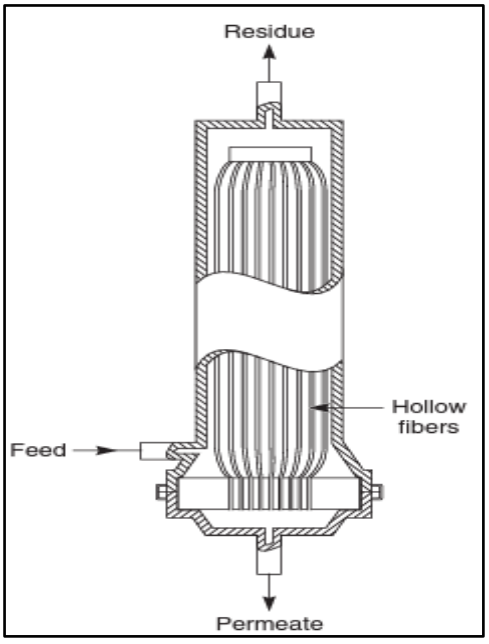

Figure 2-8: Hollow fibre shell-side feed module (Baker, 2012)

Continuing from Baker (2012) it is stated that there are two main types of gas-separation membrane materials: microporous and rubbery. These materials are opposites in their structures as microporous and ultra-microporous membranes have very small holes through which diffusion occurs, where rubbery membranes rely more heavily on adsorption and absorption to diffuse gases through their structure. The solution-diffusion model is therefore valid for the microporous membranes because of the small pore sizes involved (< 15 Å), but the sorption coefficients will be quite small for most of the gases being investigated.

The permeability of gases generally decreases as the molecules become larger and more complex in microporous membranes since the diffusion coefficient decreases. The selectivity for smaller molecules is typical of diffusion based on size and kinetic diameter, where sorption is more selective to molecules that would bond to the membrane. The effect on the permeability of each gas in two different membrane materials was graphed by Behling *et al.* (1989) as in **Figure 2-9.**

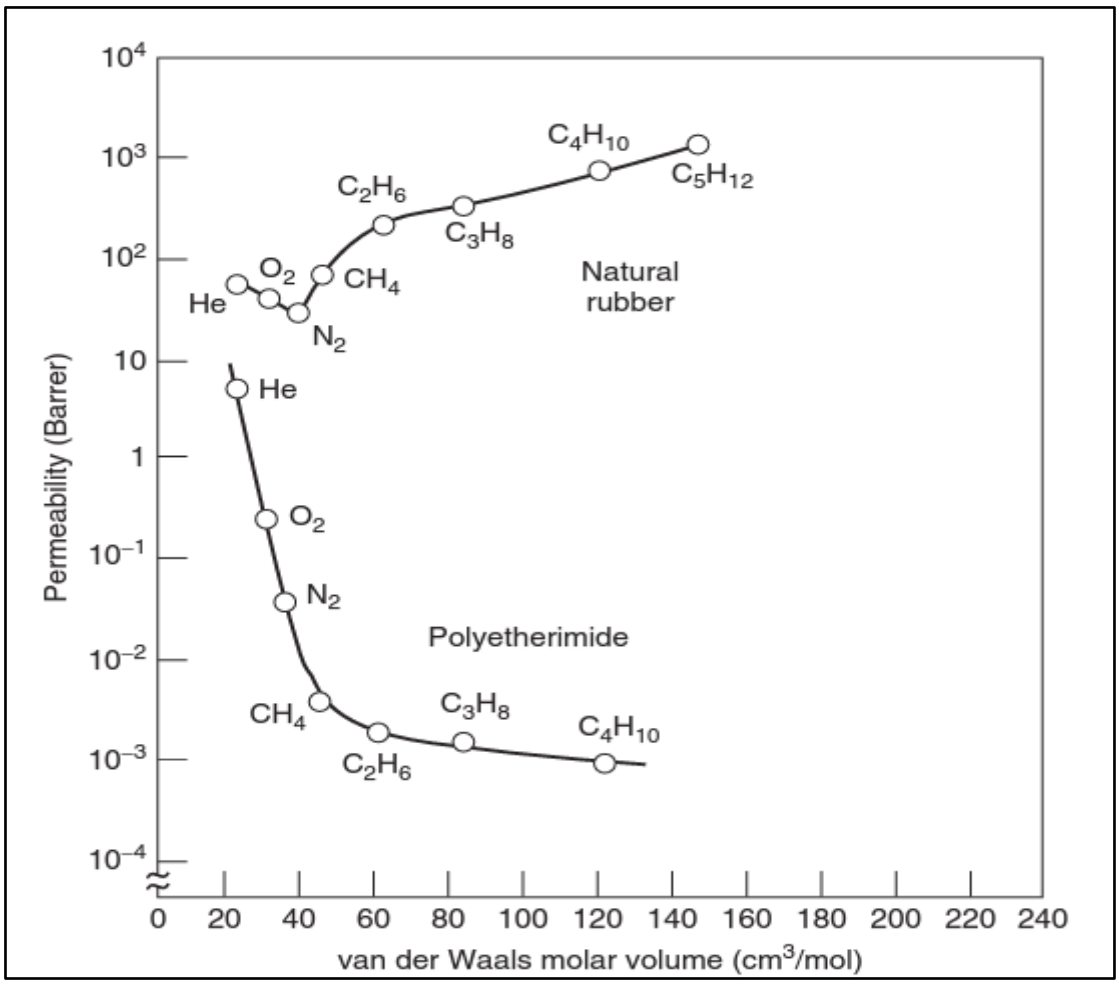

Figure 2-9: Permeabilities of different gases in the main types of gas separation membrane materials (Behling *et al*., 1989)

Silica membranes also have strong, rigid structures that can withstand long use with consistently sized, evenly-spaced pores. As long as large dust particles and water are kept away they will not be easily damaged (Barboiu *et al.*, 2009). The very high selectivity for the

low kinetic diameter gases shown in **Table 2-3**, make ultra-microporous silica membranes ideal to design and simulate the HPS for the AHTR.

There are, however, other types of membrane materials that have not been developed or researched to the same level as the ultra-microporous silica membranes. Baker (2012) explains that other possibilities exist in metal membranes, carbon membranes, or ceramic and zeolite membranes. Each of these will be examined in more depth in the following sections.

Table 2-3: Gas permeance in ultra-microporous silica membranes (Barboiu *et al.*, 2009)

Gas	Permeance ($x10^{-10}$ kmol/m^2 s Pa)	Kinetic diameter (Å)
Helium	2.5	2.6
Nitrogen	0.0435	3.64
Carbon dioxide	0.0556	3.3
Methane	0.0588	3.8

Glassy polymer membranes

The glassy polymer membrane materials are defined as such because they are used at temperatures below their glass transition temperature and are, consequently, rigid and durable (Baker, 2012). The permeation of gases through these membranes is also described by the solution-diffusion model as evidenced, in that the rate of permeation decreases very abruptly with increasing molecule size. One of the main problems with glassy polymer membranes are that they tend to have low permeabilities and as the selectivity between gases increases, the permeabilities will decrease further. In **Table 2-4**, some of the glassy type membranes are listed as per Baker (2012), along with their permeabilities being shown in Barrer and the glass transition temperatures of the membrane materials shown in ^{o}C.

Table 2-4: List of some glassy polymer membrane materials and their pure gas permeabilities (Barrer) for different gases (Baker, 2012)

Gas	Cellulose acetate 124°C	Polysulfone 186°C	Polyimide >250°C
H_2	24	14	50
He	33	13	40
O_2	1.9	1.4	3
N_2	0.33	0.25	0.6
CO_2	10	5.6	13
CH_4	0.36	0.25	0.4
C_2H_6	0.20	-	0.08
C_3H_8	0.13	-	0.015
C_4H_{10}	0.1	-	-

Metal membranes

Since the 1970s, metal membranes have been used as a special type of membrane as they have extremely high selectivity and permeation for hydrogen. Palladium-silver alloy membranes are the most commonly used membrane for the purpose of ultrapure hydrogen production (purity >= 99.9%) for use in fuel cells or the electronics industry (Baker, 2012). A serious problem faces these metallic membrane materials as they are easily poisoned by oxidation and cracks may form in the structures if they are not operated at high enough temperatures.

One such membrane material is the iron and cobalt mixtures tested by Darmawan *et al*. (2015). The mixtures were tested at different iron and cobalt quantities and different temperatures of permeation, with the figures indicated in **Table 2-5** being those for a 4 bar trans-membrane pressure and 400°C temperature at the various iron/cobalt ratios. This membrane material shows very high helium and hydrogen permeation, as well as selectivities of >100 at lower amounts of cobalt, which is very promising. One major problem with this specific membrane material is that the cobalt molecules are likely to become radioactive and may pose a risk for damage to other parts in the unit or be dangerous to humans when the unit is in maintenance.

Table 2-5: Permeabilities (GPU) of different gases in different iron/cobalt membrane mixtures (Darmawan *et al.*, 2015)

Gas	Fe/Co 10/90	Fe/Co 25/75	Fe/Co 50/50
H_2	477.9	182.2	295.7
He	851.3	328.6	537.7
N_2	6.4	20.9	62.7
CO_2	7.9	17.9	56.8

Ceramic and Zeolite membranes

Baker (2012) explains that these membrane materials have proven to be highly effective in selective separation of some gas pairs and research has improved the way these membranes are produced and supported in the membrane modules. They have been used in some commercial processes by Mitsui (Kondo *et al.*, 1997) and ECN (Castricum *et al.*, 2008), but not in mainstream commercial operations due to the high cost of production. Thus, research should be focused on making production more economically viable. As there are no economically viable options for these types of membranes available as of yet, a comparison of the permeabilities and selectivities is irrelevant here.

Polyimide membranes

Kase (2008) from UBE Industries explains that polyimides have seen a boom in commercial availability due to new production methods being discovered. These polyimides are very strong mechanically, have long maintenance-free life times, with high selectivity and permeability for gases, and are thermally and chemically stable. Furthermore, they are produced commercially by at least three business: Praxair, Medal, and UBE industries.

The specific membrane properties are completely dependent on the chemical structure of the membranes, which is decided by the constituent monomers. Therefore, there are hundreds of different polyimide membranes, each with its own advantages and disadvantages. What Kase (2008) also deems important is the fact that the polyimide materials may be easily shaped into hollow fibres that are bundled and present a very high surface area per volume occupied. These membranes are already used in commercial

hydrogen recovery processes and, as such, helium purification may be modelled with these membranes as helium and hydrogen molecules act similarly in membrane separation.

One example of these polyimides is given by Yu *et al*. (2017), where three different types of organoalkoxysilane precursors are bonded to a silica structure to produce better membrane materials. These amine precursors are 3-(triethoxysilyl)propan-1-amine (PA-Si), 3-(triethoxysilyl)-N-methylpropan-1-amine (SA-Si), and 3-(triethoxysilyl)-N,N-dimethylpropan-1-amine (TA-Si). They were tested for single gas permeances of several gases at 1 bar trans-membrane pressure and 200 ^{o}C.

Table 2-6: Permeabilities (GPU) of different gases through the different amine-silica membrane materials (Yu *et al.*, 2017)

Gas	PA-Si amine precursor	SA-Si amine precursor	TA-Si amine precursor
H_2	1852	821.4	1494
He	1852	746.8	1344
N_2	44.8	29.9	95.6
CO_2	268.8	185.2	537.7
CH_4	44.8	44.8	149.4
SF_6	0.0478	0.4481	0.2688

These materials all show high permeance for helium and hydrogen, as is evident in **Table 2-6**, but the selectivity of some of the gases make these specific membrane materials less than ideal.

Carbon membranes

Williams & Koros (2008) detail the carbon material membranes saying that they are produced by the thermal decomposition of polymer precursors and are, therefore, more easily formed than the other types of membranes. The main type of permeation in carbon membranes is the molecular sieving of molecules through pores similar in size to that of the molecules themselves. In another work Koros & Steel (2003) proposed the model of larger pores (> 5Å) being connected by smaller holes (< 5Å) whereby, the smaller the molecule is,

the faster it will permeate through the carbon membrane as a result of the difference in pore sizes.

Williams & Koros (2008) continues by stating that the reproducible production of the pore sizes carbon membranes depends on several factors;

- The post-treatment conditions.
- The time spent at the maximum treatment temperature.
- The composition of the precursor.
- The rate of heating and the maximum temperature.
- The atmosphere surrounding the carbon at the time of treatment.

As of yet, carbon membranes have not seen large-scale commercial use, but in the few instances where it was tried, the results seemed promising with packing densities of between 2000 m^2/m^3 and 2500 m^2/m^3.

Favvas *et al.* (2015) provide a very good example of the permeabilities and selectivities of these carbon membrane materials in their study, where single gas permeance is tested for the carbon precursor first, and then for the carbon materials after pyrolysis in an inert environment. The pyrolysis was carried out at 900 ^oC at varying times, while the single gas permeance tests were carried out at 60 ^oC. The results for the tests are shown in **Table 2-7** where the pyrolysis temperature and duration are shown as (^oC/minutes).

Table 2-7: Pure gas permeabilities (GPU) for different carbon membrane materials (Favvas *et al*., 2015)

Gas	Carbon precursor	Carbon (900/5)	Carbon (900/30)	Carbon (900/60)
H_2	33.20	5.99	5.50	4.41
He	33.40	3.53	3.08	2.34
N_2	5.30	0.01	0.009	0.0073
CO_2	6.10	0.42	0.31	0.2104
CH_4	6.70	0.0085	0.0051	0.0008
O_2	5.60	0.119	0.10	0.0794

It is concluded from these results that the duration of the pyrolysis directly affects the rate of permeation negatively, but increases the selectivity for the smaller molecules dramatically.

2.2.3 – Previous studies by others for this type of gas separation

Developments in membrane technology have allowed for ultra-microporous membranes (<1 nm pore sizes) to be producible on an industrial scale. Barboiu *et al.* (2006) proposed that due to the difference in kinetic diameter of helium (2.6 Å) and CO_2 (3.6 Å), these ultra-microporous membranes might be usable in high temperature reactors. Barboiu *et al.* (2009) corroborated this proposal in a later study wherein it was proved by means of experimentation that the silica-boron membrane had a selectivity of around 18-55 for helium vs. carbon dioxide, and subsequently, any kinetically larger molecules will have an even larger selectivity.

Several methods exist to produce the ultra-microporous silica membranes, which include chemical leaching as described by Beaver (1998), chemical vapour infiltration as described by Gavalas *et al.* (1989), and sol-gel synthesis as described by Barboiu *et al.* (2009) and Klein & Gallagher (1988). From several sets of experiments and characterizations by Vendanges & Colomban (1996), the sol-gel process provides the most promising results with a constant pore size and fewest defects in the membrane, as well as production being industrially viable with this process.

Mourgues & Sanchez (2012) tested different support structures for the membranes and found that the specific support structure makes insignificant difference in the permeance of helium for the conditions present in HTRs. In the same study, it was determined, through simulations, that a cascade system will purify the helium the best without the need of recycle streams or intermediary compressors as in **Figure 2-10.**

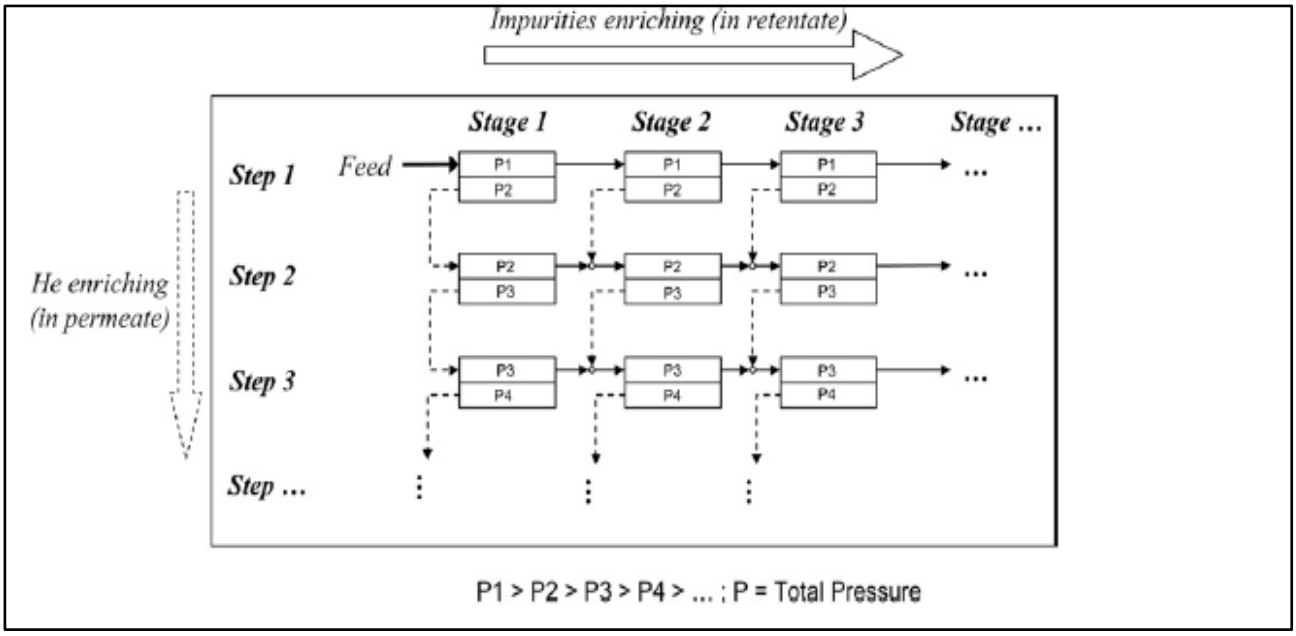

Figure 2-10: Proposed form of a cascade system for helium purification (Mourgues & Sanchez, 2012)

2.2.4 – Gas kinetic diameters, proposed membrane type, and permeances.

The gases that need to be separated from helium will all have a larger kinetic diameter and, consequently, have a lower chance of diffusing through the membranes. For this very reason, the helium will be purified, by the larger molecules remaining in the retentate and being sent out of the reactor system. The kinetic diameters of the gases that will be used as models for this design and the gases or solid molecules that may be found in the system have been listed in **Table 2-8**. This table however, is not yet complete, as no dependable tests have been done to ascertain the exact make-up of pollutants leaving the fuel pebbles or structures in the primary system.

Table 2-8: Gas kinetic diameters (Baker, 2012)

Gas	Kinetic diameter (Å)
Helium (He)	2.6
Hydrogen (H_2)	2.89
Tritium (H_3)	2.89
Oxygen (O_2)	3.46
Carbon Dioxide (CO_2)	3.3

Methane (CH_4)	3.8
Xenon (Xe)	3.96
Carbon Monoxide (CO)	3.76
Krypton (Kr)	3.6
Nitrogen (N_2)	3.64
Bromine (Br_2)	3.5
Argon (Ar)	3.4
Sulphur Hexafluoride (SF_6)	5.5

For the purpose of this work, silica membranes are to be used as the base type of membrane material. The production of silica membranes has been improved to such an extent that the pore size distribution may be assumed constant over a very large surface area membrane (Vendanges & Colomban, 1996). These membranes also display significant permeance and selectivity for the relatively small gases as is shown in parts of **Table A-8** and **Table A-9** in Appendix A. The tables are not shown here because of the length of each and the difficulty it would cause in reading the document. They also provide high mechanical strength and stability because of their rigid crystalline structure. The permeances of the gases selected to base the designs upon and the types of membranes that have been tested in literature are listed in **Table A-8** to **Table A-13**. The permeances that are to be used for the designs in this work are taken as “a workable average” of each of the gases’ permeances from the literature and are listed in **Table 2-9**.

Table 2-9: Gases' permeance that will be used in the designs

Gas	Permeance to be used (GPU)
Helium (He)	2000
Hydrogen (H_2)	1500
Carbon Dioxide (CO_2)	150
Nitrogen (N_2)	50
Methane (CH_4)	35
Sulphur Hexafluoride (SF_6)	5

2.3: Membrane simulation

In previous works, the performance calculations in the gas membranes were done either by complex mathematical models solved analytically or by simulations run in a software

environment (MATLAB, ASPEN, UniSim) where a code is written to solve the models dynamically, usually with fewer assumptions (Barboiu *et al.*, 2009, Mourgues & Sanchez, 2012, Chen *et al.*, 2016, Ahsan *et al.*, 2017, Ahmad *et al.,* 2015, Chowdhury, 2011, Rodriques, 2009).

Chen *et al.* (2016) encoded a new membrane simulation software-package, which allows for almost instant simulation of single membrane systems or hundreds of membranes in a single system. The Membrane Calculation (Memcal) software uses ASPEN Hysys as a platform to allow the user to add and remove membranes, change feed amounts and conditions, work with different stage cuts, or even different membrane characteristics. This hastens the rate of changing design features significantly, relative to having to recode the entire system, while providing accurate and trustworthy data. The Memcal system is described in more detail in Chapter 3.1.

Hysys also includes equations of state and non-ideal gas calculations that will move the data away from theoretical values and closer to experimental values. Simulating the helium purification system this way will also allow for many different designs, each with its own specific characteristics. The possible advantages and disadvantages of each design can then be compared without spending any money on equipment to run tests.

2.4: Literature review conclusion

The literature review provided a scope of the other HPS designs and HPS technologies. While still being used in many of the applications around the world, it has not grown or changed much with time. The membrane technology, however, has grown in leaps and bounds to be a widely accepted method of gas separation industrially. For now, it has mostly been implemented in natural gas purification. Membrane technology does show potential to be an innovative method of purifying helium in a passive way, but the compactness and possible purity requires further research. The rest of this work attempts to prove that a membrane system can provide the necessary compactness and purification to replace the other systems.

Chapter 3: Description and qualification of membrane simulation method

3.1: Description of the Memcal system

The Memcal system affords the user the opportunity to focus on different configurations for a system of membranes without having to reprogram the entire application. The assumptions used by Memcal are not extraordinary in the world of gas separation simulation either; they are tabulated in **Table 3-1**.

Table 3-1: List of assumptions for the Memcal software (Chen *et al.,* 2016 and Coker *et al.*, 1998)

Assumption 1	The solution-diffusion mechanism is the governing factor for gas transport across the membrane.
Assumption 2	The effects of pressure build-up in the feed side can be ignored.
Assumption 3	There is no axial dispersion, but the shell side flow does display plug flow.
Assumption 4	Temperature has no effect on the membrane permeability.
Assumption 5	Deformation of the hollow fibre because of pressure is negligible.
Assumption 6	All the fibres have identical separation surface thickness.
Assumption 7	The unit is operated at steady state.
Assumption 8	A single hollow fibre is calculated and these results are scaled for the total gas flow.
Assumption 9	All separation takes place solely on the separation membrane surface and not because of the supports.

The inputs for the Memcal system are also quite simple; an example of a Memcal unit is shown in Appendix A as **Figure A-4**. The important inputs for each Memcal unit are listed below:

- The permeance of each gas in GPU
- The inner and outer diameter of each membrane fibre
- The active length of each membrane fibre
- The pressure of the permeate in kPa
- The flow pattern of the membrane unit
- The membrane type between hollow fibre and spiral-wound
- And the membrane area in m^2

Memcal was coded with the set of differential equations shown in **Equation 19** to **Equation 23**, along with a set of symbols used included after the equations in **Table 3-2**. The differential equations may be solved with any of a number of numerical algebraic algorithms, but in this case specifically, the finite difference method is used. The differential equations for the Memcal software are derived from the full single-membrane module simulation equations given thoroughly in Coker *et al*. (1998). These equations have become the standard in single membrane separation simulation. The model is derived from the solution-diffusion model, but the differential equations used by the Memcal code are much simpler in that they ask only for a permeance to be specified.

Equation 19 $$d(F_r x_i) = -J_i\left(P_f x_i - P_p y_i\right)dA$$ **Chen *et al.* (2016)**

Equation 20 $$d\left(F_p y_i\right) = J_i\left(P_f x_i - P_p y_i\right)dA$$ **Chen *et al.* (2016)**

Equation 21 $$dF_r = \sum_{i=1}^{c} -J_i\left(P_f x_i - P_p y_i\right)dA$$ **Chen *et al.* (2016)**

Equation 22 $$dF_p = \sum_{i=1}^{c} J_i\left(P_f x_i - P_p y_i\right)dA$$ **Chen *et al.* (2016)**

Equation 23 $$\frac{dP_p}{dL} = -\frac{\frac{64}{Re}}{2d_i^j}\rho^j(v^j)^2$$ **Chen *et al.* (2016)**

Table 3-2: List of symbols for equations 19 to 23 (Chen *et al.*, 2016)

Symbol	Explanation	Units
i	The component being investigated	N/A
F_p	The flow rate of the permeate	mol/s
F_r	The flow rate of the retentate	mol/s
x_i	The mole fraction of component i in the retentate	N/A
y_i	The mole fraction of component i in the permeate	N/A

J_i	The membrane permeance of component i	GPU
P_f	The pressure of the feed	Pa
P_p	The pressure of the permeate	Pa
A	The membrane area	m^2
c	The total number of components	N/A
L	The membrane fibre active length	m
Re	Reynolds number	N/A
j	Used to indicate the specific membrane	N/A
d_i^j	The thickness of the membrane in membrane j	m
ρ^j	The density of the mixture in membrane j	mol/m^3
v^j	The molar flow rate in membrane j	mol/s

3.2: Memcal method qualification

The method of designing a helium purification using mathematical software simulations has been discussed in the literature review and the previous section, but the Memcal system has not been qualified independently from what the authors have done in Chen *et al.* (2016). The qualification of the method is presented before the design work to show that the method employed in the designs can be trusted and shows accuracy, since no work from literature can be used for comparison with the actual designs. By qualifying the method first, accurate and trustworthy results can be produced and compared for passive, compact membrane gas separation systems.

The process of qualifying the Memcal system will be uniform in steps where the data from literature is gathered into a table of important properties and a similar configuration of membranes will be built in Hysys with the Memcal units. An example of a membrane unit is shown in Appendix A as **Figure A-1** and its configuration as **Figure A-4**. Each qualification design and test has its own set of Memcal units and configurations, all displayed in Appendix A. The Memcal simulation is then executed and the results are compared with those from literature, whether empirical or simulated.

3.2.1 – Qualification test from Sada et al. (1992)

For the first qualification test, a single membrane unit was configured with the empirical data shown in Sada *et al.* (1992) as shown in **Table 3-3**. The qualification process was followed

as described above and the results were generated using the simulation method described in section 3.1 and can be seen in **Figure A-5** to **Figure A-8** in Appendix A. In **Table 3-4**, the results from the Memcal simulation are compared with the results from Sada *et al.* (1992). A mass balance for both Sada *et al*. (1992) and the Memcal calculations are included in Appendix A as **Table A-1** and **Table A-2**.

Table 3-3: Hollow fibre membrane module characteristics (Sada et al., 1992)

Membrane material	Asymmetric cellulose triacetate hollow fibre
Number of fibres	270
Fibre inner diameter (μm)	63
Fibre outer diameter (μm)	156
Active length (cm)	26
Feed flow rate (mol/sec)	0.0002518
Feed composition	50.0% CO_2 10.5% O_2 39.5% N_2
Temperature (K)	303
Permeance (GPU)	CO_2: 60.99 O_2: 17.98 N_2: 3.913
Flow configuration	Shell side feed, Counter-current
Feed pressure (kPa)	1570
Permeate pressure (kPa)	101.3

Table 3-4: Memcal results vs. Sada *et al.* (1992)

Component mole fraction	**Memcal**	**Sada *et al.* (1992)**
CO_2	0.6228	0.62
N_2	0.2559	0.25
O_2	0.1212	0.12
Total molar flow (mol/s)	2.01×10^{-4}	2×10^{-4}
Stage cut (%)	80%	80%

The results clearly show that the Memcal system compares very well with the results from Sada *et al.* (1992). The values from Sada are empirical and thus the Memcal system is proven accurate for the first test.

3.2.2 – Qualification test from Chowdhury (2011), membrane setup 1

Chowdhury (2011) presented many different membrane systems to test his membrane simulation coding. He first validated his own simulation system with a few sources before moving on to calculations. For this qualification test, the configuration specified in **Table 3-5** and displayed in **Figure 3-1** was used with the results presented for his calculations as well as that of the Memcal software for this qualification in **Table 3-6**. The Memcal simulation for this setup is also displayed in **Figure A-9** to **Figure A-12** in Appendix A, which is the same process as for the first qualification test.

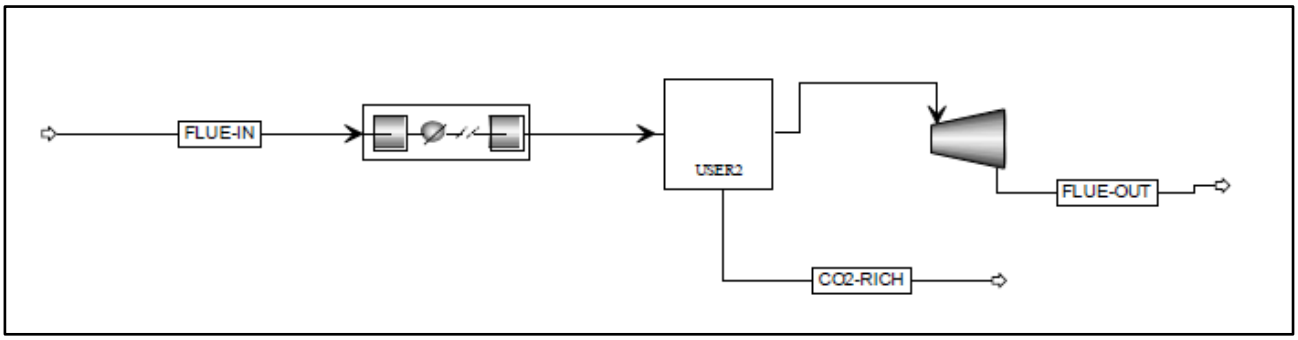

Figure 3-1: Chowdhury (2011) membrane setup 1 configuration

Table 3-5: Chowdhury (2011) membrane setup 1 characteristics

Total flow (kmol/sec)	20.95
Temperature (K)	313
Feed pressure (kPa)	101
Permeate pressure (kPa)	5.05
Membrane area (m^2)	107000
Feed composition	14.95% CO_2 80.20% N_2 3.90% O_2 0.95% Ar
Fibre inner diameter (µm)	300

Fibre outer diameter (μm)	500
Fibre active length (m)	0.5
Flow configuration	Counter-current, shell-side feed
Permeance (GPU)	CO_2: 1001 N_2: 20.01 O_2: 50.18 Ar: 50.18

Table 3-6: Chowdhury (2011) setup 1 vs. Memcal results

Mole fraction	Chowdhury Setup 1	Memcal
CO_2	65.3%	65.12%
N_2	30.47%	30.66%
O_2	3.40%	3.39%
Ar	0.84%	0.825%
Molar flow rate (kmol/hr)	14688	14625

The results show encouraging accuracy for the Memcal software with differences being minute. A mass balance for the Memcal system and Chowdhury's simulations are shown in **Table A-3** and **Table A-4**, respectively, in Appendix A.

3.2.3 – Qualification test from Chowdhury (2011), membrane setup 2

The second membrane setup chosen for the qualification test is the seventh configuration tested by Chowdhury (2011), as shown in **Figure 3-2**. The specific details of this setup are given in **Table 3-7** and the results of his calculations are compared with the results from the Memcal software in **Table 3-8**. The Memcal setup and process, similar to the first test, is displayed in Appendix A in **Figure A-13** to **Figure A-16**.

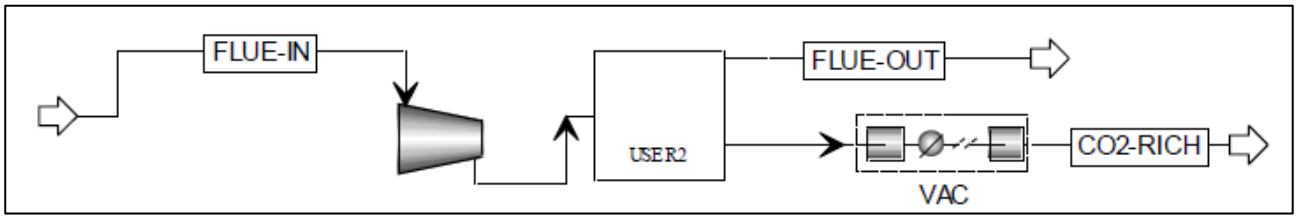

Figure 3-2: Chowdhury (2011) membrane system 7, referred to as setup 2

Table 3-7: Chowdhury (2011) membrane setup 2 characteristics

Total flow (kmol/sec)	20.95
Temperature (K)	313
Feed pressure (kPa)	150
Permeate pressure (kPa)	10
Membrane area (m^2)	227000
Feed composition	14.95% CO_2 80.20% N_2 3.90% O_2 0.95% Ar
Fibre inner diameter (μm)	300
Fibre outer diameter (μm)	500
Fibre active length (m)	0.5
Flow configuration	Counter-current, shell-side feed
Permeance (GPU)	CO_2: 1001 N_2: 20.01 O_2: 50.18 Ar: 50.18

Table 3-8: Chowdhury (2011) setup 2 vs. Memcal results

Mole fraction	Chowdhury Setup 2	Memcal
CO_2	55.03%	55.59%
N_2	39.81%	39.38%
O_2	4.15%	4.045%
Ar	1.02%	0.9855%
Molar flow rate (kmol/hr)	17280	17379

These results correlate well, as differences are within 1% of each other and a more complete mass balance of both Chowdhury's simulation and the Memcal simulation is presented in Appendix A as **Table A-5** and **Table A-6**, respectively.

3.2.4 – Qualification test of cascade membrane system from Mourgues & Sanchez (2012)

The research done by Mourgues & Sanchez (2012) tested the idea that for membranes with a certain permeability or higher, the supports do not have any effect on the actual permeation of the gases present. The test was successful for all the permeabilities tested, after which they continued tests on the membranes with a cascade system shown in **Figure 2-10** above.

This cascade membrane system had the characteristics shown in **Table 3-9**, and after they did the permeation experiments mentioned in their previous work (Barboiu *et al.*, 2009), they ran simulations with the assumptions listed in **Table 3-10**. It is important to note here that the exact permeances for the simulations done by Mourgues and Sanchez were not explicitly given and, as such, the values in **Table 3-9** are the ones used for the Memcal simulation. The Memcal setup for this qualification test is also shown in **Figure A-17** to **Figure A-21**. The results for this configuration are generated in the same way as the first test, except for the process where the area of each Memcal unit is changed until a permeate stage cut of 90% is reached for each unit.

Table 3-9: Mourgues & Sanchez (2012) cascade membrane system validation membrane characteristics

Total flow (kg/hr)	135
Temperature (K)	573.15
Feed pressure (kPa)	7000
Transmembrane pressure (kPa)	4000
Feed Composition	0.0002% CO_2 0.0001% N_2 99.9996% He 0.0001% CH_4
Fibre inner diameter (µm)	400
Fibre outer diameter (µm)	N/A
Fibre active length (m)	1.02
Flow configuration	Counter-current, shell-side feed
Permeance (GPU)	CO_2: 21.57 N_2: 19.42 He: 388.3 CH_4: 22.84

Table 3-10: Mourgues & Sanchez (2012) list of assumptions

Assumption number	Assumption
1	Steady state
2	Ideal gas law
3	Isothermal conditions
4	The permeability is constant and not a function of the relative quantity of the gases
5	Axial diffusion is negligible
6	Counter-current flow module
7	The inside and outside boundary layers and the porous support resistance are negligible
8	The axial pressure drop is negligible

These simulations provided the results which are compared with the Memcal results as reflected in **Table 3-11.** A mass balance cannot be included for these results as the results for Mourgues & Sanchez (2012) are not explicitly given. The notable differences are most likely caused by the fact that Mourgues & Sanchez used a different selectivity than the one used for the gases in the Memcal units, as it was not explicitly specified, but the most likely selectivities were used for the Memcal simulation. This argument would explain why the simulation by Mourgues & Sanchez performed better separation, if the selectivity they used was higher compared with the ones chosen for the Memcal units. This would also explain why the helium recovery and total membrane area is so similar but the separation differs. This proves that the model used for Memcal works if the correct values for permeances are given.

Table 3-11: Mourgues & Sanchez (2012) cascade system results vs. Memcal results

Recovery	M & S (2012)	Memcal
Impurities in retentate	59%	46.7%
Impurities in permeate	41%	53.3%
Helium in retentate	1.0%	1.03%
Helium in permeate	99.0%	98.97%
Total membrane area (m^2)	804	805.27

3.2.5 – Conclusion of the qualification tests

Concluding the method qualification section, the results clearly show that each test has different properties but that they all prove the Memcal system to be accurate. The final test differs slightly in helium purity but this is largely attributed to the selectivities not being explicitly defined for the simulations done by the authors. Following these results, the Memcal system is used with a trusted level of accuracy for the development of the compact, passive helium purification system for the AHTR.

Chapter 4: Design requirements, specifications, and process

4.1: – Design requirements

Since this helium purification system is intended to replace the system used in the PBMR project, the system will have to fulfil similar requirements. The requirements of the PBMR system have already been shown in **Table 2-1**, but in **Table 4-1**, the updated requirements for the AHTR are listed and compared with the PBMR system.

Table 4-1: AHTR and PBMR HPS requirements compared

Type of impurity	Required concentration of the impurity at the HPS outlet for the AHTR system (ppm)	Specified concentration of the impurity at the HPS outlet for the PBMR system (PBMR Pty Ltd., 2010) (ppm)
Carbon Monoxide (CO)	0	3.9
Carbon Dioxide (CO_2)	< 10	< 0.1
Hydrogen (H_2)	<0.001	3.9
Methane (CH_4)	< 5	< 0.1
Nitrogen (N_2)	< 5	126
Oxygen (O_2)	0	< 0.1
Water (H_2O)	0	< 0.1
Sulfurhexafluoride (SF_6)	< 1	0
Total flow (kg/hr)	100	100

It is also important to note that the AHTR system required, at all costs, that molecules like hydrogen and methane do not exist in the system. The much higher operating temperature presents a serious hazard if these molecules should be present. They are, however, included in this list since they have been investigated thoroughly in literature and their kinetic diameter present a good spread of different sizes as shown in **Table 2-8**. As the chosen membrane type is rigid in structure and ultra-microporous silica in nature, the gases will rely predominantly on molecular diffusion to move through the membrane, and as such, molecules with similar kinetic diameter may be compared with reliable accuracy.

4.2: – Design Specifications

Since the characteristics of the AHTR differs so much in temperature and operating structure from the old PBMR system, the expected influx of gases will not be the same as in the PBMR system. Both the expected inlet compositions are displayed in **Table 4-2** while the operating conditions for the intended membrane system are tabled in **Table 4-3**. Owing to their kinetic diameter and their thoroughly studied characteristics in literature, hydrogen and methane are ideal candidates for the development of the designs presented and are included in the designs as part of the gases that are to flow into the membrane. The gases and molecules that are to be expected in reality will however only be seen when the plant is built and operated. Thus, the molecules that are already included in the designs will be theoretically removed to at least the purity specified, and the molecules that have similar, or predominantly larger kinetic diameters, will be removed to a higher purity than the gases used for the designs in this work.

It should also be noted that, as previously mentioned, if the kinetic diameter of the molecule were larger than the pore size of the membrane there would be no diffusion of this molecule through the membrane. The inclusion of sulphur hexafluoride is seen as a “maximum molecule size” that the membranes may be exposed to. As with the PBMR HPS design, a compressor shall be included at the start of the HPS so that the pressure and flow fed to the membranes is constant. Additionally, a dust filter will be fitted to this compressor so that any particles that are larger than most gases will be removed before they can cause physical damage or blockages in the membranes.

Table 4-2: AHTR HPS theoretical inlet properties vs. PBMR HPS expected inlet properties

Gas	AHTR HPS inlet flow that will be used for designs (ppm)	PBMR HPS inlet expected flow (ppm)
Carbon Monoxide (CO)	0	3.9 – 19.5
Carbon Dioxide (CO_2)	10	< 0.1
Hydrogen (H_2)	0.001 (1 ppb)	3.9 – 19.7
Methane (CH_4)	5	< 0.5
Nitrogen (N_2)	5	37-131
Oxygen (O_2)	0	< 0.5
Water (H_2O)	0	< 0.5

Sulphur Hexafluoride (SF_6)	1	0
Helium (He)	Balance	Balance
Total flow (kg/hr)	100	100

Table 4-3: Operating conditions of the possible membrane system

Operating condition	Value
Temperature	300°C
Inlet pressure	7000 kPa
Max. pressure drop over entire system	6000 kPa
Max. volume of the system	~3 m^3

4.3 – Design process

The design process begins with the creation of a feed stream with the properties displayed in **Table 4-2**, with a temperature of 300°C and a pressure of 7000 kPa or 70 bar. This is connected to the first of a series of Memcal membrane units; a single unit is shown in the appendix as **Figure A-1**. Each of the membrane units has a permeate stream and a retentate stream exiting the unit and flowing to their respective destinations. Additionally, each of the membranes are configured as counter-current flow membranes with shell-side feed, as is suggested in literature above.

There are five different designs, each with its own specific characteristics and its own argument as to why this configuration might work, as detailed in the following section. The transmembrane pressure for each unit is set at 3 bar, for four of the five designs, so that the pressure loss in the system is not too great but is also sufficient to provide meaningful permeation. Each design was first completed in Microsoft Excel. This process focused on finding the required permeate flow rate in a specific membrane unit for its set stage-cut, as this differs from design to design. The membrane area for each unit could then be calculated iteratively by changing the area until the permeate flow in Hysys matched that of the Excel calculation. An example of this process is presented in **Figure A-22** to **Figure A-26** in the appendix.

Each of the designs follow the same assumptions, listed above in **Table 3-1** for the Memcal software, and any assumptions that Aspen Hysys works into the simulation. It is also very important to note that the permeances used for the development of the designs in this work are single gas permeances in the membranes, thus tests will have to be conducted to see if the mixed flow of the gases has an effect on the permeances. The Peng-Robinson fluid package was chosen for the equations of state (EOS) and any datasets that Hysys would require to do the calculations, not only because it is one of the most well-known fluid packages for Hysys, but also because it is used in many of the simulations in literature.

The designs each begin with the feed shown in **Figure A-2** and **Figure A-3** in the appendix. The designs are all some form of a cascade system each with the membranes being named as “Membrane 1,1” for membrane row x, column x; an example of this is shown in **Figure A-1.** From there, each membrane system has its own characteristics to maximize the separation of the gases, as is explained in the next section, but they all have the same configurations and properties as those shown in **Figure A-4** in Appendix A. These properties include the permeances shown in **Table 2-9**, the membrane active length of 1 m, and the membrane thickness of 200 µm.

A maximum pressure loss of 6 MPa or 60 bar is fixed for each design, but this maximum should only be reached in the final row of each design which is at the maximum number of rows of 20. Thus, the total pressure loss of the combined permeate and retentate streams is minimized. A compressor is added at the end of the final HPS to deliver the helium return flow to the primary system at the full 7 MPa pressure. Below, in **Table 4-4** the constant operating specifications for the membrane units are shown as a summation of all the important data required for the designs. There are other factors that may play a role in the real designs as listed below:

- Whether the materials to be used would leak helium.
- The specific position of the membrane system in the primary loop.
- The real required purity for the system.
- The possibility of a secondary, larger system to clean the helium that flows out in the retentate stream.

Table 4-4: Membrane design constant specifications

Characteristic	Value	Units
$\Delta P_{membrane}$	3	bar
ΔP_{system}	60	bar
Feed temperature	300	^{o}C
Feed pressure	70	bar
Maximum number of rows	20	N/A
Membrane active length	1	m
Membrane thickness	2×10^{-4}	m
Membrane feed side	Shell-side	N/A
Membrane flow orientation	Counter current	N/A
Helium permeance(He)	2000	GPU
Hydrogen permeance(H_2)	1500	GPU
Carbon Dioxide permeance(CO_2)	150	GPU
Nitrogen permeance(N_2)	50	GPU
Methane permeance(CH_4)	35	GPU
Sulphur Hexafluoride permeance (SF_6)	5	GPU

4.4: Different designs

4.4.1 – Design 1

Design 1 has a set stage-cut of 90% per membrane and operates in a cascade system similar to that of Mourgues & Sanchez (2012), but it differs in that it has more membranes toward the end of the system, i.e. in the later rows and columns. The argument for this setup is that the helium can be permeated more readily through the membranes and thus the other gases will remain in the retentate. This design has the maximum 20 rows and features, at most, 7 columns of membranes. These membranes vary from sizes as large as 250 m^2 to as small as 0.5 m^2.

One of the outcomes of this system is that separation occurs and the majority of the helium is permeated back into the primary loop. There are, however, negative effects from each type of design. The negative aspects for this system include that the membranes will vary quite widely in size and will include membrane units that are simply too small to be constructed for industrial use. The other effect this causes is that the small membranes will waste substantial space because of their casings only being able to shrink down to a certain size. Another problem this system may encounter is that a very large number of membranes

could be required. Because the desired physical volume occupied by the system is limited by the AHTR design, the number of membranes may cause this limit to be exceeded.

4.4.2 – Design 2

Design 2 has variable stage cuts starting with 50% for the first membrane in each row, 65% for the next membrane, followed by 80%, and ending with 90% stage cut membranes until a minimum amount of helium is left in the retentate. The argument for this system is to have membrane units of a similar size, which might make for less membranes being needed while separating the gas to an acceptable level.

A few specific “rules” were added for design 2; namely, as soon as the permeate from the first membrane in a row reaches a flow of 15 kg/hr or less, it is sent directly out to the main permeate flow back to the primary loop, and as soon as the retentate of the last membrane in a row reaches a flow of 1.5 kg/hr or above, a new column is added to the system. These limits will help to decide when a column should be added or removed from the system. This system will also ultimately employ the maximum 20 rows and possibly provide better purification than design 1, while using fewer membranes and having fewer impractically small membranes.

4.4.3 – Design 3

Design 3 will follow a similar route as in design 1, however, the main difference is that as soon as a retentate flow from the last membrane in a row is equal to or below 1 kg/hr, it is sent out to the collected retentate flows. The argument for this setup is that the membranes can only separate the minute pollutants marginally in this simulation, as the figures used for permeances in the membranes are those of single gas permeances through the membrane, as stated previously.

Design 3 also attempts to maximize the separation by using 20 rows of membranes, but has no membranes that are so small that they are not suited for industrial use. Additionally, if the membranes are more equally sized, they may be produced more economically.

4.4.4 – Design 4

Design 4 focuses on a different pressure drop through each membrane; the transmembrane pressure being 5 bar instead of 3 bar. This design tests the effect that a different pressure ratio has on separation and membrane size. The results from design 4 are compared with design 1 and 5. Design 4 has a maximum of 12 rows due to the pressure drop exceeding the maximum allowable if any more rows are added, accompanied with a 90% stage cut, and, at most, 5 columns of membrane units. The rationale behind design 4 is that the higher pressure drop will cause faster separation and will allow better purification with fewer membranes. It must be noted that the literature does specify a transmembrane pressure of 6 bar as the maximum, due to the fact that many membrane materials may break at higher transmembrane pressures.

4.4.5 – Design 5

Design 5 is not an entirely new and different design, but a shortened version of design 1. All the membrane sizes and properties remain the same as in design 1, but it has the same amount of membrane units as design 4, so that the results from these two designs may be compared.

Chapter 5: Results and discussion

The results for each of the designs' retentate and permeate streams are presented separately in this chapter so that they may be compared and discussed. It is important to note that to make the graphs clearer, each of the results' values are multiplied by 10^{10} and then plotted on a logarithmic scale. For each of the graphs, the feed value is illustrated as the blue bar, while the design in question is marked as the red bar.

5.1: Results for design 1

The results for design 1 shows that the helium recovery is significant at 98.74%, and allows for 30% of the impurities in the feed inlet flow to be captured. The complete results are shown below in **Table 5-1** and **Table 5-2**, and graphed in **Figure 5-1** and **Figure 5-2**. A complete table of the mass balance for both the retentate and permeate flows in each membrane is given in Appendix A as **Table A-14**. Additionally, the total membrane area for design 1 is found to be 4345 m^2 and the complete list of membrane areas is shown in **Table A-14**. In **Figure 5-3** below, the setup of the membrane system is shown from Aspen Hysys with a picture of the entire setup shown in Appendix A as **Figure A-27**.

Table 5-1: Design 1 retentate results

Retentate		
Total flow rate	0.30809	**kmol/hr**
Total flow rate	1.2394	**kg/hr**
Retentate composition	**Concentration**	**Flow rate (kmol/hr)**
Helium	99.9506%	0.30794
Hydrogen	1.0743 ppb	3.3100×10^{-10}
Carbon Dioxide	62.382 ppm	1.9219×10^{-5}
Nitrogen	140.578 ppm	4.3311×10^{-5}
Methane	209.485 ppm	6.4541×10^{-5}
Sulphur Hexafluoride	80.828 ppm	2.4902×10^{-5}
Impurities flow rate	1.5197×10^{-4}	**kmol/hr**
% Impurities in Retentate	28.97%	
% Helium lost in Retentate	1.23%	

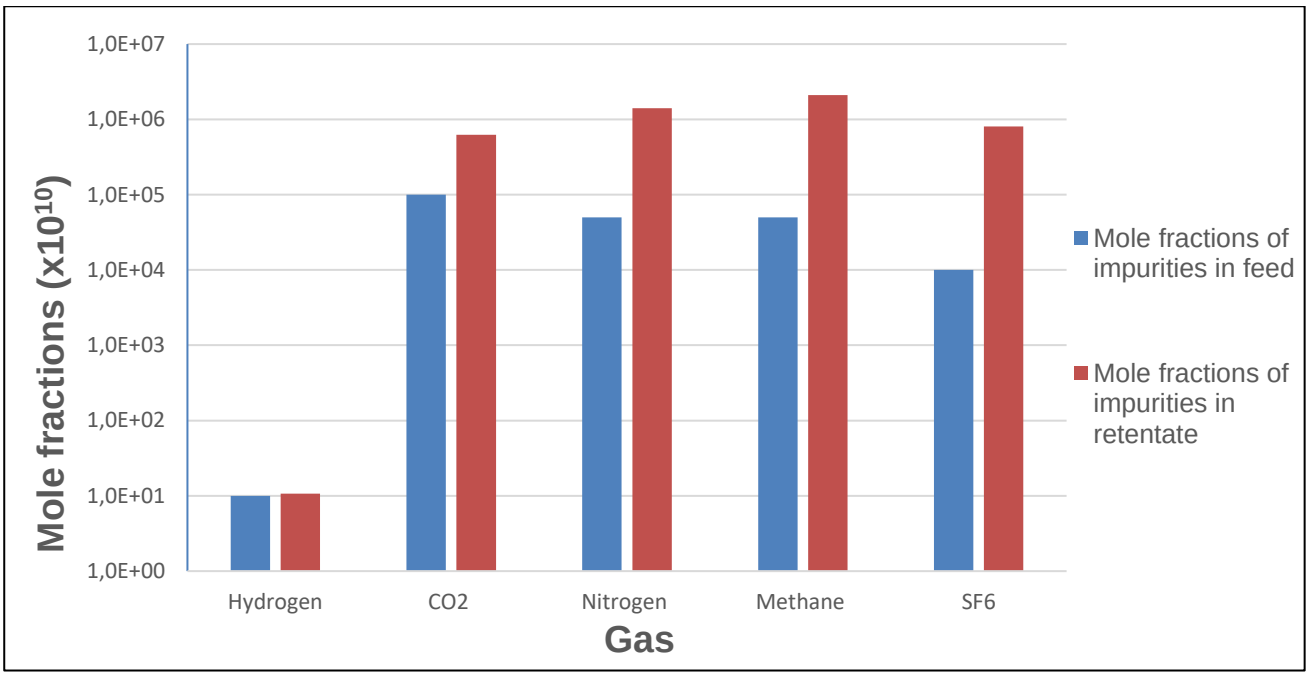

Figure 5-1: Mole fractions of the impurities in the retentate and the feed of design 1

Table 5-2: Design 1 permeate results

Permeate		
Total flow rate	24.662	**kmol/hr**
Total flow rate	98.735	**kg/hr**
Permeate composition	**Concentration**	**Flow rate (kmol/hr)**
Helium	99.9985%	24.6620
Hydrogen	0.99903 ppb	2.4639×10^{-8}
Carbon Dioxide	9.3268 ppm	2.3002×10^{-4}
Nitrogen	3.2804 ppm	8.0902×10^{-5}
Methane	2.4169 ppm	5.9607×10^{-5}
Sulphur Hexafluoride	2.4689 ppb	6.0889×10^{-8}
Impurities flow rate	3.7062×10^{-4}	**kmol/hr**
% Impurities in Permeate	70.66%	
% Helium recovered	98.74%	

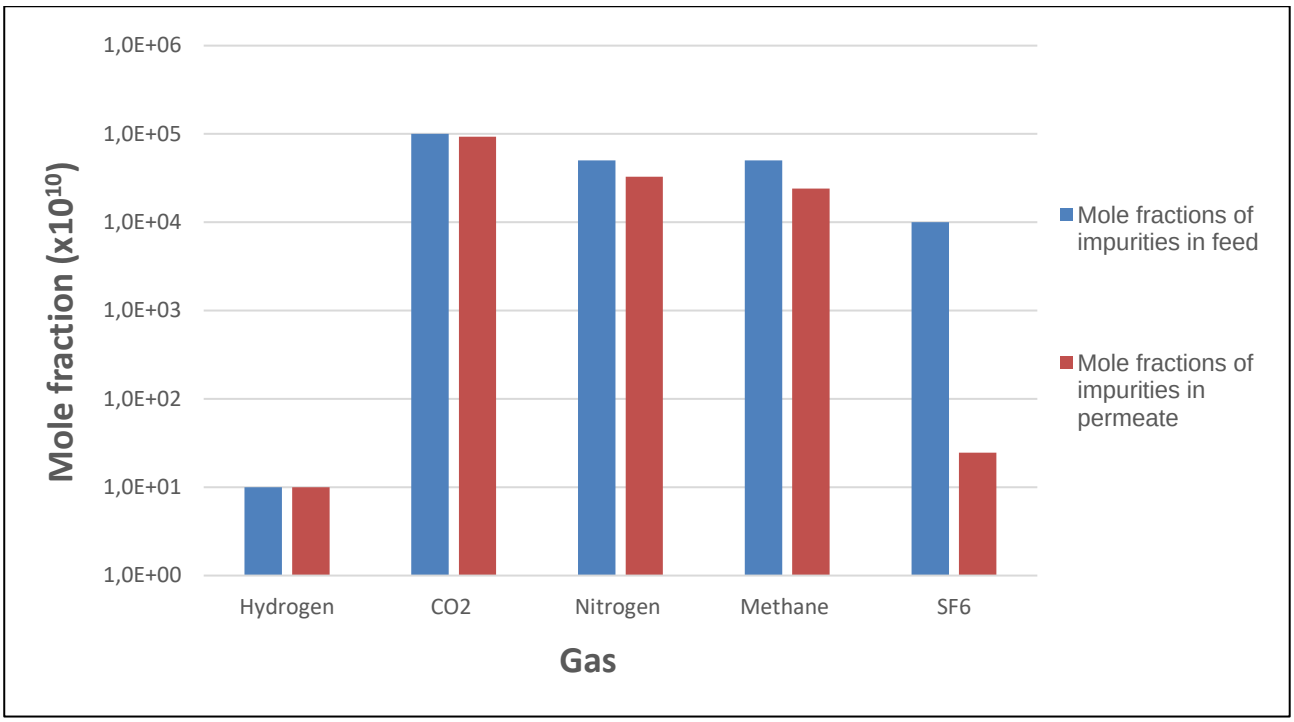

Figure 5-2: Mole fractions for impurities in the permeate and the feed for design 1

It is possible to compare the results from design 1 with that of Mourgues & Sanchez (2012), since the setup of the membrane unit systems are similar. The results for design 1, Mourgues & Sanchez (2012) simulation results, and the Memcal validation results of Mourgues & Sanchez' work are shown in **Table 5-3**.

Table 5-3: Comparison of design 1 results with that of Mourgues & Sanchez (2012)

Characteristic	Design 1	M & S	M & S qualification
Retentate impurity removal	28.97%	59%	46.7%
Permeate impurity retention	70.66%	41%	53.3%
Total membranes	91	22	22
Total membrane area (m^2)	4345	804	805.3
Helium recovery	98.74%	99%	98.97%
Helium lost in retentate	1.23%	1%	1.03%
Impurity flow removed (kmol/hr)	1.5197×10^{-4}	7.9588×10^{-5}	6.2996×10^{-5}

The results for design 1 show that the membrane system configuration suggested by Mourgues & Sanchez (2012) could work, but the separation done by Mourgues & Sanchez would seem more effective. This difference is attributed to the higher level of impurities involved in the designs for this study. This argument is corroborated by the flow rate of impurities removed being almost double for design 1 than for the other two sets of results. Design 1 does, however, have more than five times the membrane separation area, and almost four and a half times as many membranes as Mourgues & Sanchez. **Figure 5-3** shows an entire membrane unit system where (1) is the feed side of the membrane system, (2) is the direction of increasing rows, and (3) is the direction of increasing columns.

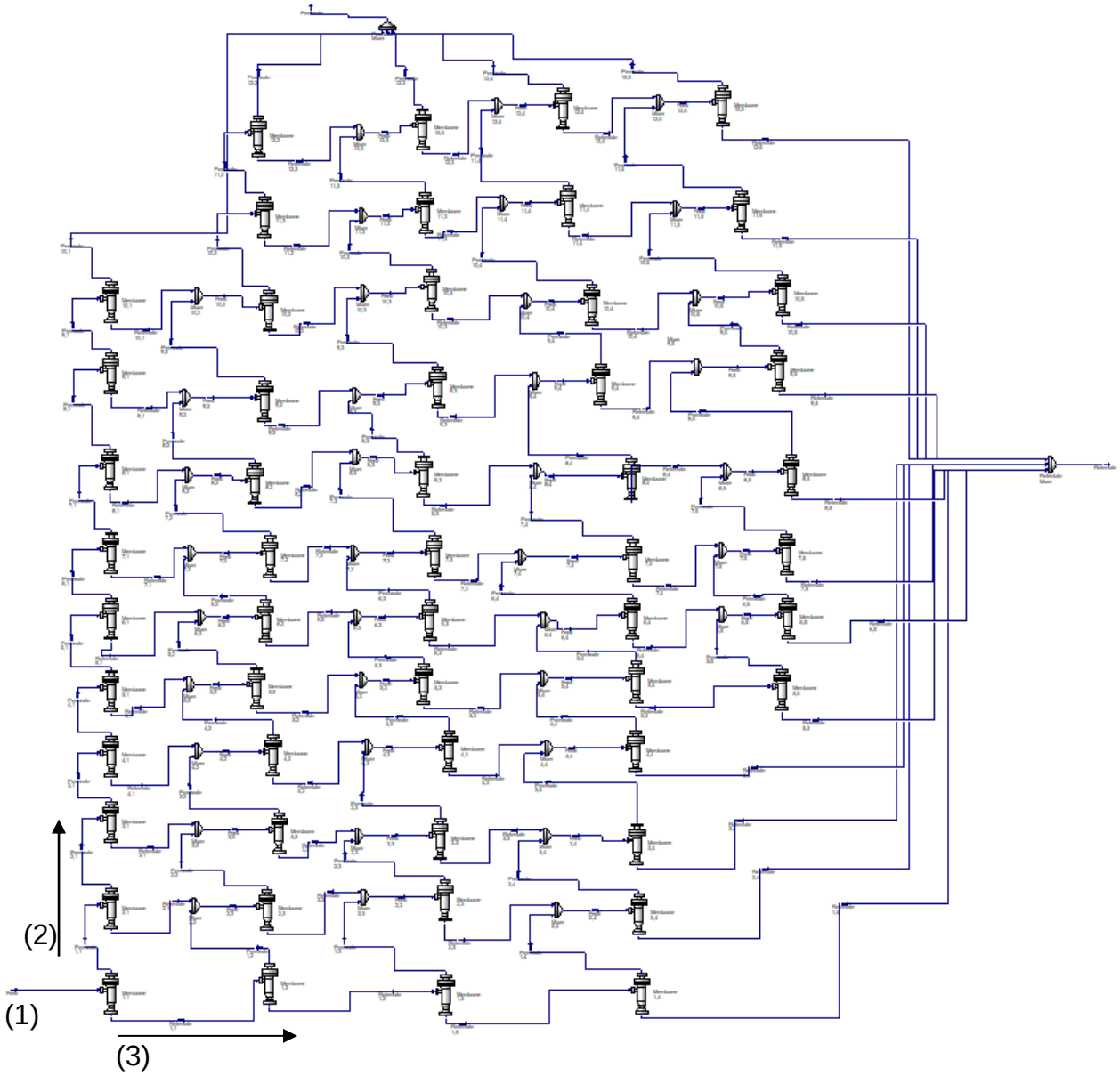

Figure 5-3: Memcal full system of membrane units

5.2: Results for design 2

Design 2 separates the impurities more thoroughly, with an impurity removal of 60.4%, while 84.27% of the helium is recovered in the permeate stream. These results are shown in **Table 5-4** for the retentate flow, and **Table 5-5** for the permeate flow, with their respective graphs in **Figure 5-4** and **Figure 5-5**. The total membrane area for design 2 is calculated as 4192 m^2. The flows and areas for all the membrane units are shown in **Table A-15,** while the setup is displayed in **Figure A-28**, although the picture may not be clear the membranes are setup in a similar manner as **Figure 5-3** above. When comparing the two complete systems, it becomes clear that only the specific configurations differ.

Table 5-4: Design 2 retentate results

Retentate		
Total flow rate	3.92165	**kmol/hr**
Total flow rate	15.7091	**kg/hr**
Retentate composition	**Concentration**	**Flow rate (kmol/hr)**
Helium	99.9919%	3.92133
Hydrogen	1.0398 ppb	4.0777×10^{-9}
Carbon Dioxide	24.9550 ppm	9.7865×10^{-5}
Nitrogen	23.1183 ppm	9.0662×10^{-5}
Methane	26.4180 ppm	1.0360×10^{-4}
Sulphur Hexafluoride	6.3444 ppm	2.4880×10^{-5}
Impurities flow rate	3.1701×10^{-4}	**kmol/hr**
% Impurities in Retentate	60.44%	
% Helium lost in Retentate	15.70%	

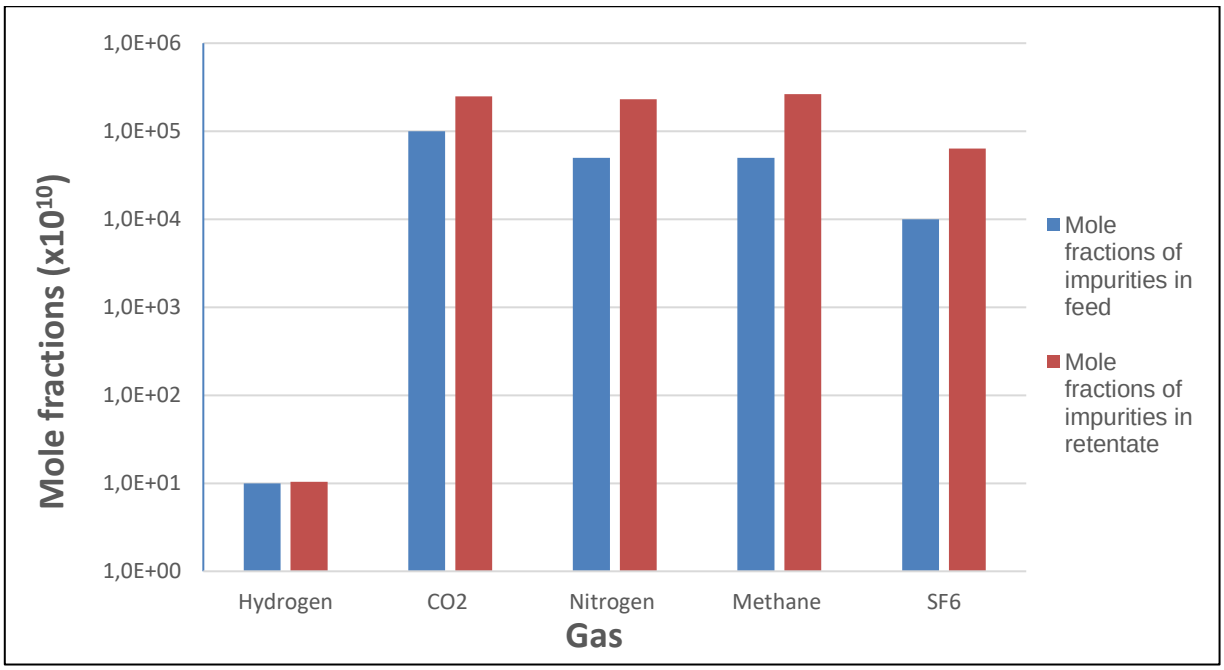

Figure 5-4: Mole fractions of the impurities in the retentate and feed of design 2

Table 5-5: Design 2 permeate results

Permeate		
Total flow rate	21.0481	**kmol/hr**
Total flow rate	84.2622	**kg/hr**
Permeate composition	**Concentration**	**Flow rate (kmol/hr)**
Helium	99.9990%	21.0479
Hydrogen	0.9925 ppb	2.0890×10^{-8}
Carbon Dioxide	7.1924 ppm	1.5139×10^{-4}
Nitrogen	1.6120 ppm	3.3929×10^{-5}
Methane	1.0003 ppm	2.1055×10^{-5}
Sulphur Hexafluoride	4.4668 ppb	9.4017×10^{-8}
Impurities flow rate	2.0649×10^{-4}	**kmol/hr**
% Impurities in permeate	39.36%	
% Helium recovered	84.27%	

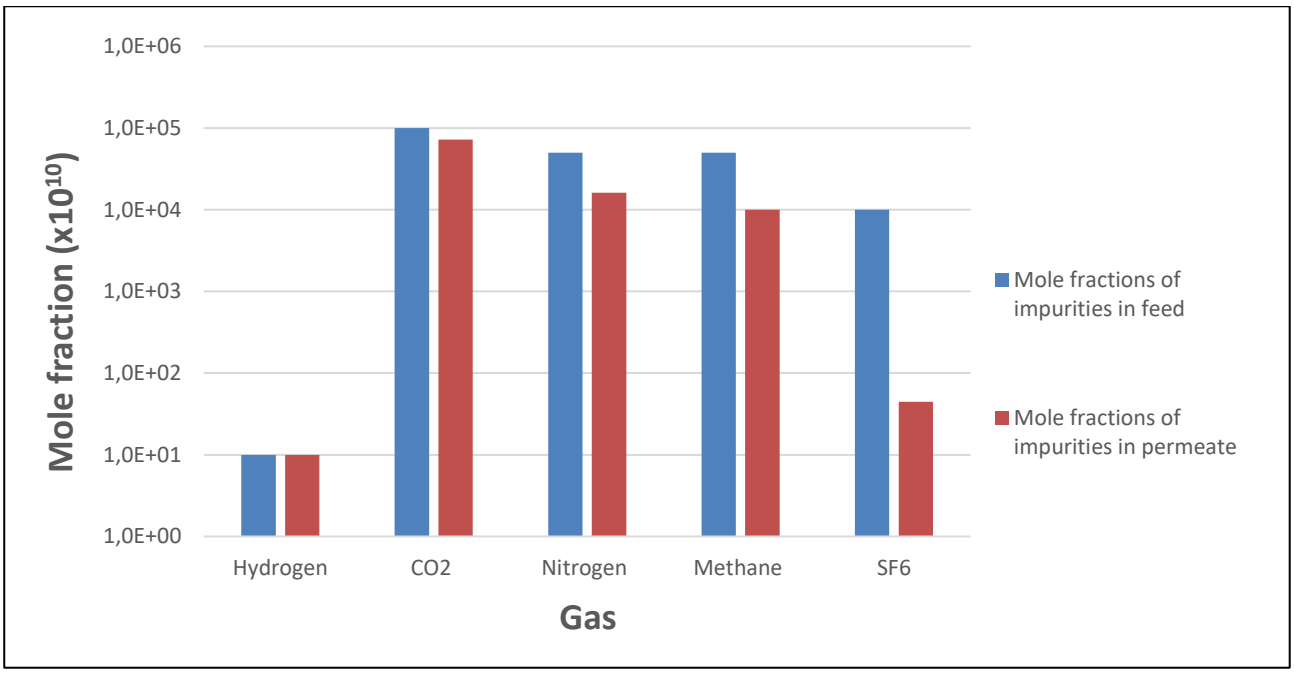

Figure 5-5: Mole fractions of the impurities in the permeate and feed of design 2

The results for design 2 are compared with that of Mourgues & Sanchez (2012) and its qualification test in **Table 5-6,** as this provides a point to evaluate all the designs independently.

Table 5-6: Comparison of design 2 results with that of Mourgues & Sanchez (2012)

Characteristic	Design 2	M & S	M & S qualification
Retentate impurity removal	60.44%	59%	46.7%
Permeate impurity retention	39.36%	41%	53.3%
Total membranes	60	22	22
Total membrane area (m^2)	4192	804	805.3
Helium recovery	84.27%	99%	98.97%
Helium lost in retentate	15.70%	1%	1.03%
Impurity flow removed (kmol/hr)	3.1701×10^{-4}	7.9588×10^{-5}	6.2996×10^{-5}

One very important aspect of this comparison is that the flow rate of impurities removed is almost four times higher for design 2 than for Mourgues & Sanchez, while the total feed flow is smaller for design 2. However, a large portion of the helium is not recovered in design 2. The amount of membrane units used is only ~three times larger for design 2, but the total separation area is still more than five times larger.

5.3: Results for design 3

Simulation of design 3 leads to 52% of the impurities being removed and 89.4% of the helium being recovered in the permeate flow, with the complete results listed in **Table 5-7** and **Table 5-8.** The mole fractions of impurities in each stream is graphed in **Figure 5-6** and **Figure 5-7.** The membrane system setup is similar to that of design 1, but the specific configuration for design 3 is shown in Appendix A as **Figure A-29,** while the complete flows and areas for each membrane in the system is tabled in **Table A-16**.

Table 5-7: Design 3 retentate results

Retentate		
Total flow rate	2.6269	**kmol/hr**
Total flow rate	10.5251	**kg/hr**
Retentate composition	**Concentration**	**Flow rate (kmol/hr)**
Helium	99.9895%	2.6267
Hydrogen	1.0428 ppb	2.7394×10^{-9}
CO2	28.0489 ppm	7.3682×10^{-5}
Nitrogen	30.4083 ppm	7.9880×10^{-5}
Methane	36.5504 ppm	9.6015×10^{-5}
F6S	9.4965 ppm	2.4947×10^{-5}
Impurities flow rate	2.7453×10^{-4}	**kmol/hr**
% Impurities in Retentate	52.34%	
% Helium lost in Retentate	10.52%	

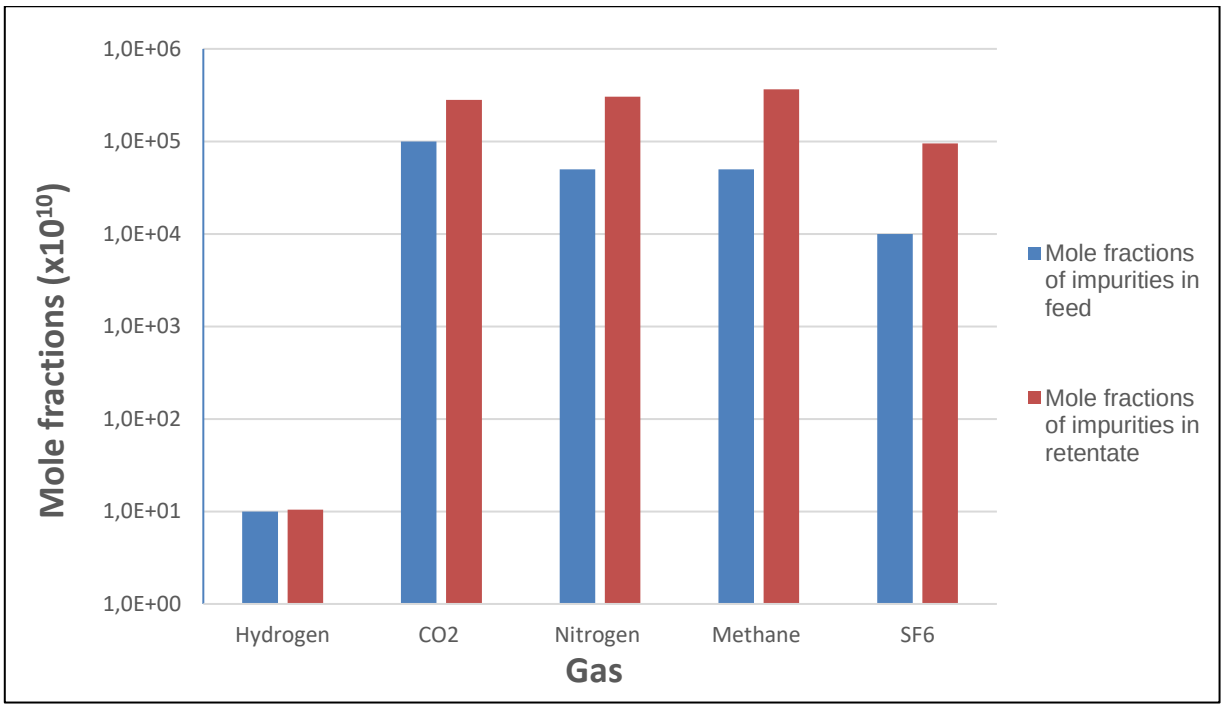

Figure 5-6: Mole fractions of impurities in the retentate and feed of design 3

Table 5-8: Design 3 permeate results

Permeate		
Total flow rate	22.3356	**kmol/hr**
Total flow rate	89.4175	**kg/hr**
Permeate composition	**Mole fraction**	**Flow rate (kmol/hr)**
Helium	99.9989%	22.3354
Hydrogen	0.9491 ppb	2.2222×10^{-8}
CO2	7.8600 ppm	1.7556×10^{-4}
Nitrogen	1.9986 ppm	4.4640×10^{-5}
Methane	1.2782 ppm	2.8549×10^{-5}
F6S	1.1390 ppm	2.5440×10^{-8}
Impurities flow rate	2.4879×10^{-4}	**kmol/hr**
% Impurities in permeate	47.43%	
% Helium recovered	89.43%	

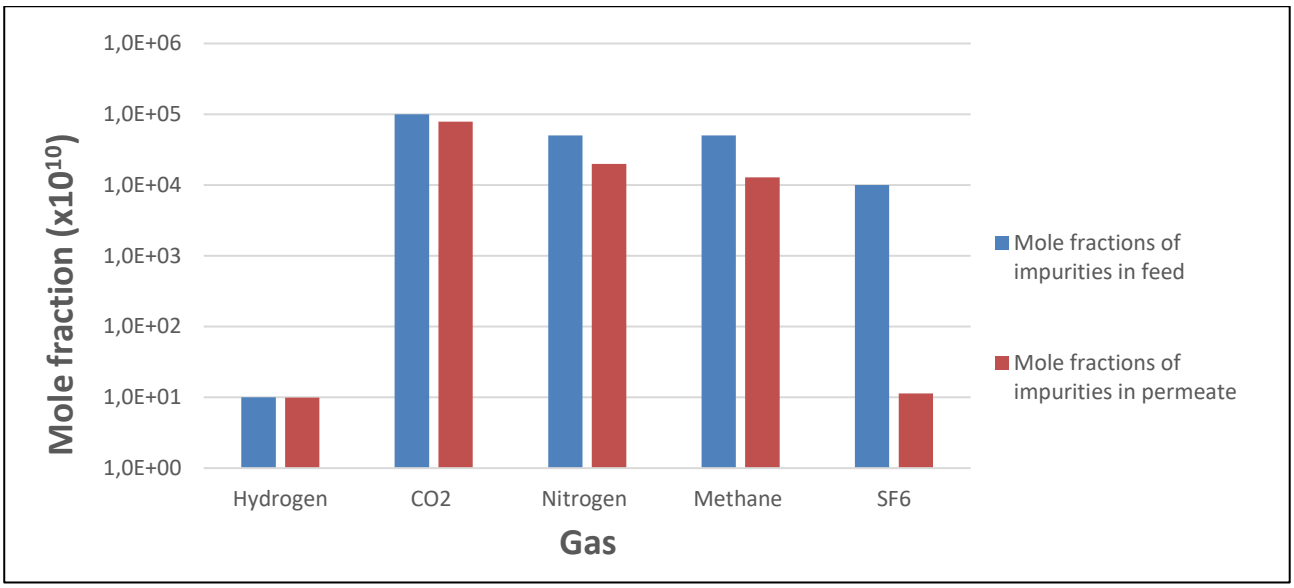

Figure 5-7: Mole fractions of the impurities in the permeate and feed of design 3

The results for design 3 are listed in **Table 5-9**, along with the results from Mourgues & Sanchez (2012), and the accompanying qualification test so that a comparison may be drawn. These results show that better separation is not guaranteed in a membrane system with fewer membranes that have a great total separation area. However, more than half of the impurities entering the system are removed from this design and only ~10% of the helium is lost in the retentate.

Table 5-9: Comparison of results of design 3 with that of Mourgues & Sanchez (2012)

Characteristic	Design 3	M & S	M & S qualification
Retentate impurity removal	52.34%	59%	46.7%
Permeate impurity retention	47.43%	41%	53.3%
Total membranes	60	22	22
Total membrane area (m^2)	4685	804	805.3
Helium recovery	89.43%	99%	98.97%
Helium lost in retentate	10.52%	1%	1.03%
Impurity flow removed (kmol/hr)	2.7453×10^{-4}	7.9588×10^{-5}	6.2996×10^{-5}

5.4: Results for design 4

The results for design 4 show that a change in the transmembrane pressure makes a difference in the purification abilities of the membrane system. While only having 54 membranes and 2983m^2 separation area, 98.21% of the helium is recovered while 33.35% of the impurities are removed. The complete results for design 4 are tabled in **Table 5-10** and **Table 5-11**. Graphs for the mole fractions of impurities remaining in the streams have also been displayed in **Figure 5-8** and **Figure 5-9**, for the retentate and permeate, respectively. A screenshot of the membrane system setup is included as **Figure A-30** in Appendix A, with a table of the membrane areas and mass balance as **Table A-17**. A comparison of the results for design 4 is done with the results for design 5 in the next section, as they are related.

Table 5-10: Design 4 retentate results

Retentate		
Total flow rate	0.31087	**kmol/hr**
Total flow rate	1.2509	**kg/hr**
Retentate composition	**Concentration**	**Flow rate (kmol/hr)**
Helium	99.9463%	0.31070
Hydrogen	1.0990 ppb	3.4165×10^{-10}
CO_2	79.2540 ppm	2.4638×10^{-5}
Nitrogen	157.1024 ppm	4.8838×10^{-4}
Methane	220.8039 ppm	6.8641×10^{-5}
SF_6	79.9576 ppm	2.4856×10^{-5}
Impurities flow rate	1.6697×10^{-4}	**kmol/hr**
% Impurities in retentate	33.35%	
% Helium lost	1.79%	

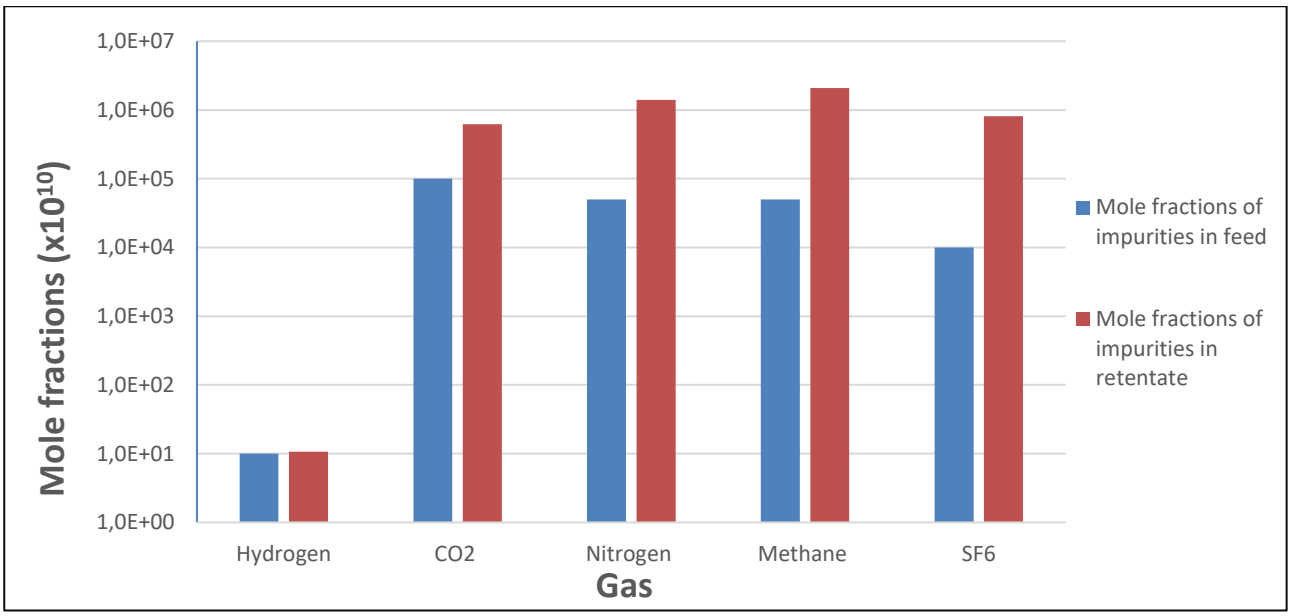

Figure 5-8: Mole fraction of the impurities for the retentate and the feed of design 4

Table 5-11: Design 4 permeate results

Permeate		
Total flow rate	24.5296	**kmol/hr**
Total flow rate	98.2027	**kg/hr**
Permeate composition	**Mole fraction**	**Flow rate (kmol/hr)**
Helium	99.9986%	24.5292
Hydrogen	0.9984 ppb	2.4490×10^{-8}
CO_2	9.0275 ppm	2.2144×10^{-4}
Nitrogen	3.0087 ppm	7.3802×10^{-5}
Methane	2.2118 ppm	5.4256×10^{-5}
SF_6	4.0178 ppb	9.8555×10^{-8}
Impurities flow rate	3.4962×10^{-4}	**kmol/hr**
% Impurities in permeate	66.65%	
% Helium recovered	98.21%	

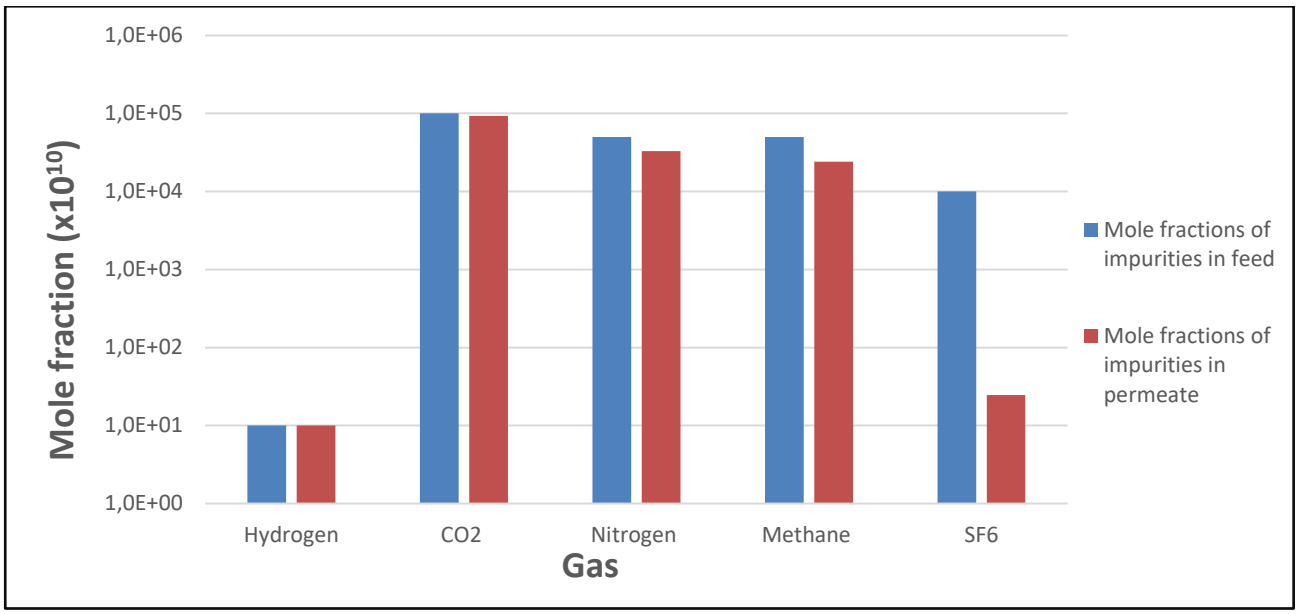

Figure 5-9: Mole fractions of the impurities in the permeate and the feed of design 4

5.5: Results for design 5

Design 5 is formed by shortening the amount of membranes in design 1 to that of design 4. The helium recovery was found to be 98.21% with 23.07% of the total impurities leaving the system with the retentate. The complete results are reflected in **Table 5-12** and **Table 5-13**. The results for the mole fractions of impurities remaining in the retentate and permeate streams are graphed below in **Figure 5-10** and **Figure 5-11**, respectively. A screenshot of the membrane units is included in Appendix A as **Figure A-31** and a complete table of the membranes and their respective separation surface area and flow is included as **Table A-18** in Appendix A.

Table 5-12: Design 5 retentate results

Retentate		
Total flow rate	0.45215	**kmol/hr**
Total flow rate	1.8155	**kg/hr**
Retentate composition	**Concentration**	**Flow rate (kmol/hr)**
Helium	99.9733%	0.45203
Hydrogen	1.0548 ppb	4.7693×10^{-10}
CO_2	39.8302 ppm	1.8009×10^{-5}
Nitrogen	70.1075 ppm	3.1699×10^{-5}
Methane	103.3730 ppm	4.6741×10^{-5}
SF_6	54.0218 ppm	2.4426×10^{-5}
Impurities flow rate	1.2088×10^{-4}	**kmol/hr**

% Impurities in retentate	23.07%	
% Helium lost	98.21%	

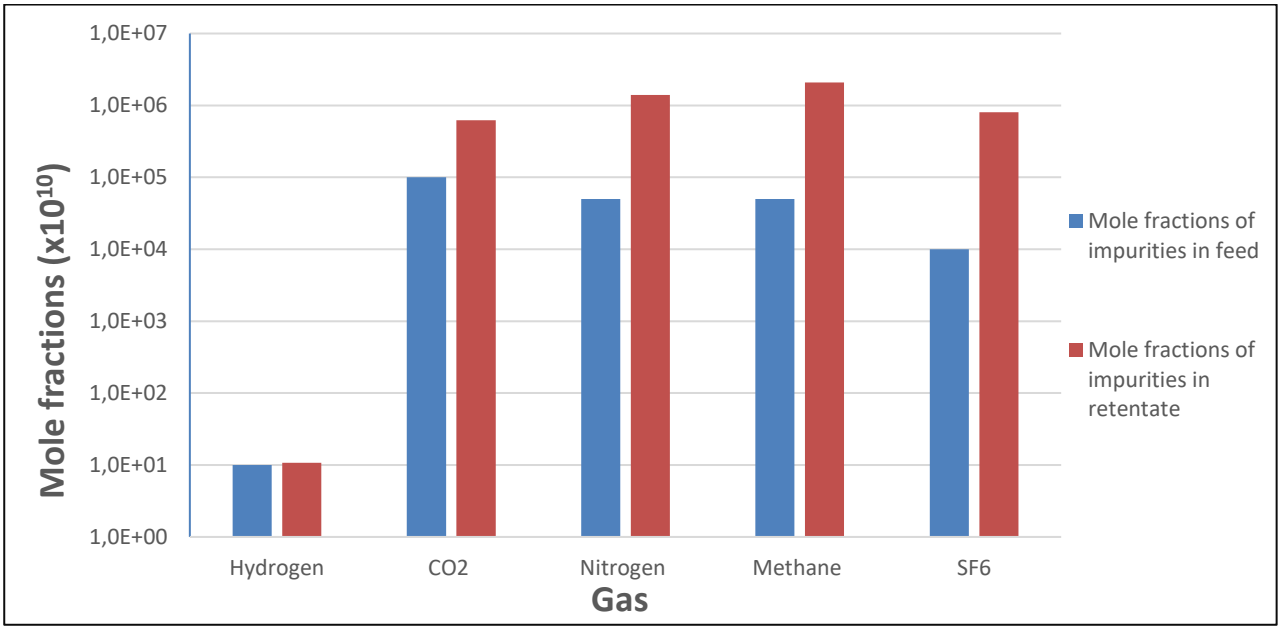

Figure 5-10: Mole fractions of the impurities of the retentate and the feed of design 5

Table 5-13: Design 5 permeate results

Permeate		
Total flow rate	24.5293	**kmol/hr**
Total flow rate	98.2027	**kg/hr**
Permeate composition	**Concentration**	**Flow rate (kmol/hr)**
Helium	99.9984%	24.5289
Hydrogen	0.9990 ppb	2.4504×10^{-8}
CO2	9.4475 ppm	2.3174×10^{-4}
Nitrogen	3.7971 ppm	9.3140×10^{-5}
Methane	3.1835 ppm	7.8089×10^{-5}
F6S	2.2163 ppb	5.4364×10^{-7}
Impurities flow rate	4.0354×10^{-4}	**kmol/hr**
% Impurities in permeate	76.93%	
% Helium recovered	98.21%	

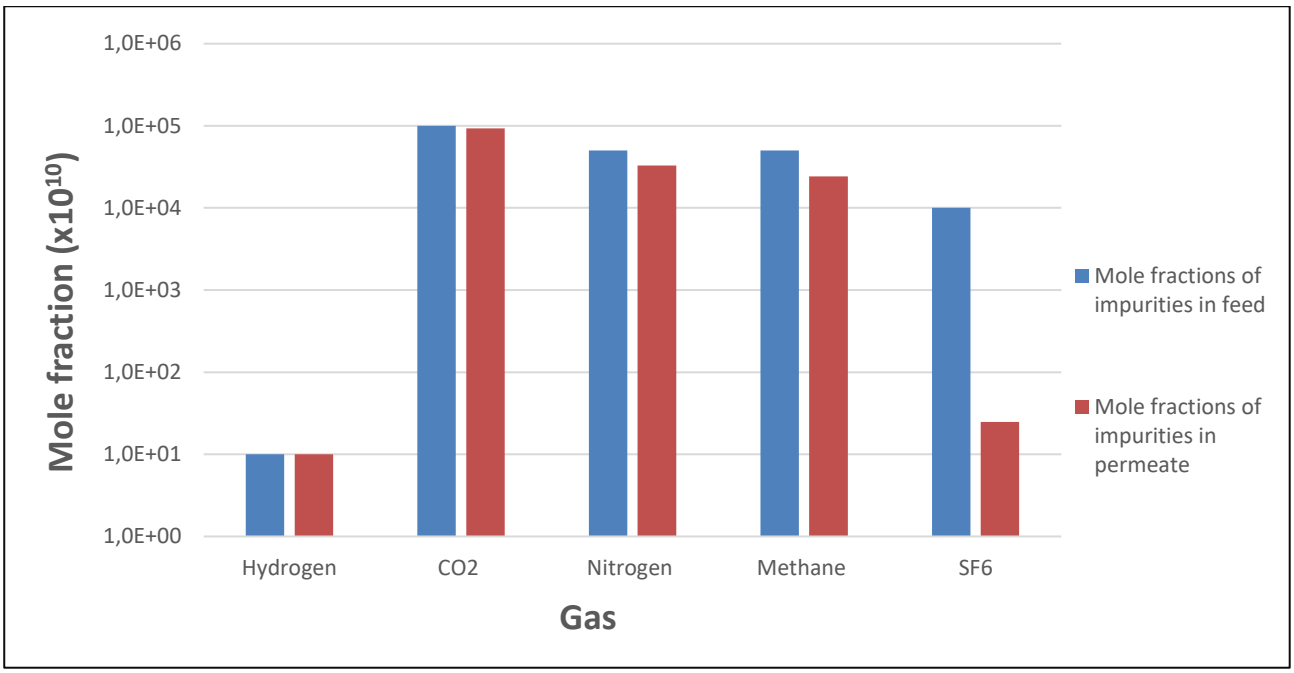

Figure 5-11: Mole fractions of the impurities of the permeate and the feed of design 5

In **Table 5-14** the results for design 1, 4, and 5 are compared. The helium recovery is equal for both design 4 and 5, which shows that the amount of helium recovered is independent of transmembrane pressure. Instead, helium recovery is a function of stage cut and amount of membranes, since design 4 and 5 have the same stage cut and amount of membranes. The removal of impurities is better for design 4 than for both design 1 and 5, showing that the change in transmembrane pressure does have an effect on the separation ability of the membranes. Furthermore, the decrease in total membrane area and the amount of membranes for design 4 compared to design 1 is noteworthy. Because design 5 is not optimised as a complete solution, it will only be used for comparison purposes and is not a valid solution for the AHTR's HPS.

Table 5-14: Comparison of results from designs 1, 4, and 5

Characteristic	Design 1	Design 4	Design 5
Retentate impurity removal	29.34%	33.35%	23.07%
Permeate impurity retention	70.66%	66.65%	76.93%
Total membranes	91	54	54
Total membrane area (m^2)	4345.25	2983.14	3607.75
Helium recovery	98.74%	98.21%	98.21%
Helium lost in retentate	1.26%	1.79%	1.79%
Impurity flow removed (kmol/hr)	1.5197×10^{-4}	1.6697×10^{-4}	1.2088×10^{-4}

5.6: Discussion and comparison of results

In comparing the results of the five designs, as shown in **Table 5-15**, key differences are easily noted in the degree of separation. Design 1 contains the most membranes, but separates the least amount of impurities from the helium, while recovering almost as much helium as design 5. Design 2 and 3, on the other hand, lose more than 10% of the helium to the retentate stream, but they remove more than 50% of the impurities. Design 4 presents similar helium recovery to design 1, but removes more impurities with fewer membranes. Design 5, although it is only meant for comparison, did perform well with the same helium recovery as design 4, but it removes 10% less impurities.

The next important point to take note of, is that the total area of the membranes does not vary proportionally for impurity separation or helium recovery. Helium recovery seems to be much more closely related to stage cut and the setup of the membrane system in terms of the number of rows and columns of membranes in the design. This is definitively shown by design 1 having similar helium recovery to design 4 and 5 despite having 8 more rows, 2 more columns, and 37 more membranes. The transmembrane pressure plays a large role in membrane area too. This is evident due to the fact that design 4 and 5 have the same amount of membranes and a similar helium recovery but vary in area by ~600m^2.

Table 5-15: Comparison of results between the different designs

Property	Design 1	Design 2	Design 3	Design 4	Design 5
No. of membranes	91	60	60	54	54
Area (m^2)	4345.25	4192.19	4685.22	2983.14	3607.75
Helium recovery	98.74%	84.27%	89.43%	98.21%	98.21%
Impurity removal	28.97%	60.64%	47.43%	31.83%	23.07%

In **Figure 5-12** and **Figure 5-13** the mole fractions of the impurities in the different designs' retentate and permeate streams are compared with that of the feed so that the separation can be seen. There are a few very important points to take note of from these comparisons, starting with the fact that the hydrogen (2.89 Å) concentration does not change very much in any stream; it varies between 0.992 ppb and 1.10 ppb. Sulfurhexafluoride (5.5 Å), on the other hand, undergoes a massive change in concentration, from the original 1 ppm, it varies

toward 80 ppm in the retentate streams, and as low as 1.14 ppb in the permeate streams. This major difference in separation is due to the different kinetic diameters of the gases. It can also be seen from the other gases that the separation is performed more efficiently as the kinetic diameter increases; the separation for methane (3.8 Å) is more pronounced than the separation for nitrogen (3.64 Å) or carbon dioxide (3.3 Å).

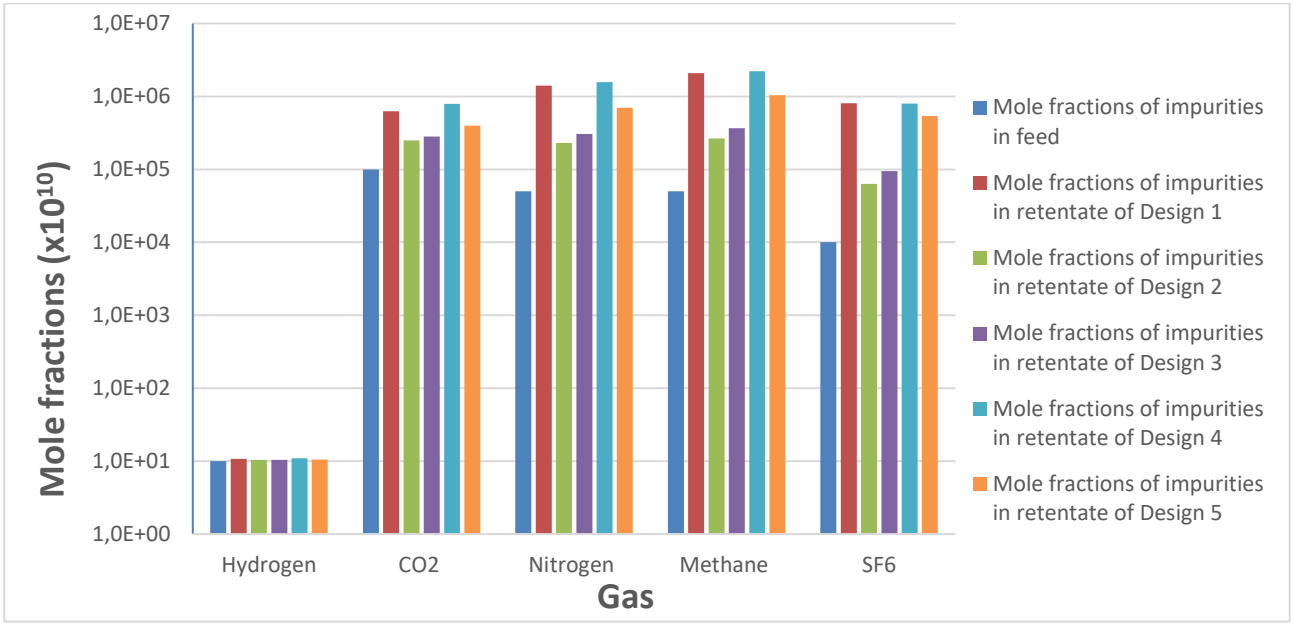

Figure 5-12: Comparison between the mole fractions of the impurities in the retentates and feed of the different designs

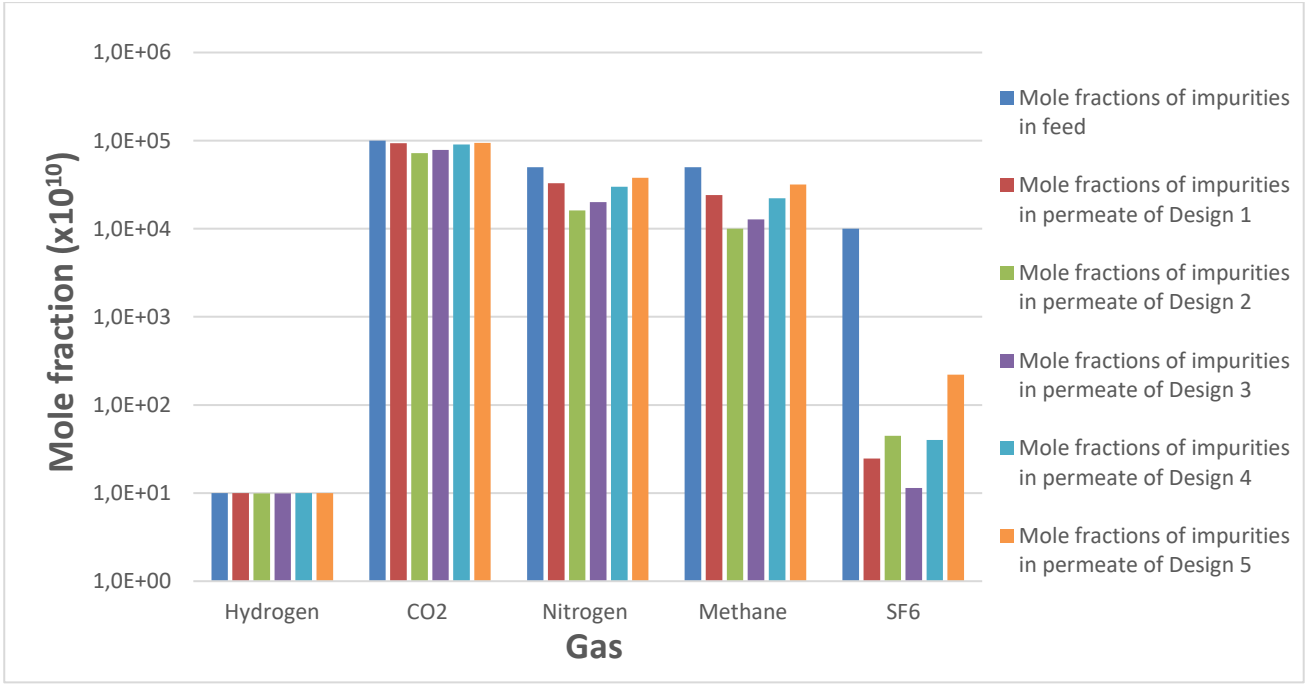

Figure 5-13: Comparison between the mole fractions of the impurities in the permeates and feed of the different designs

The next comparisons are important because they prove that the removal of impurities and the recovery of helium is not a function of area, but rather of membrane setup. This is evident in **Figure 5-14** where the results are plotted as bar graphs for each design, and in **Figure 5-15** where a line is drawn to find a linear relationship for the helium recovery vs. impurities remaining. This relationship is close to linearity, $R^2 = 0.9873$, which points to the possibility of calculating a theoretical helium recovery for 100% impurity removal; this theoretical helium recovery is 66.27%, although this would almost never work.

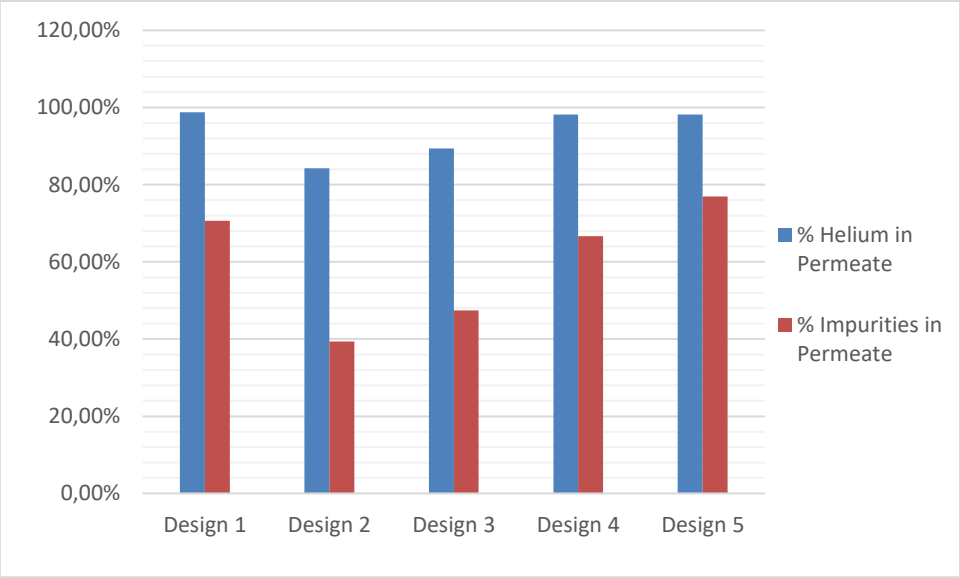

Figure 5-14: Comparison of membrane areas vs. permeate composition

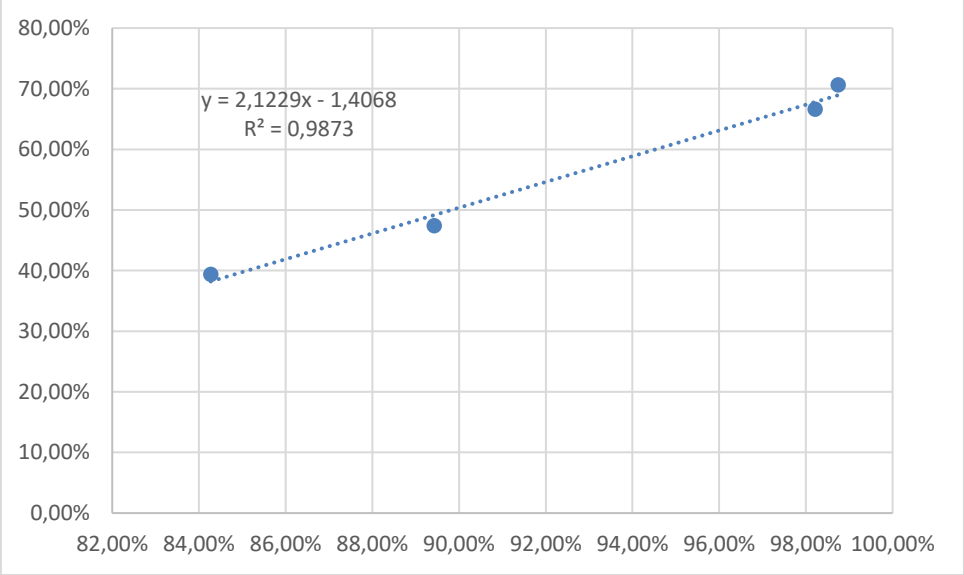

Figure 5-15: Graph of helium recovery vs. impurity retention in different designs

More comparisons are done in **Figure 5-16** to **Figure 5-21** below to illustrate the percentage of each impurity that is in the total impurities leaving the membrane system for each design, as well as the amount of helium lost for each design. These results all clearly point to the membrane system removing changing amounts of the contaminants. This is displayed in the fact that, for example, design 4 has much lower hydrogen removal than design 2, but a much higher removal of methane. This proves that separation is not based solely on the transmembrane pressure nor on stage cut. It is clear from the results for design 2 and 3 that when a larger amount of helium is lost, more hydrogen and carbon dioxide is removed.

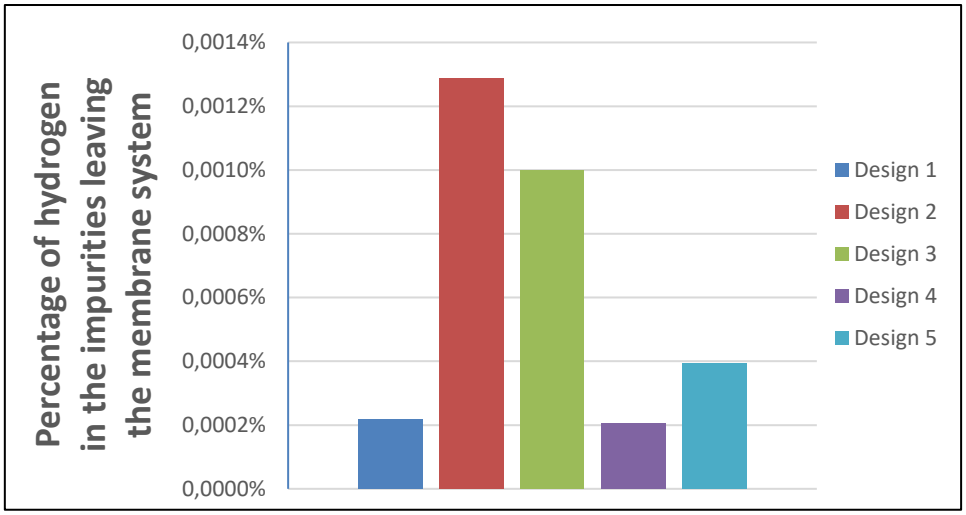

Figure 5-16: Comparison of the percentage of hydrogen in the impurities removed in the different designs

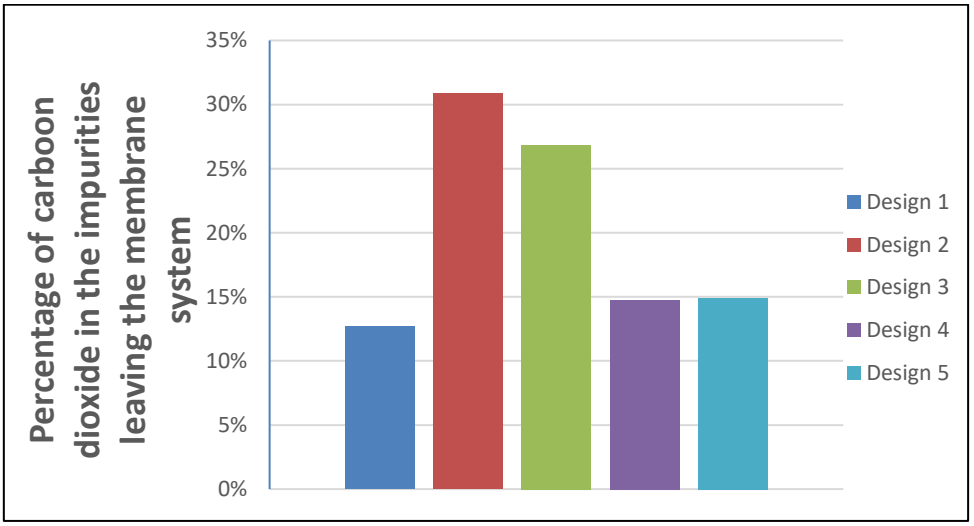

Figure 5-17: Comparison of the percentage of carbon dioxide in the impurities removed in different designs

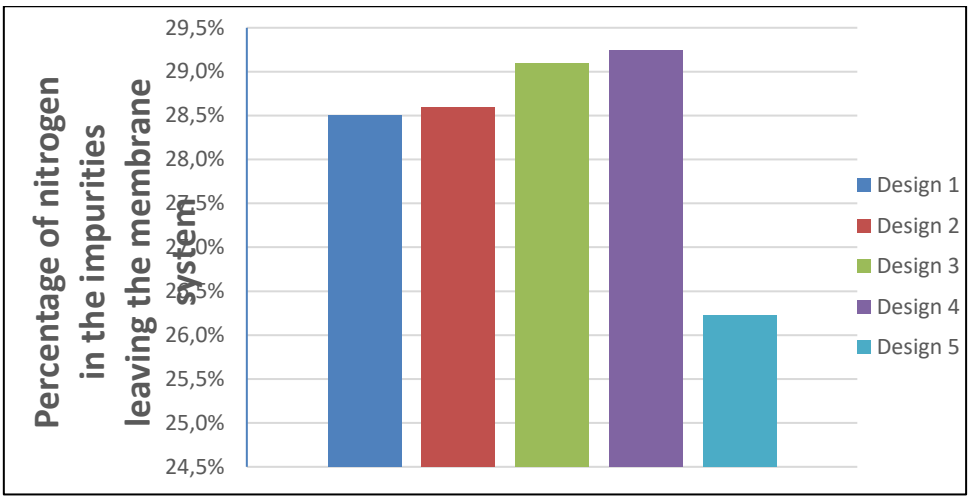

Figure 5-18: Comparison of the percentage of nitrogen in the impurities removed in different designs

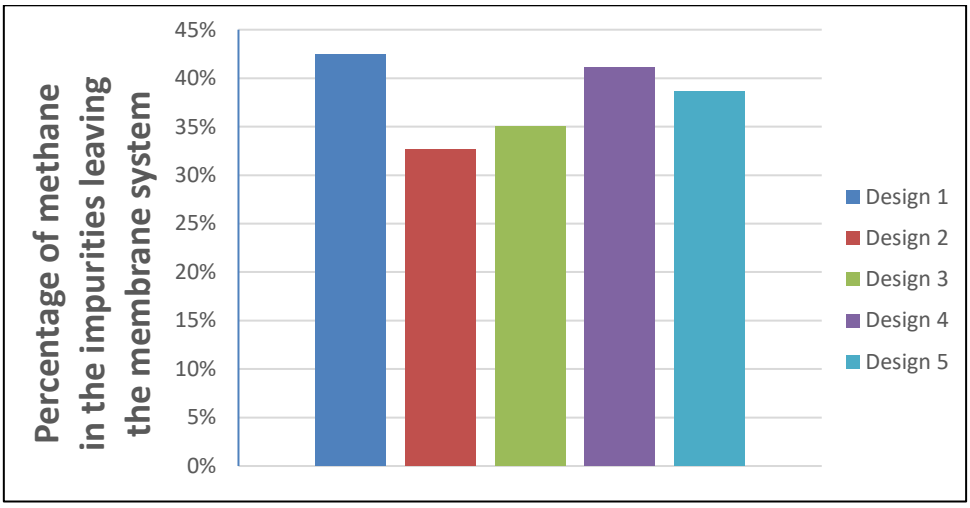

Figure 5-19: Comparison of the percentage of methane in the impurities removed in different designs

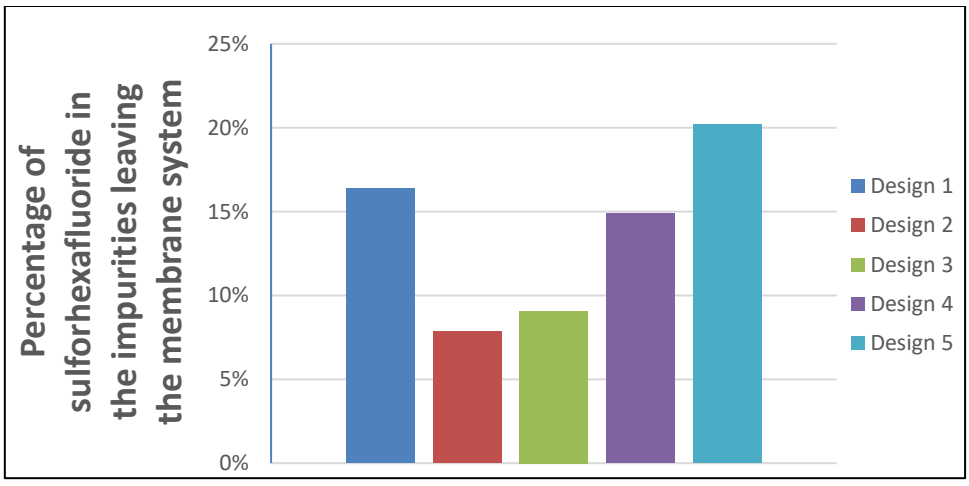

Figure 5-20: Comparison of the percentage of sulfurhexafluoride in the impurities removed in different designs

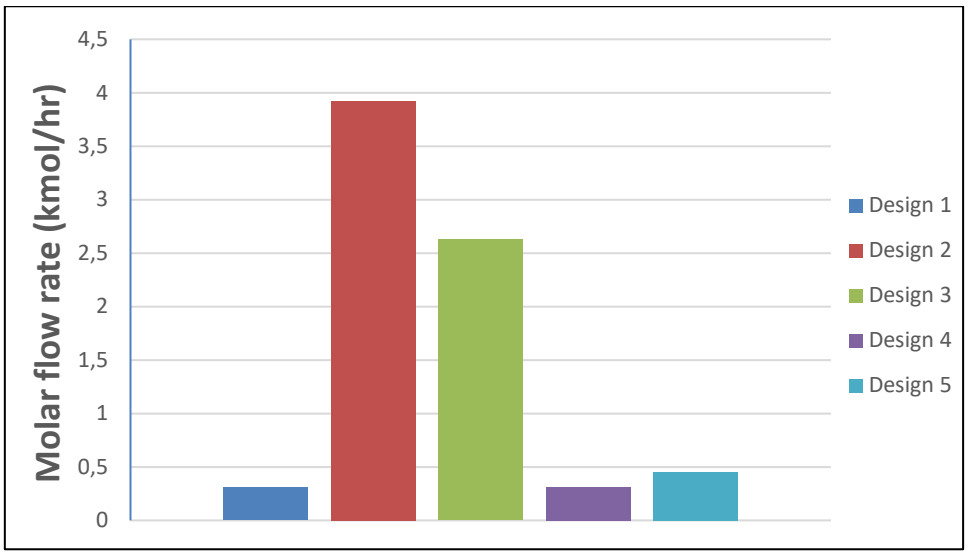

Figure 5-21: Comparison of helium flow rate lost in different designs

Chapter 6: Conclusion and recommendations

The development of these designs have proven the idea that the old helium purification system from the PBMR may be replaced by a passive, compact system that will likely fit inside the power conversion unit of each AHTR plant, as shown above in **Figure 1-2**. This system contains no moving parts and requires minimal maintenance over time; making it a prime candidate to be implemented, not only in the AHTR system, but also in other industrial systems. All information gathered for this work has become part of a larger picture that may lead to an industrially viable method of separating gases. However, problems such as the manufacturability of large enough membranes or radiation damage to the membrane materials persist.

This study has also provided a wide-ranging summary of all the applicable membrane materials and types, as seen in the literature review and various pure gas permeance tables shown as **Table A-8** to **Table A-13** in Appendix A. The Memcal software provided by Chen *et al*. (2016) was qualified for use by simulations and comparisons with the work of other authors and provided meaningful and accurate results for the design simulations. The largest membrane system area was ~4700 m^2 and the smallest was ~3000m^2.

The membrane units would ideally be arranged in a manner that would allow all inlet and outlet pipes to be on the same side on the ends of a column of membrane units, a rough illustration is shown in **Figure 6-1**. This arrangement would be to ease any maintenance or replacement of a specific membrane unit, but the specific dimensions of such a system can only be calculated once testing membrane units have been purchased.

This study shows that the membrane configuration and the order in which the membranes are arranged changes the purity that is generated at the end. Additionally, it is self-evident in **Figure 5-16** to **Figure 5-21** that each contaminant is not removed at the same rate as the designs change. Design 4 performed “more efficiently,” meaning that it recovered similar amounts of helium to design 1 but used fewer membranes and surface area; this is due to the increased transmembrane pressure. It is, however, worth mentioning that design 2 and 3, which lost more helium than the others, removed the hydrogen and carbon dioxide to a greater extent when compared to the total amount of impurities removed for these designs.

All the designs have proven that a membrane system could be designed to satisfy the necessary purification of helium for the AHTR, some more efficiently than others as seen in **Table 6-1.** A final design will be done once the AHTR project has finished empirical testing of the fuel pellets and reactor system, such that the species of contaminants can be measured and designed for. Another possibility exists, where two differently designed HPS could be designed for the AHTR; the first would fit inside the PCU and would be the main HPS, while a secondary system situated outside the reactor building could purify the helium from any contaminants so that the helium may be sent back to the primary system. This dual HPS design would assist in recovering helium leaked into the containment building, as well as any helium that would need purification after the start-up of the reactor.

Table 6-1: Table of required purities in the AHTR system compared to the results of the permeate streams for the different designs (ppm)

Type of impurity	Carbon Dioxide (CO_2)	Hydrogen (H_2)	Nitrogen (N_2)	Methane (CH_4)	Sulfurheaxfluoride (SF_6)
Required outlet for the AHTR system	< 10	<0.001	< 5	< 5	< 1
Design 1	9.33	9.99×10^{-4}	3.28	2.42	0.0025
Design 2	7.19	9.92×10^{-4}	1.61	1.00	0.0045
Design 3	7.86	9.95×10^{-4}	2.00	1.28	0.0011
Design 4	9.03	9.98×10^{-4}	3.01	2.21	0.0040
Design 5	9.45	9.99×10^{-4}	3.80	3.18	0.0222

Further recommendations would be the testing of a membrane unit with single gases and mixtures of gases, to ascertain the specific permeances of the gases in the membrane material. These tests will help to improve the design by removing the assumption that single gas permeances are accurate for mixtures. Research concerning shape, size, volume, cost, strength, and reproducibility of membrane surface will also be required for a final design of an HPS that will fit inside the AHTR PCU.

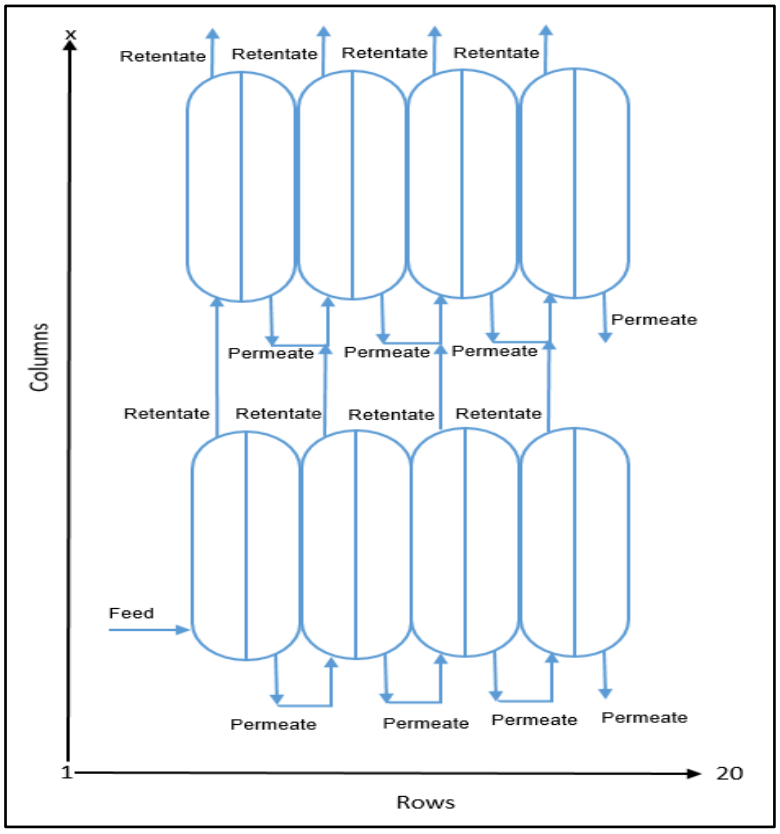

Figure 6-1: Schematic drawing of membrane system

A final research process flow diagram is also included below as **Figure 6-2** to show the final research process. Three other membrane simulation processes were tested before the Memcal system was decided upon, the first being the model given by Mourgues & Sanchez (1) (2012), the second being the simulation software created by Chowdhury (2) (2011), and the last being the simulation method coded by Rodrigues (3) (2009). A preliminary Microsoft Excel attempt at solving the equations to calculate permeance and required membrane area was made, but this was found to be a fool's errand and abandoned before too much time was wasted. It is important to note, that unlike Chowdhury or Rodrigues, the goal for this thesis was not to create a new simulation method for gas separation membranes but to design a system that could separate impurities from helium to the required purity for the AHTR primary system.

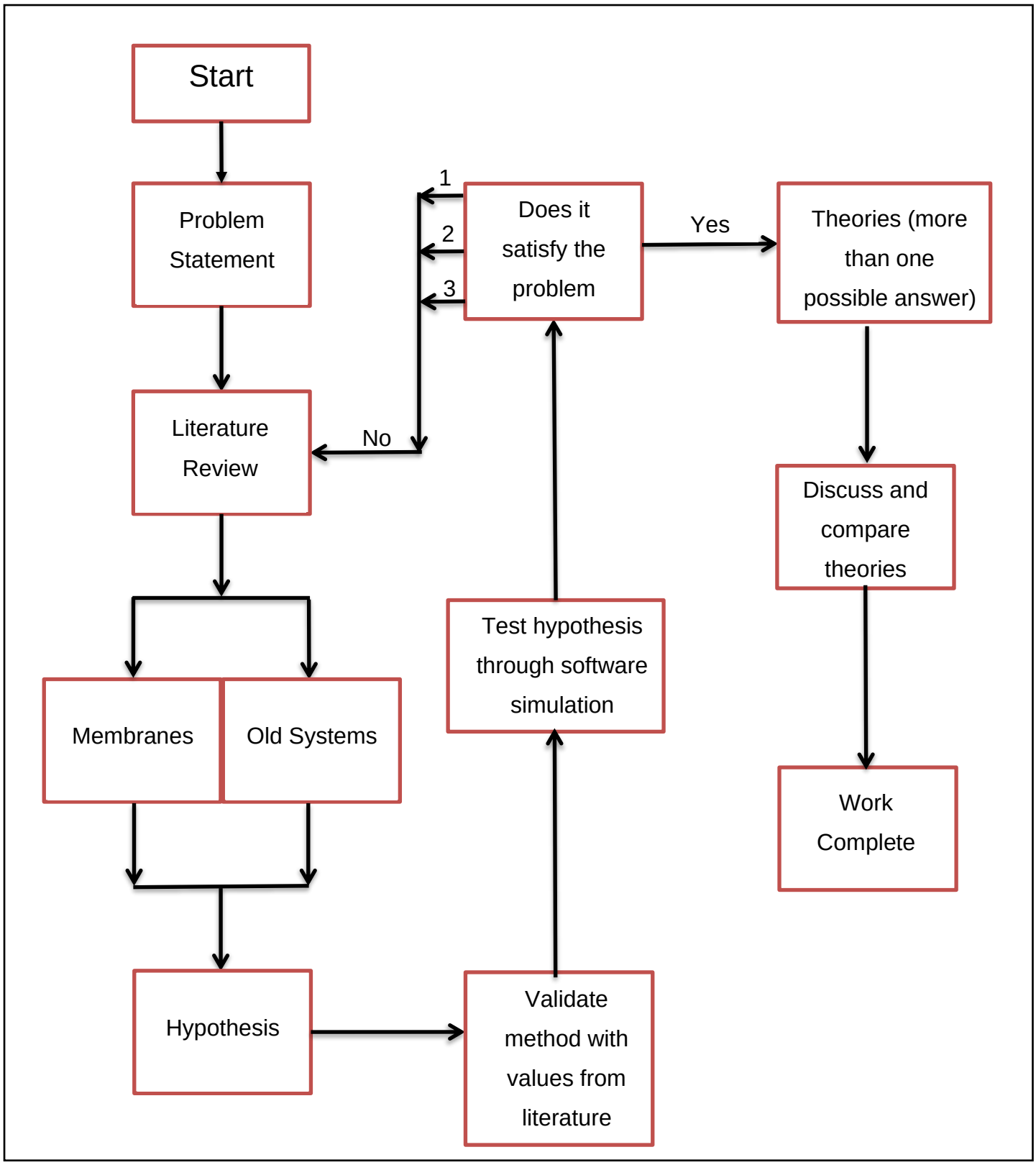

Figure 6-2: Final research process flow diagram

References

Ahmad, F., Lau, K.K., Lock, S.S.M., Rafiq, S., Khan, A.U., Lee, M. 2015. Hollow fiber membrane model for gas separation: Process simulation, experimental validation and module characteristics study. Journal of industrial and engineering chemistry, 21: 1246 – 1257.

Ahsan, M., Sweeney, O.M., Hussain, A. 2017. Development of user-defined extension for the simulation of membrane process in Aspen Hysys. Sigma journal of engineering and natural sciences, 35: 35-45.

Baker, R.W. 2008. Vapor and gas separation by membranes. (*In* Li, N.N., Fane, A.G., Ho, W.S.W., & Matsuura, T., *ed.* Advanced membrane technology and applications. Hoboken, NJ: John Wiley & Sons. p. 559-580).

Baker, R.W. 2012. Membrane technology and applications. 3rd ed. Chichester: John Wiley & Sons.

Barboiu, C., Mourgues, A., Sala, B., Julbe, A., Sanchez, J., de Perthuis, S., & Hittner, D. 2006. Ultra-microporous silica membranes for He purification. Desalination, 200: 89-91.

Barboiu, C., Sala, B., Bec, S., Pavan, S., Petit, E., Colomban, Ph., Sanchez, J., de Perthuis, S., & Hittner, D. 2009. Structural and mechanical characterizations of microporous silica-boron membranes for gas separation. Journal of Membrane Science, 326: 514-525.

Beaver, R.P. 1998. Method of producing porous hollow silica-rich fibers. US Patent 4,778,499.

Behling, R.D., Ohlrogge, K., Peinemann, K.V., & Kyburz, E. 1989. The separation of hydrocarbons from waste vapor streams. In Membrane Separations in Chemical Engineering, AIChE Symposium Series Number 272, Vol. 85 (eds A.E. Fouda, J.D. Hazlett, T. Matsuura, and J. Johnson). AIChE, New York: 68.

Berka, J., Hlincik, T., Viden, I., Hudsky, T., & Vit, J. 2015. The design and utilization of a high-temperature helium loop and other facilities for the study of advanced gas-cooled reactors in the Czech Republic. Progress in Nuclear Energy, 85: 156-163.

Boffa, V., Blank, D.H.A., & ten Elshof, J.E. 2008. Hydrothermal stability of microporous silica and niobia-silica membranes. Journal of membrane science, 319: 256-263.

Brands, K., Uhlmann, D., Smart, S., Bram, M., & Diniz da Costa, J.C. 2010. Long-term flue gas exposure effects of silica membranes on porous steel structure. Journal of membrane science, 359: 110-114.

Castricum, H.L., Kreiter, R., van Veen, H.M., Blank, D.H.A., Vente, J.F., & ten Elshof, J.E. 2008. High-performance hybrid pervaporation membranes with superior hydrothermal and acid stability. Journal of membrane science, 324: 111-118.

Castricum, H.L., Qureshi, H.F., Nijmeijer, A., & Winnubst, L. 2015. Hybrid silica membranes with enhanced hydrogen and CO_2 separation properties. Journal of membrane science, 488: 121-128.

Chen, B., Jiang, X., Xiao, W., Dong, Y., Hamouti, I.E., He, G. 2016. Dual-membrane natural gas pretreatment process as CO_2 source for enhanced gas recovery with synergy hydrocarbon recovery. Journal of natural gas science and engineering, 34: 563 – 574.

Chowdhury, M.H.M. 2011. Simulation, design and optimization of membrane gas separation, chemical absorption and hybrid processes for CO_2 capture. Waterloo: University of Waterloo. (Thesis – PhD.).

Coker, D.T., Freeman, B.D., Fleming, G.K. 1998. Modeling multicomponent gas separation using hollow-fiber membrane contactors. AIChE Journal, 44: 1289 - 1302.

Darmawan, A., Motuzas, J., Smart, S., Julbe, A., & Diniz da Costa, J.C. 2015. Binary iron cobalt oxide silica membrane for gas separation. Journal of membrane science, 474: 32-38.

Favvas, E.P., Heliopoulos, N.S., Papageorgiou, S.K., Mitropoulos, A.C., Kapantaidakis, G.C., & Kanellopoulos, N.K. 2015. Helium and hydrogen selective carbon hollow fiber membranes: the effect of pyrolysis isothermal time. Separation and purification technology, 142: 176-181.

Gao, X., Diniz da Costa, J.C., & Bhatia, S.K. 2013. The transport of gases in supported mesoporous silica membrane. Journal of membrane science, 438: 90-104.

Gavalas, G.R., Megiris, C.E., & Nam, S.W. 1989. Deposition of H_2 permselective SiO_2-films. Chemical Engineering Science, 44: 1829–1835.

Kanezasi, M., Sasaki, T., Tawarayama, H., Nagasawa, H., Yoshioka, T., Ito, K., & Tsuru, T. 2014. Experimental and theoretical study on small gas permeation properties through

amorphous silica membranes fabricated at different temperatures. The journal of physical chemistry, 118: 20323-20331.

Kase, Y. 2008. Gas separation by polyimide membranes. (*In* Li, N.N., Fane, A.G., Ho, W.S.W., & Matsuura, T., *ed.* Advanced membrane technology and applications. Hoboken, NJ: John Wiley & Sons. p. 581-598).

Klein, L.C. & Gallagher, D. 1988. Pore structure of sol–gel silica membrane. Journal of Membrane Science, 39: 213–220.

Kondo, M., Komori, M., Kita, H., & Okamoto, K. 1997. Tubular-type pervaporation module with zeolite NaA membrane. Journal of membrane science, 133: 133-141.

Lee, H.R., Shibata, T., Kanezashi, M., Mizumo, T., Ohshita, J., & Tsuru, T. 2011. Pore-size-controlled silica membranes with disiloxane alkoxides for gas separation. Journal of membrane science, 383: 152-158.

Morgues, A. & Sanchez, J. 2012. Theoretical considerations about a membrane process for helium purification in multichannel monoliths for high temperature nuclear reactors. Nuclear Engineering and Design, 247: 88-97.

Nitodas, S.F., Favvas, E.P., Romanos, G.E., Papadopoulou, M.A., Mitropoulos, A.C., & Kanellopoulos, N.K. 2008. Development and characterization of silica-based membranes for hydrogen separation. Journal of porous materials, 15: 551-557.

Pan, C.Y. & Habgood, H.W. 1974. An analysis of the single-stage gaseous permeation process. Journal of industrial & engineering chemistry, 13: 323 - 331.

Park, H.B. & Lee, Y.M. 2008. Polymeric membrane materials and potential use in gas separation. (*In* Li, N.N., Fane, A.G., Ho, W.S.W., & Matsuura, T., *ed.* Advanced membrane technology and applications. Hoboken, NJ: John Wiley & Sons. p. 633-670).

PBMR Pty. Ltd. 2010. PBMR helium inventory control system development specification.

Qureshi, H.F., Nijmeijer, A., & Winnubst, L. 2013. Influence of sol-gel process parameters on the micro-structure and performance of hybrid silica membranes. Journal of membrane science, 446: 19-25.

Rodrigues, D.F. 2009. Model development of a membrane gas permeation unit for the separation of Hydrogen and Carbon Dioxide. Lisbon: Technical University of Lisbon. (Thesis – M.).

Sakaba, N., Hamamoto, S., & Takeda, Y. 2010. Helium Chemistry for Very High Temperature Reactors. Journal of Nuclear Science and Technology, 47: 269-277.

Steel, K.M. & Koros, W.J. 2003. Investigation of porosity of carbon materials and related effects on gas separation properties. Carbon, 41: 253-266.

Vendanges, V. & Colomban, P.H. 1996. How to tailor the porous structure of alumina and aluminosilicate gels and glasses. Journal of Material Research, 11: 518–528.

Williams, P.J. & Koros, W.J. 2008. Gas separation by carbon membranes. (*In* Li, N.N., Fane, A.G., Ho, W.S.W., & Matsuura, T., *ed.* Advanced membrane technology and applications. Hoboken, NJ: John Wiley & Sons. p. 599-632).

Yao, M.S., Wang, Z.Y., Liu, X.D., & He, J.L. 2002. The helium purification system of the HTR-10. Nuclear Engineering and Design, 218: 163-167.

Yu, L., Kanezashi, M., Nagasawa, H., & Tsuru, T. 2017. Fabrication and CO_2 permeation properties of amine-silica membranes using a variety of amine types. Journal of membrane science, 541: 447-456.

Appendix A

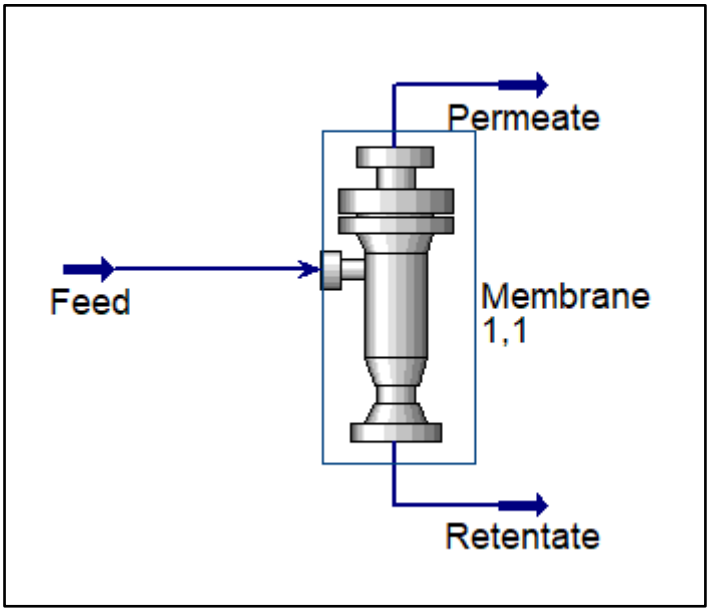

Figure A-1: Single membrane module appearance in Aspen Hysys

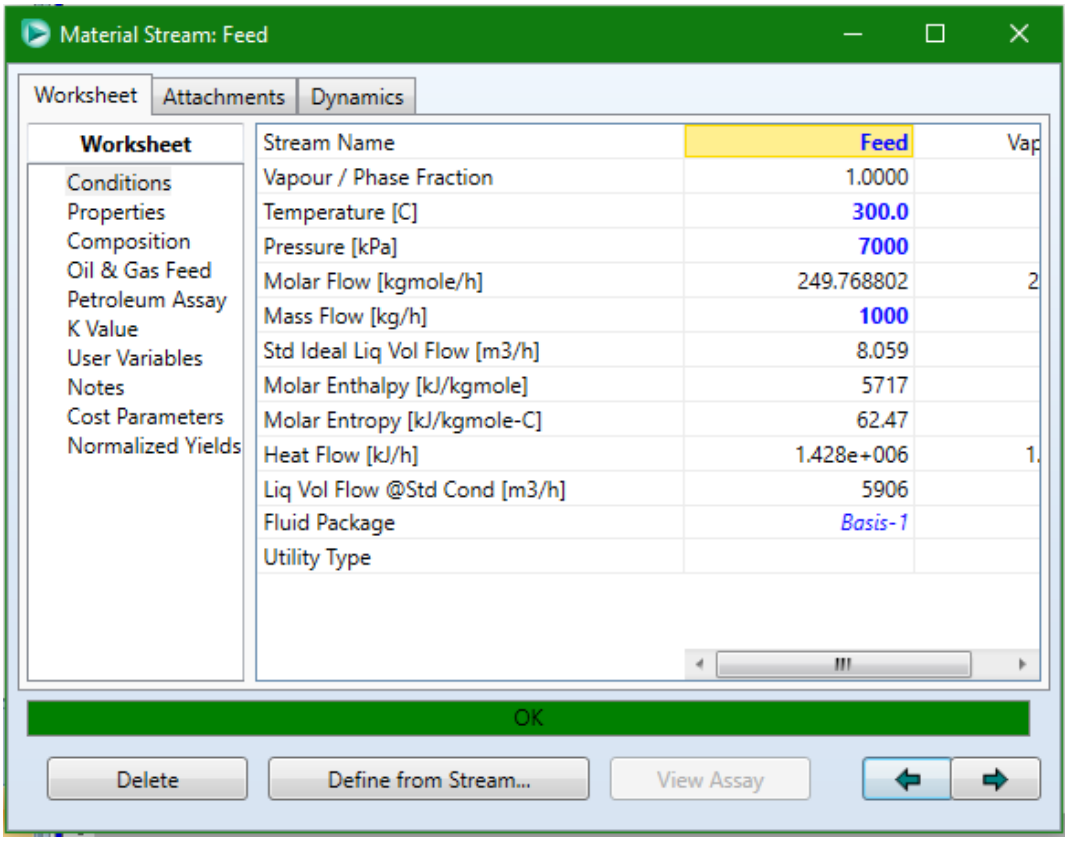

Figure A-2: Feed stream conditions for each design

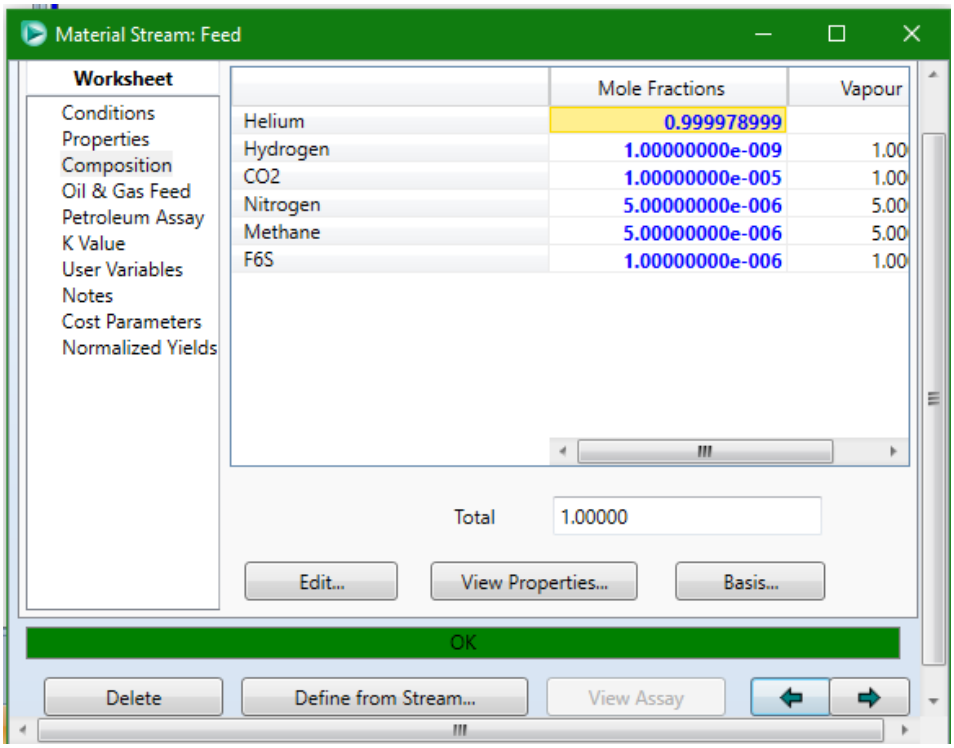

Figure A-3: Feed stream composition for all the designs

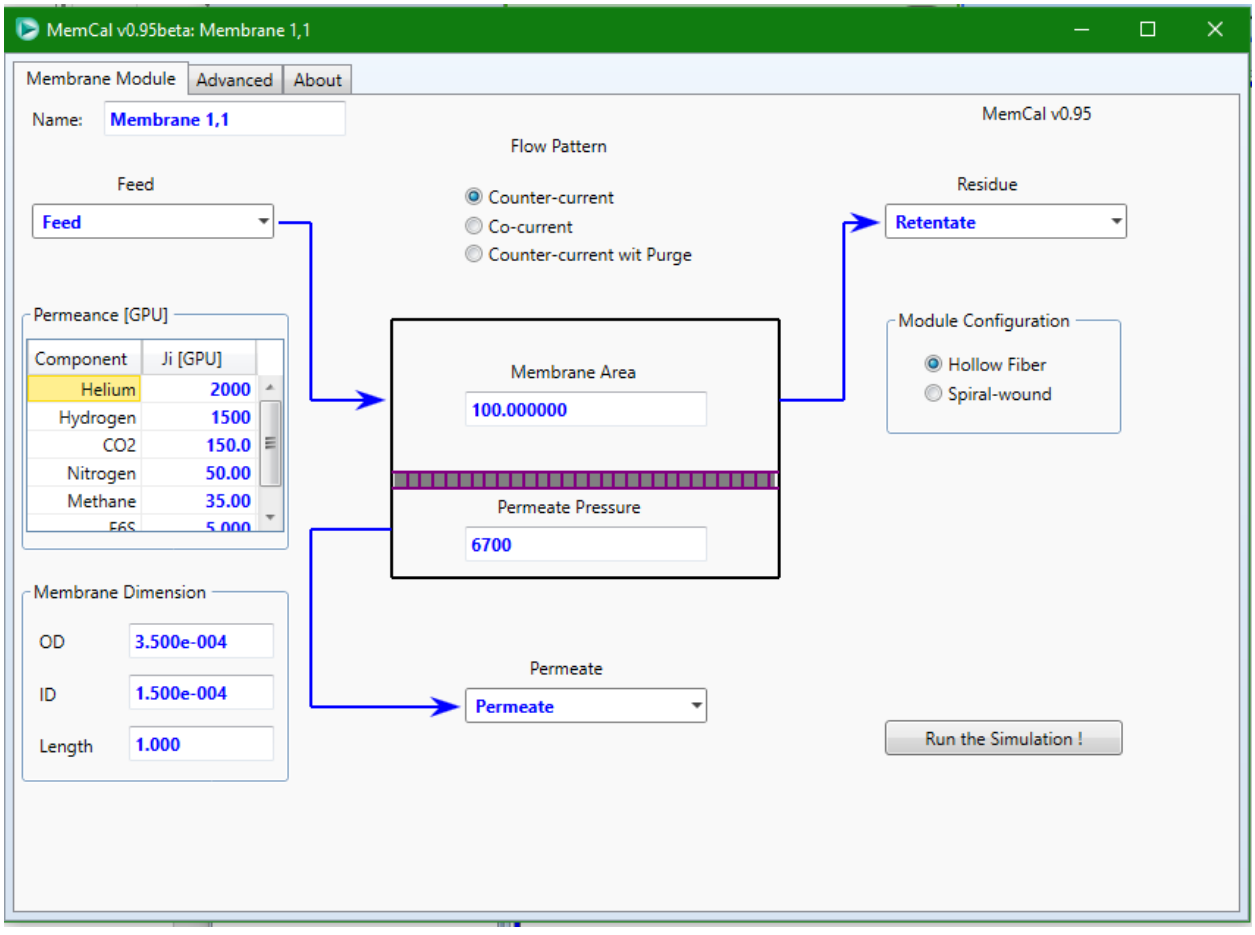

Figure A-4: Example of the membrane configuration for the designs

Sada *et al.* (1992) empirical data qualification test

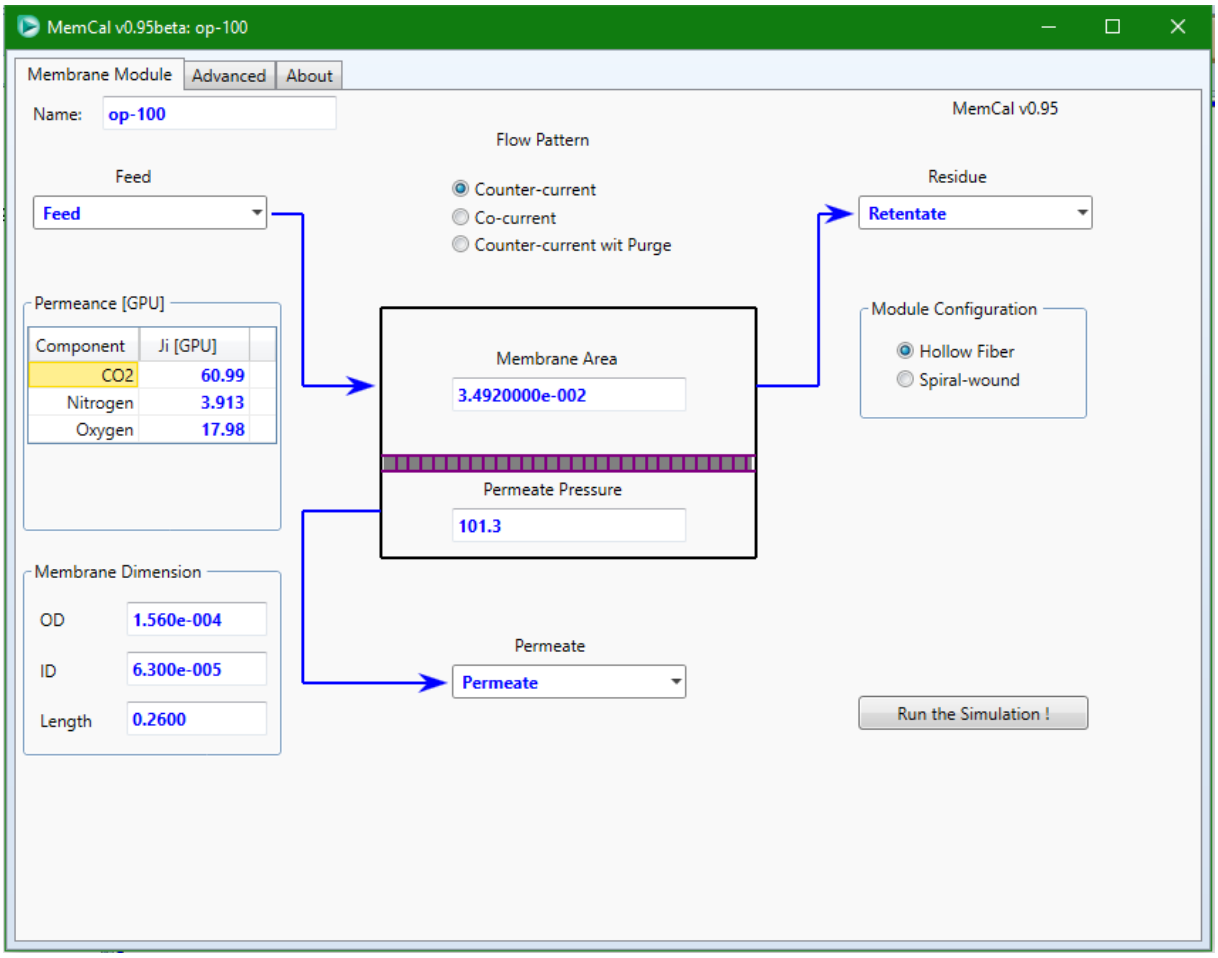

Figure A-5: Sada *et al.* (1992) qualification test membrane configuration

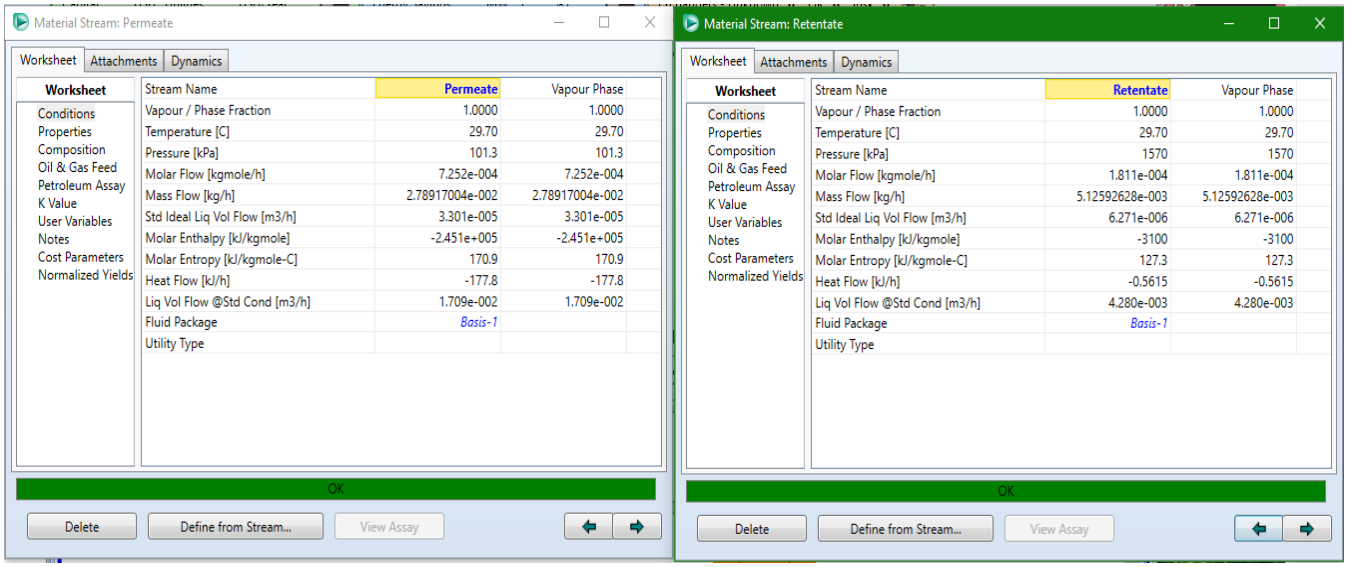

Figure A-6: Sada *et al.* (1992) qualification test permeate and retentate flows

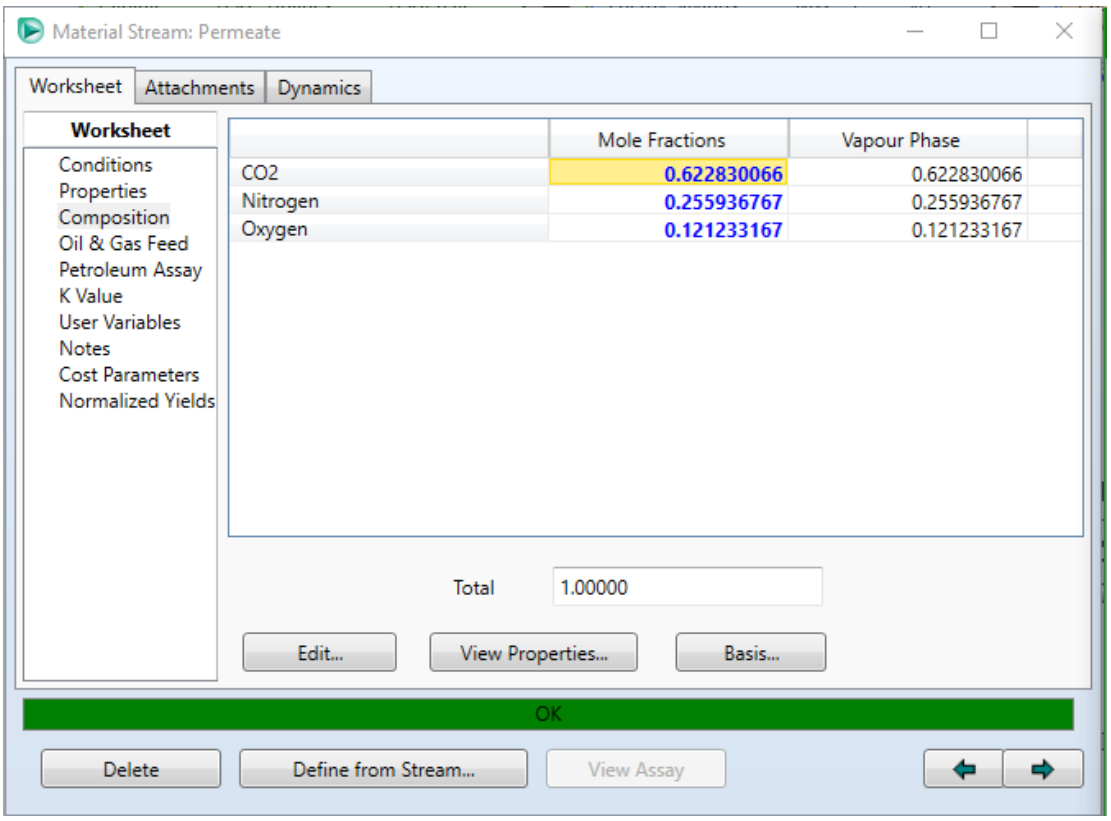

Figure A-7: Sada *et al.* (1992) qualification test permeate composition

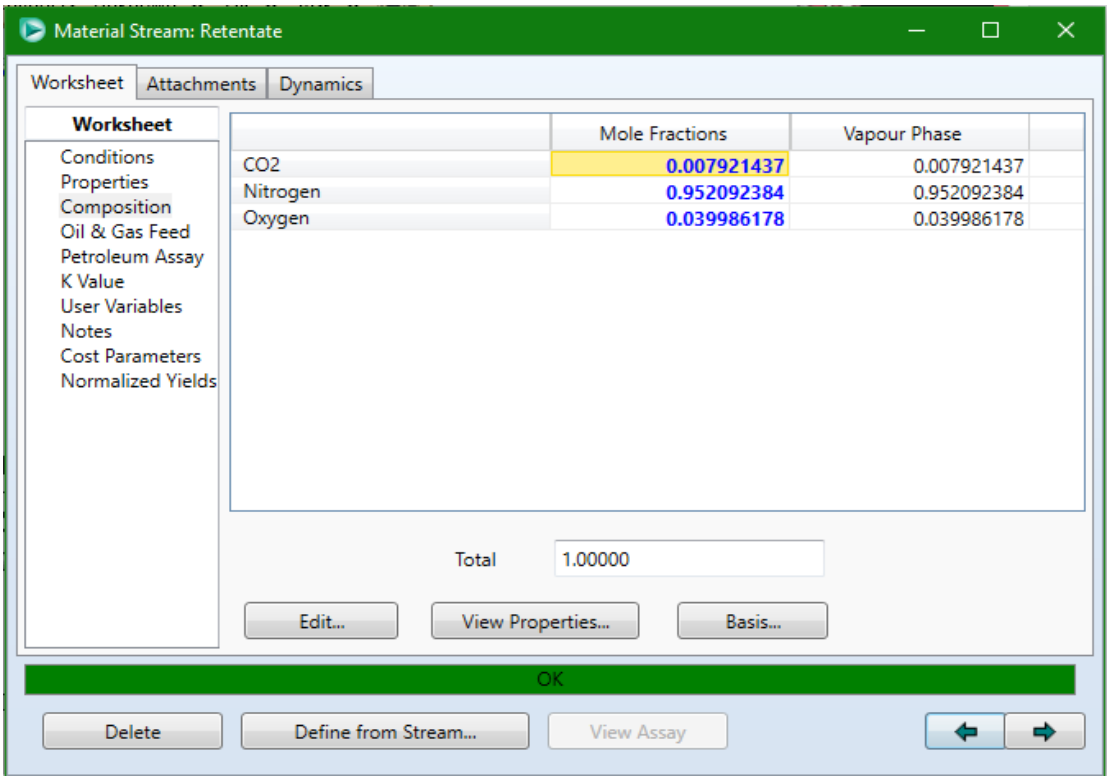

Figure A-8: Sada *et al*. (1992) qualification test retentate composition

Table A-1: Mole fractions for Sada *et al*. (1992) qualification test mass balance

Gas	Mole fraction in feed	Mole fraction in retentate	Mole fraction in permeate	Source
CO_2	5.00E-01	3.67E-02	6.20E-01	Sada *et al.*
O_2	1.05E-01	4.71E-02	1.20E-01	Sada *et al.*
N_2	3.95E-01	9.55E-01	2.50E-01	Sada *et al.*
CO_2	5.00E-01	1.41E-02	6.23E-01	Memcal
O_2	1.05E-01	4.09E-02	1.21E-01	Memcal
N_2	3.95E-01	9.45E-01	2.56E-01	Memcal

Table A-2: Mass balance for Sada *et al*. (1992) qualification test

Gas	Molar flow rate in feed (mol/s)	Molar flow rate in retentate (mol/s)	Molar flow rate in permeate (mol/s)	Source
CO_2	1.26E-04	1.90E-06	3.21E-05	Sada *et al.*
O_2	2.64E-05	2.44E-06	3.02E-05	Sada *et al.*
N_2	9.95E-05	4.95E-05	6.30E-05	Sada *et al.*
Total	2.52E-04	5.18E-05	2.00E-04	Sada *et al.*
CO_2	1.26E-04	7.17E-07	1.25E-04	Memcal
O_2	2.64E-05	2.08E-06	2.44E-05	Memcal
N_2	9.95E-05	4.80E-05	5.14E-05	Memcal
Total	2.52E-04	5.08E-05	2.01E-04	Memcal

Chowdhury (2011) first membrane setup qualification test

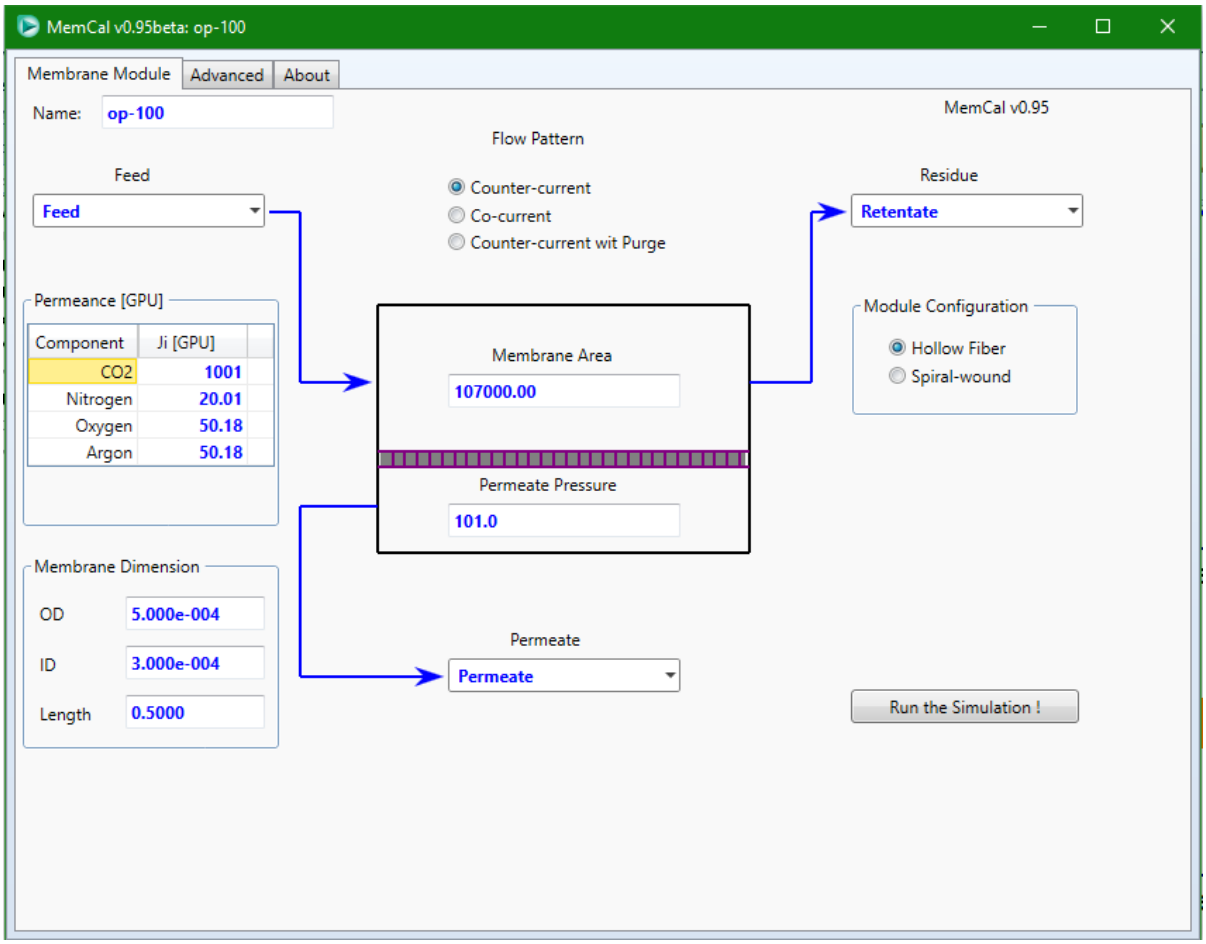

Figure A-9: Chowdhury (2011) first membrane setup qualification test membrane configuration

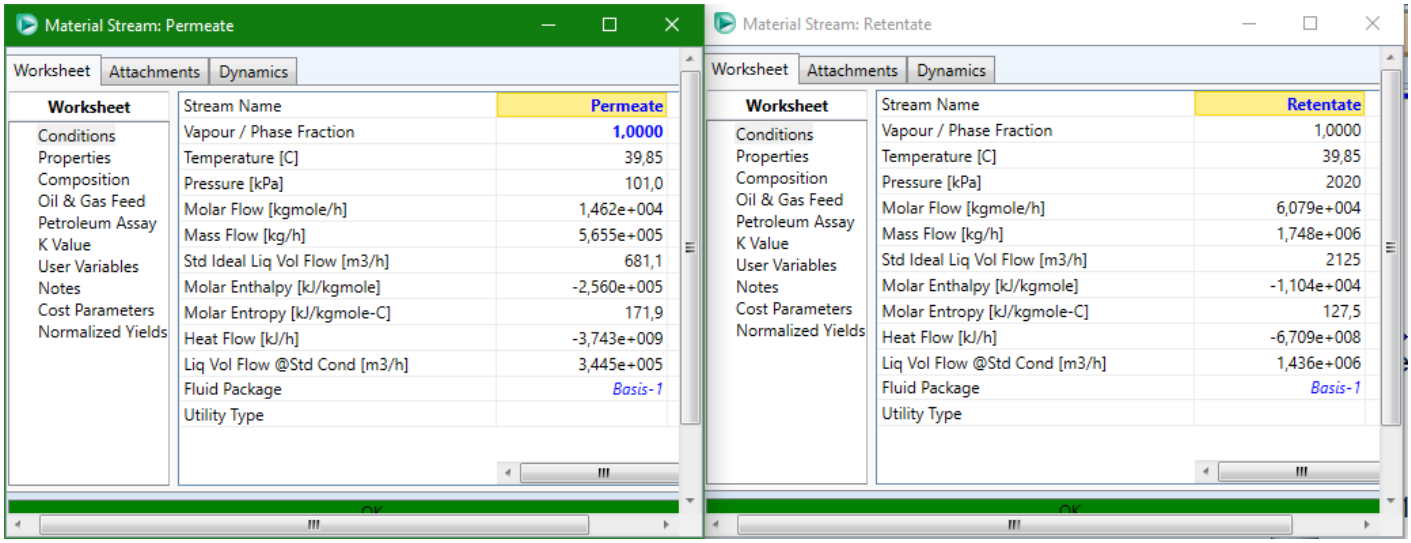

Figure A-10: Chowdhury (2011) first membrane setup qualification test permeate and retentate flow

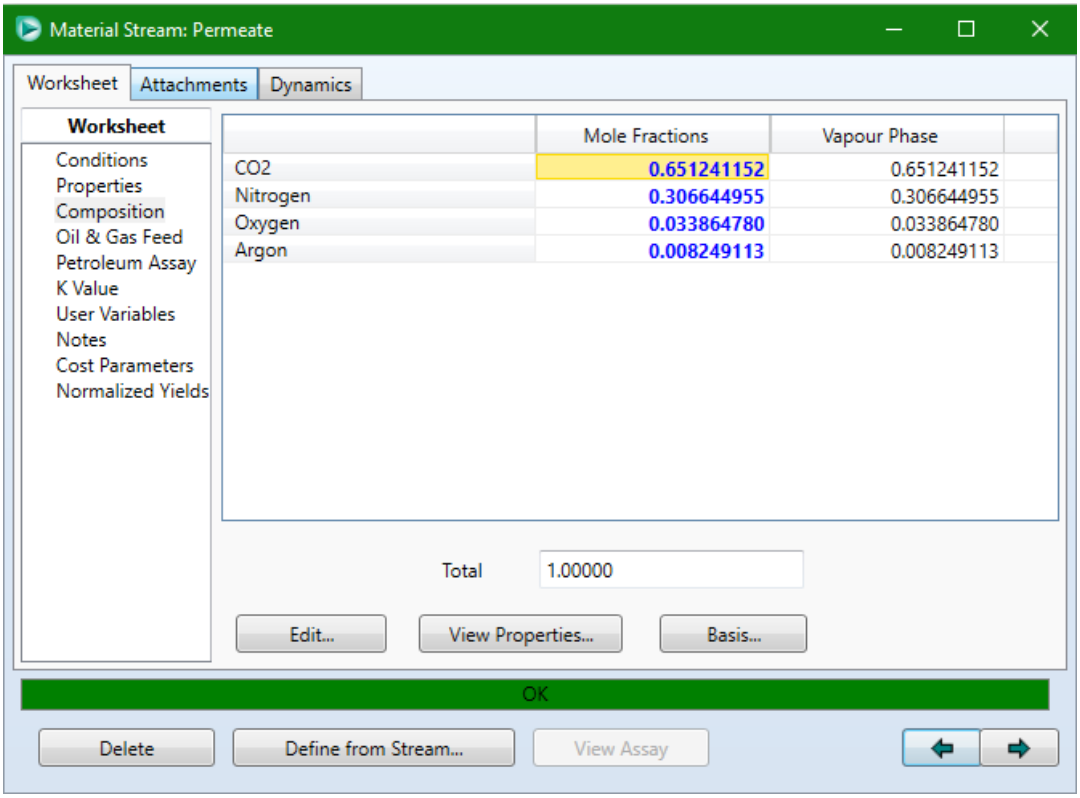

Figure A-11: Chowdhury (2011) first membrane setup qualification test permeate composition

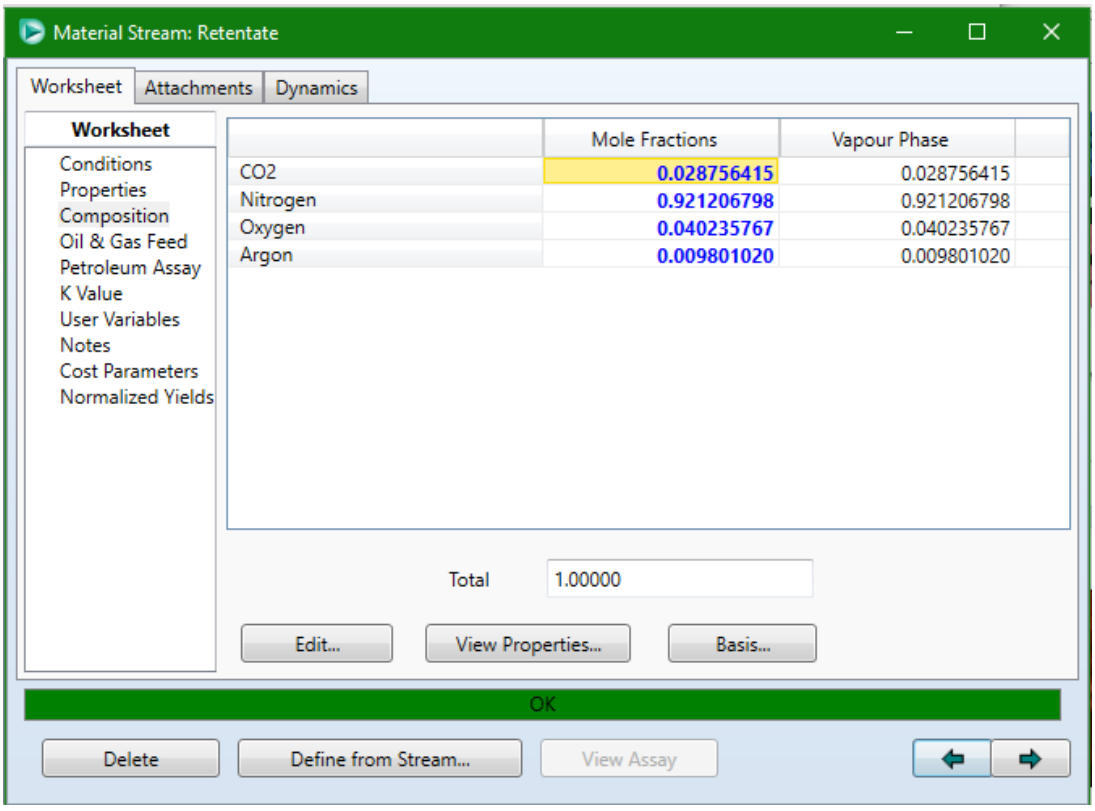

Figure A-12: Chowdhury (2011) first membrane setup qualification test retentate composition

Table A-3: Mole fractions for the Chowdhury (2011) setup 1 qualification test mass balance

Gas	Mole fractions in feed	Mole fractions in retentate	Mole fractions in permeate	Source
CO_2	1.495E-01	6.530E-01	2.773E-02	Chowdhury 1
N_2	8.020E-01	3.047E-01	9.223E-01	Chowdhury 1
O_2	3.900E-02	3.400E-02	4.021E-02	Chowdhury 1
Ar	9.500E-03	8.400E-03	9.766E-03	Chowdhury 1
CO_2	1.495E-01	6.512E-01	2.876E-02	Memcal
N_2	8.020E-01	3.066E-01	9.212E-01	Memcal
O_2	3.900E-02	3.386E-02	4.024E-02	Memcal
Ar	9.500E-03	8.249E-03	9.801E-03	Memcal

Table A-4: Mass balance for Chowdhury (2011) setup 1 qualification test

Gas	Molar flow rate in feed (kmol/s)	Molar flow rate in retentate (kmol/s)	Molar flow rate in permeate (kmol/s)	Source
CO_2	3.132E+00	2.664E+00	4.678E-01	Chowdhury 1
N_2	1.680E+01	1.243E+00	1.556E+01	Chowdhury 1
O_2	8.171E-01	1.387E-01	6.783E-01	Chowdhury 1
Ar	1.990E-01	3.427E-02	1.648E-01	Chowdhury 1
Total	20.95	4.08	1.687E+01	Chowdhury 1
CO_2	3.132E+00	2.646E+00	4.856E-01	Memcal
N_2	1.680E+01	1.246E+00	1.556E+01	Memcal
O_2	8.171E-01	1.376E-01	6.794E-01	Memcal
Ar	1.990E-01	3.351E-02	1.655E-01	Memcal
Total	2.095E+01	4.062E+00	1.689E+01	Memcal

Chowdhury (2011) qualification test of second membrane setup

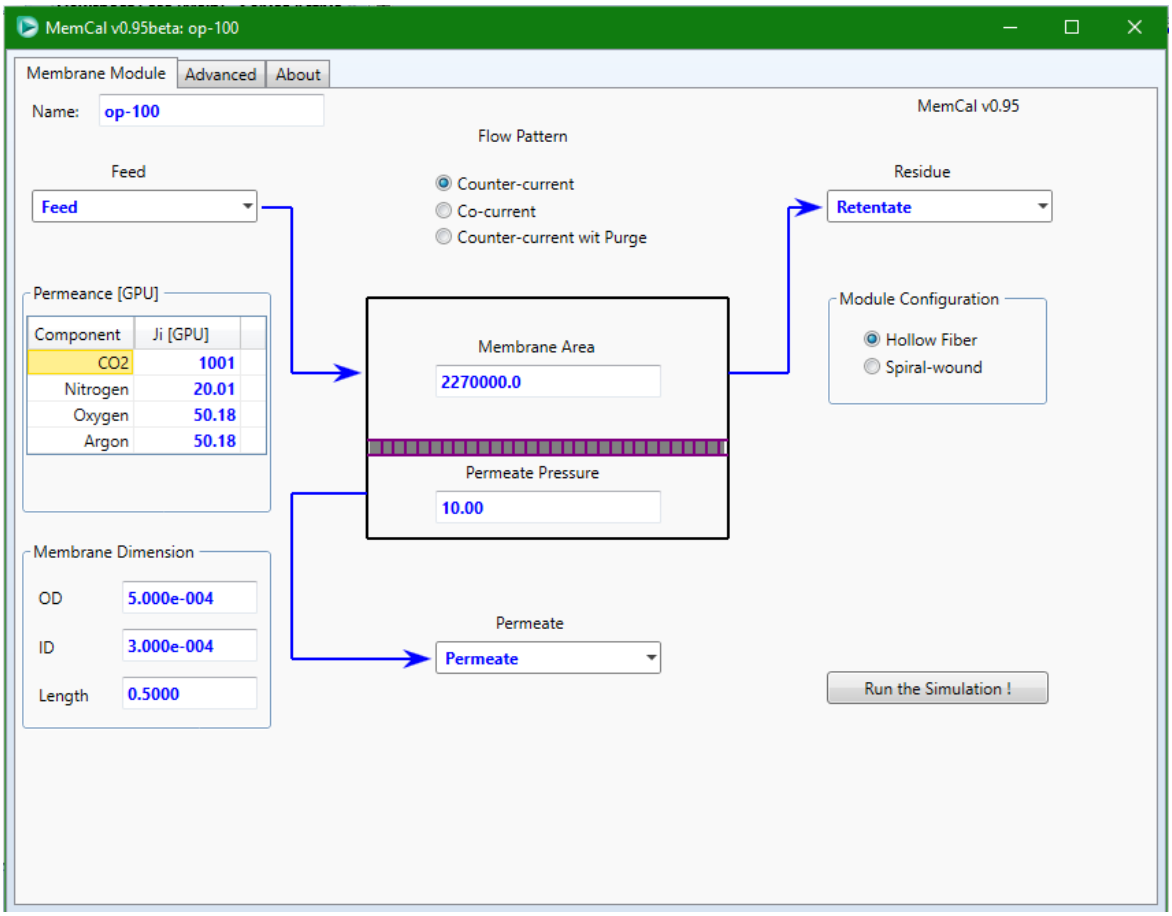

Figure A-13: Chowdhury (2011) second membrane setup qualification test membrane configuration

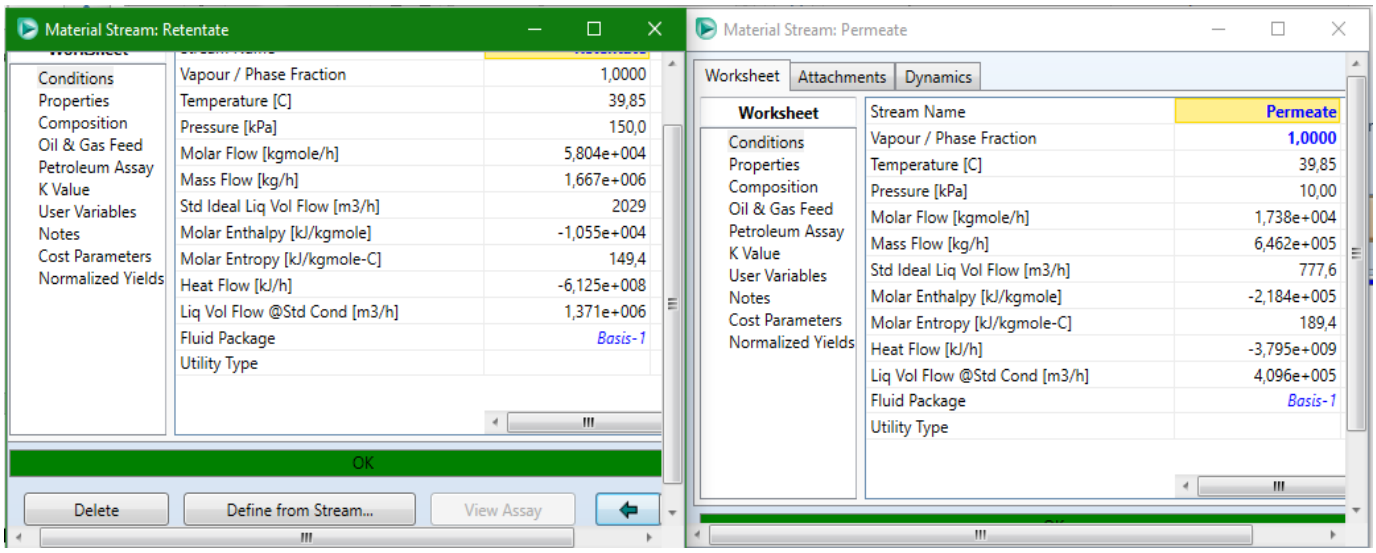

Figure A-14: Chowdhury (2011) second membrane setup qualification test permeate and retentate flow

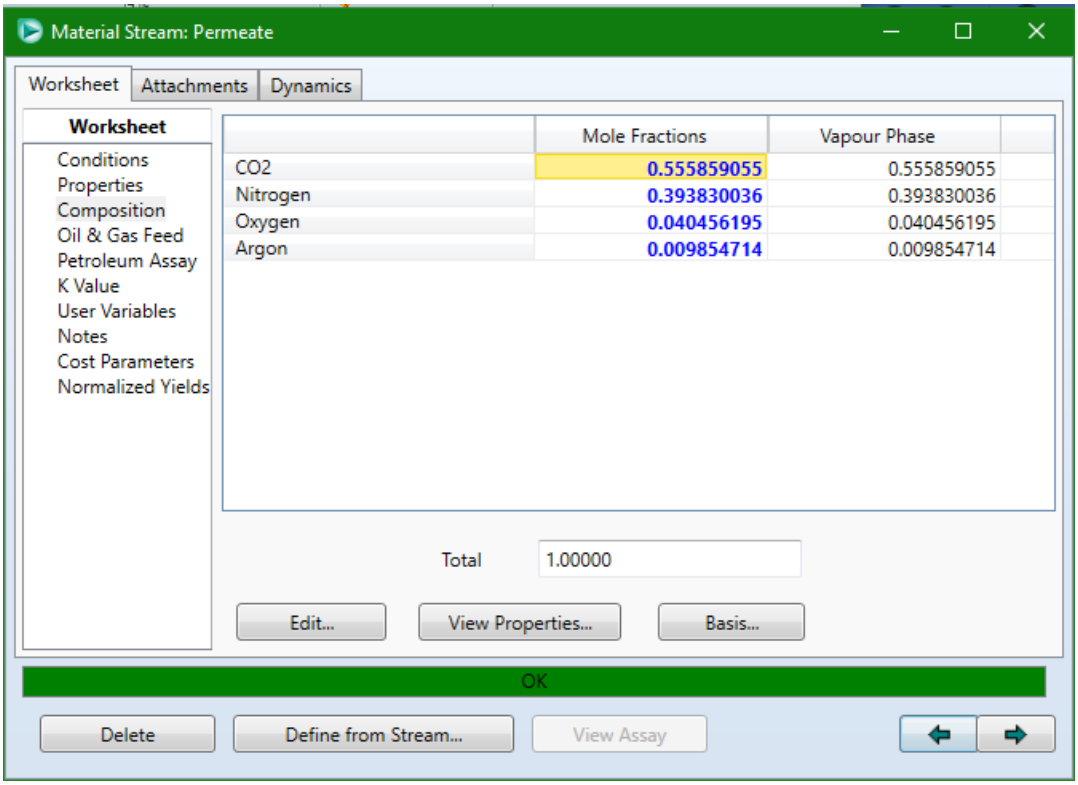

Figure A-15: Chowdhury (2011) second membrane setup qualification test permeate composition

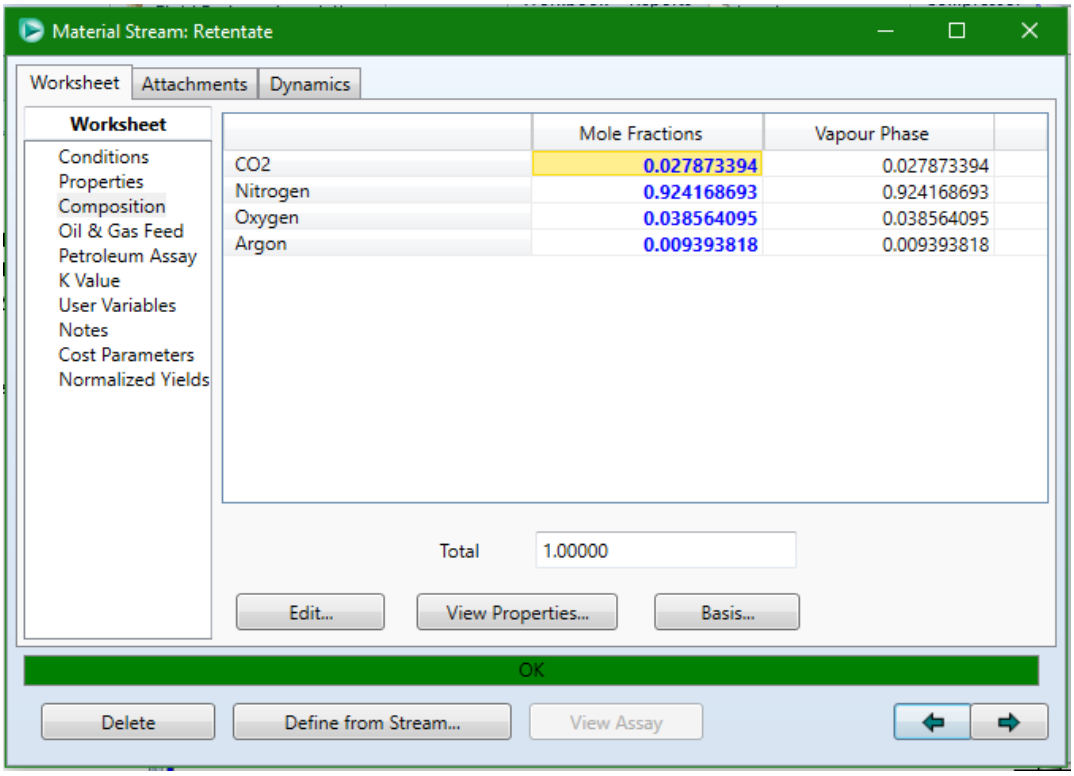

Figure A-16: Chowdhury (2011) second membrane setup qualification test retentate composition

Table A-5: Mole fractions of the Chowdhury (2011) setup 2 qualification test mass balance

Gas	Mole fractions in feed	Mole fractions in retentate	Mole fractions in permeate	Source
CO_2	1.495E-01	5.503E-01	5.491E-02	Chowdhury 2
N_2	8.020E-01	3.981E-01	9.398E-01	Chowdhury 2
O_2	3.900E-02	4.150E-02	4.011E-02	Chowdhury 2
Ar	9.500E-03	1.020E-02	9.747E-03	Chowdhury 2
CO_2	1.495E-01	2.787E-02	5.559E-01	Memcal
N_2	8.020E-01	9.242E-01	3.938E-01	Memcal
O_2	3.900E-02	3.856E-02	4.046E-02	Memcal
Ar	9.500E-03	9.394E-03	9.855E-03	Memcal

Table A-6: Mass balance of the Chowdhury (2011) setup 2 qualification test

Gas	Molar flow rate in feed (kmol/s)	Molar flow rate in retentate (kmol/s)	Molar flow rate in permeate (kmol/s)	Source
CO_2	3.132E+00	2.245E+00	8.868E-01	Chowdhury 2
N_2	1.680E+01	1.624E+00	1.518E+01	Chowdhury 2
O_2	8.171E-01	1.693E-01	6.477E-01	Chowdhury 2
Ar	1.990E-01	4.162E-02	1.574E-01	Chowdhury 2
Total	2.095E+01	4.800E+00	1.615E+01	Chowdhury 2
CO_2	3.132E+00	1.346E-01	8.962E+00	Memcal
N_2	1.680E+01	4.461E+00	6.350E+00	Memcal
O_2	8.171E-01	1.862E-01	6.523E-01	Memcal
Ar	1.990E-01	4.535E-02	1.589E-01	Memcal
Total	2.095E+01	4.827E+00	1.612E+01	Memcal

Mourgues & Sanchez (2012) cascade system qualification test

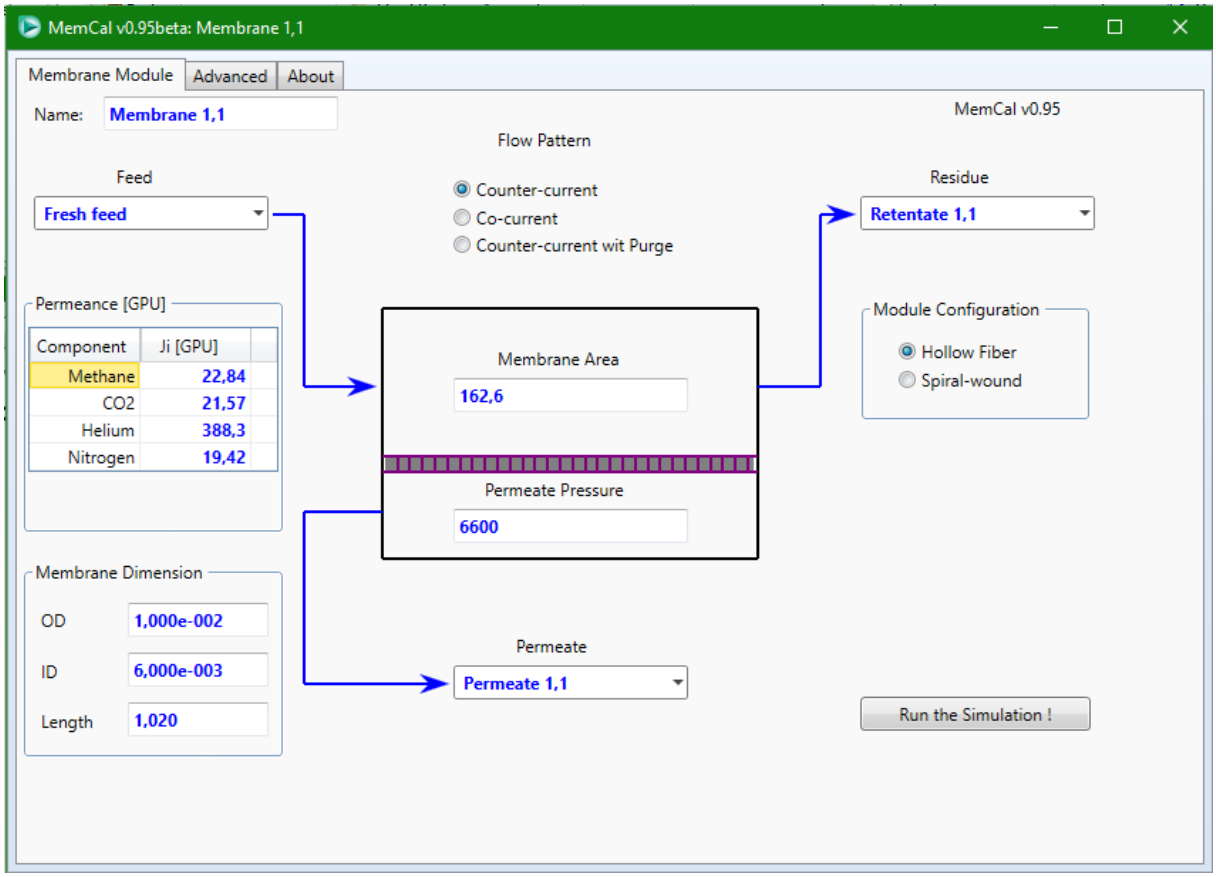

Figure A-17: Mourgues & Sanchez (2012) cascade system qualification test example of one membrane's configuration

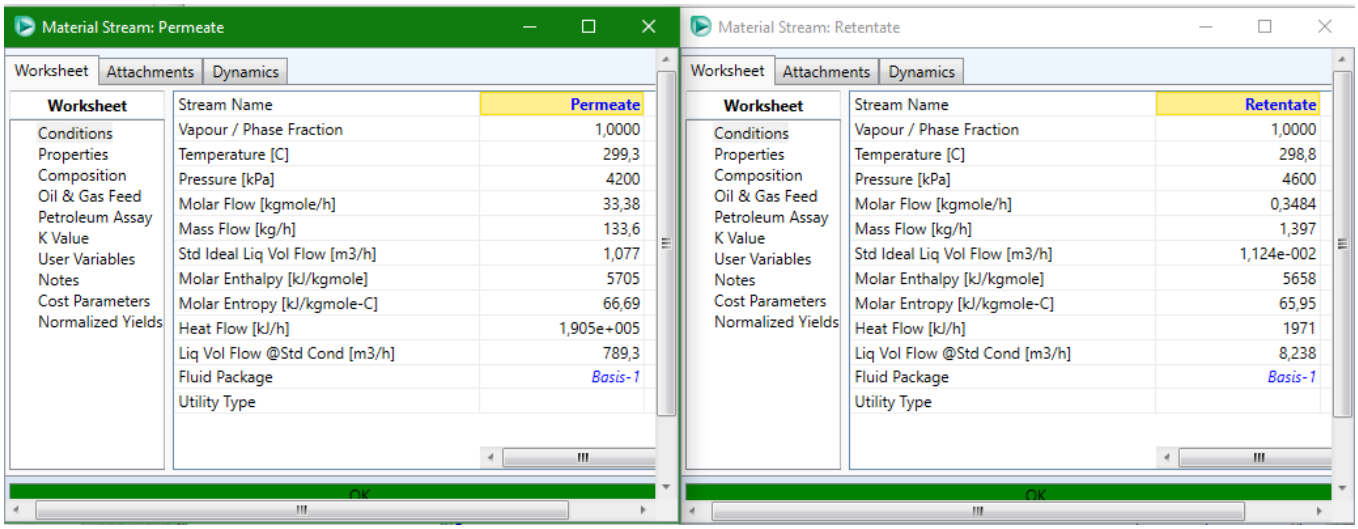

Figure A-18: Mourgues & Sanchez (2012) cascade system qualification test permeate and retentate flow

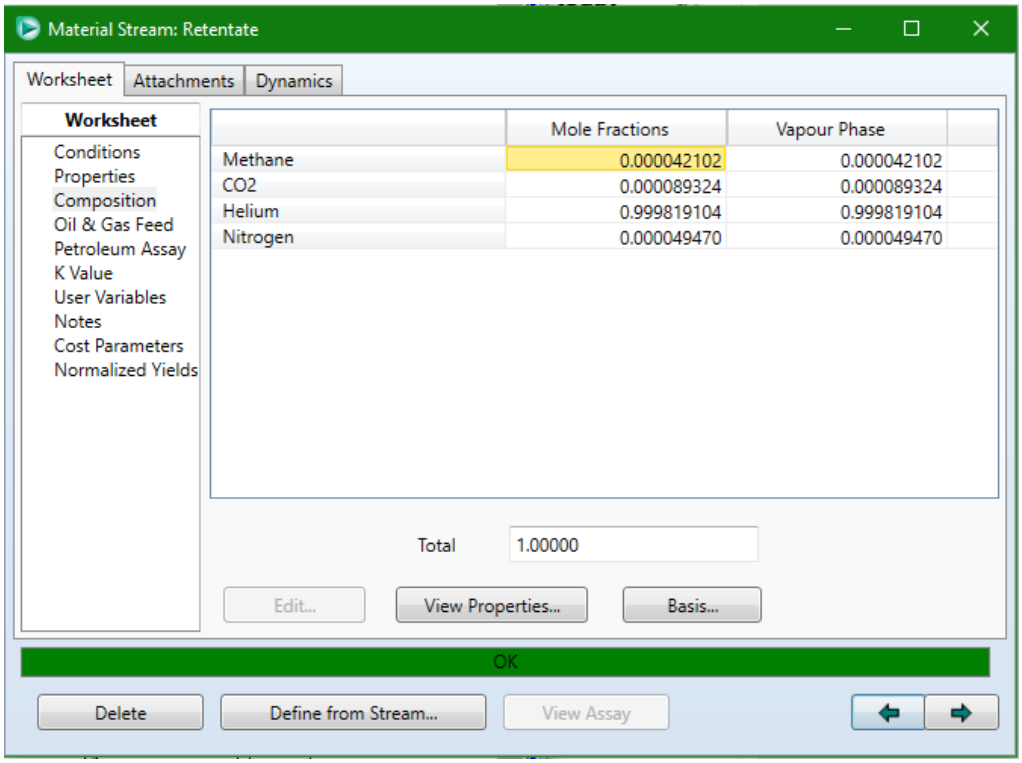

Figure A-19: Mourgues & Sanchez (2012) cascade system qualification test retentate composition

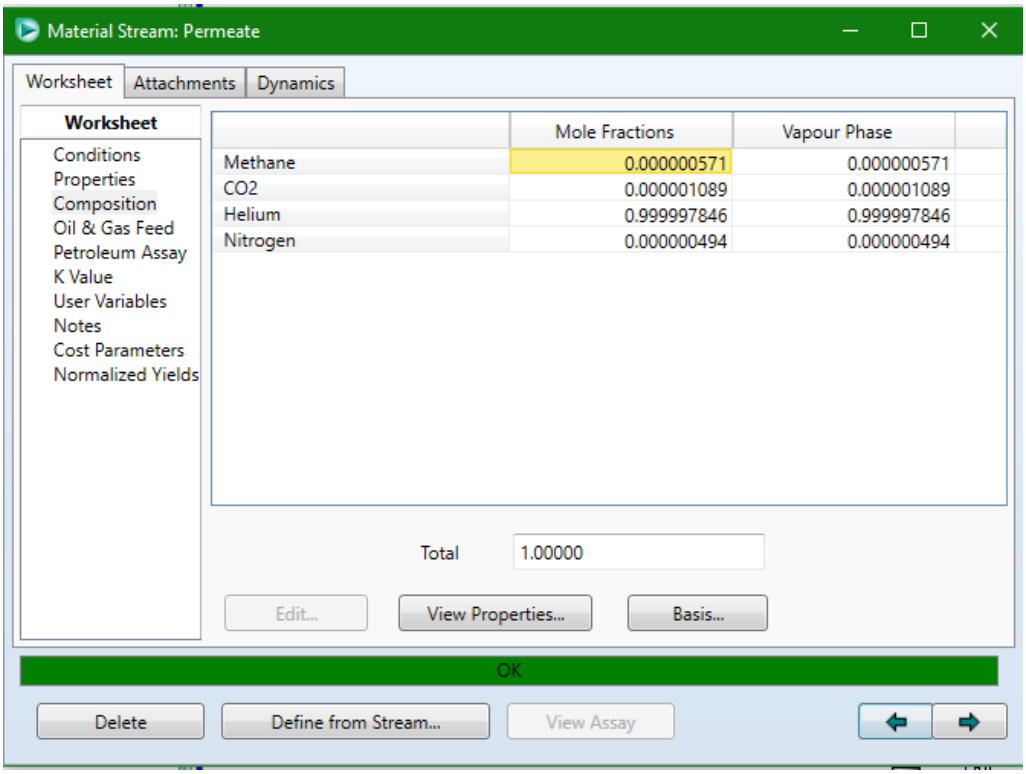

Figure A-20: Mourgues & Sanchez (2012) cascade system qualification test permeate composition

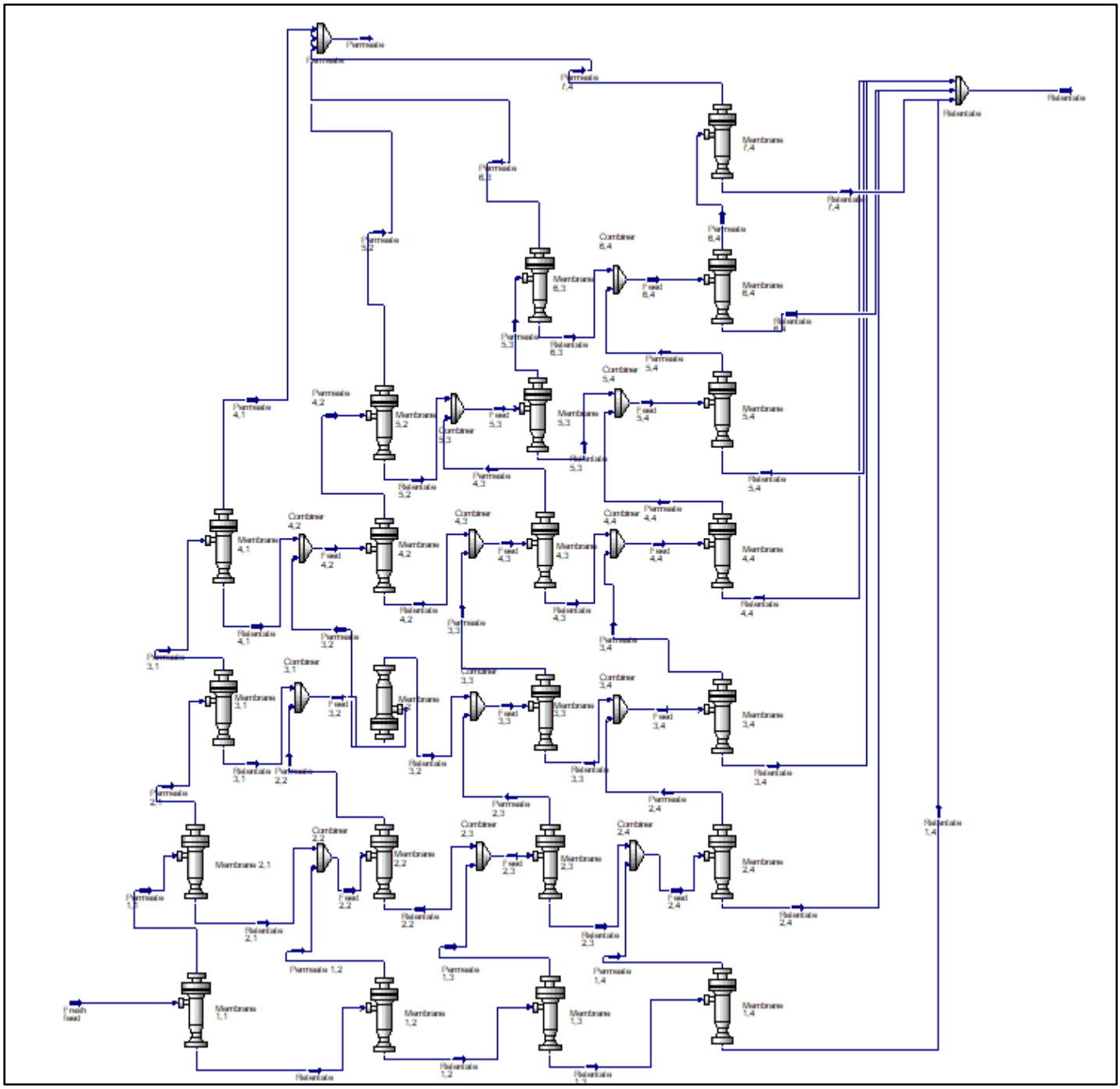

Figure A-21: Mourgues & Sanchez (2012) cascade system qualification test membrane system setup

Table A-7: Table of membrane areas for Mourgues & Sanchez (2012) cascade system qualification test

Membrane number (Row, Column)	Area (m^2)
Membrane (1,1)	162.643
Membrane (1,2)	16.2660
Membrane (1,3)	1.6270
Membrane (1,4)	0.16282
Membrane (2,1)	146.352
Membrane (2,2)	29.2675
Membrane (2,3)	4.39025
Membrane (2,4)	0.58566
Membrane (3,1)	131.703
Membrane (3,2)	39.5058
Membrane (3,3)	7.90016
Membrane (3,4)	1.31749
Membrane (4,1)	118.520
Membrane (4,2)	47.4000
Membrane (4,3)	11.8504
Membrane (4,4)	2.37084
Membrane (5,2)	42.6589
Membrane (5,3)	14.9304
Membrane (5,4)	3.62679
Membrane (6,3)	13.4351
Membrane (6,4)	4.60695
Membrane (7,4)	4.14540
Total	805.2655

Table A-8: Helium permeances and characteristics from literature

Temperature (ºC)	Feed pressure (Bar)	Permeate pressure (Bar)	Permeance (kmol/Pa s m^2)	Permeance (GPU)	Type of membrane	Source
200	3	1	4.78E-10	1.43E+03	Cobalt silica	Brands *et al.,* 2010.
200	3	1	1.85E-11	5.53E+01	Cobalt silica after flue gas exposure	Brands *et al.,* 2010.
60	N/a	N/a	1.11818E-11	33.4	Carbon precursor	Favvas *et al*., 2015.
60	N/a	N/a	1.18179E-12	3.53	Carbon 5 minute pyrolysis	Favvas *et al*., 2015.
60	N/a	N/a	1.03113E-12	3.08	Carbon 30 minute pyrolysis	Favvas *et al*., 2015.
60	N/a	N/a	7.83395E-13	2.34	Carbon 60 minute pyrolysis	Favvas *et al*., 2015.
100	2	0.01	1.809E-10	540.3483	Al2O3 fresh	Nitodas *et al*., 2008.
100	2	0.01	4.02E-11	120.0774	Al2O3 1h SiO2 deposition	Nitodas *et al*., 2008.
100	2	0.01	3.4E-13	1.01558	Al2O3 9h SiO2 deposition	Nitodas *et al*., 2008.
200	5	1	6.1E-10	1822.07	Pure silica	Boffa *et al.*, 2008.
200	5	1	3.7E-10	1105.19	PS at 150C hydrothermal exposure	Boffa *et al.*, 2008.
200	5	1	3.7E-10	1105.19	PS at 200C hydrothermal exposure	Boffa *et al.*, 2008.

200	5	1	7.2E-11	215.064	Niobia-doped silica	Boffa *et al.*, 2008.
200	5	1	5.2E-11	155.324	NS at 150C hydrothermal exposure	Boffa *et al.*, 2008.
200	5	1	4E-11	119.48	NS at 200C hydrothermal exposure	Boffa *et al.*, 2008.
300	1	0.01	6.7E-10	2001.29	Silica with sol fired at 550C	Kanezashi *et al.*, 2014.
300	1	0.01	2.3E-10	687.01	Silica with sol fired at 750C	Kanezashi *et al.*, 2014.
400	1	0.01	7.85E-10	2344.795	Silica with sol fired at 550C	Kanezashi *et al.*, 2014.
400	1	0.01	3.25E-10	970.775	Silica with sol fired at 750C	Kanezashi *et al.*, 2014.
500	1	0.01	8.8E-10	2628.56	Silica with sol fired at 550C	Kanezashi *et al.*, 2014.
500	1	0.01	4.2E-10	1254.54	Silica with sol fired at 750C	Kanezashi *et al.*, 2014.
30	1.97	1.01	8.60E-09	25688.2	Silica substrate	Gao *et al*., 2013
30	1.97	1.01	1.00E-09	2987	Disordered silica 3.7nm pores	Gao *et al*., 2013
300	1.97	1.01	5.50E-09	16428.5	Silica substrate	Gao *et al*., 2013
300	1.97	1.01	1.00E-09	2987	Disordered silica 3.7nm pores	Gao *et al*., 2013

200	5	1	1.70E-10	507.79	Iron cobalt oxide silica membrane 10/90	Darmawan *et al*., 2015
300	5	1	2.30E-10	687.01	Iron cobalt oxide silica membrane 10/90	Darmawan *et al*., 2015
400	5	1	2.85E-10	851.295	Iron cobalt oxide silica membrane 10/90	Darmawan *et al*., 2015
200	5	1	6.90E-11	206.103	Iron cobalt oxide silica membrane 25/75	Darmawan *et al*., 2015
300	5	1	9.00E-11	268.83	Iron cobalt oxide silica membrane 25/75	Darmawan *et al*., 2015
400	5	1	1.10E-10	328.57	Iron cobalt oxide silica membrane 25/75	Darmawan *et al*., 2015
200	5	1	6.50E-11	194.155	Iron cobalt oxide silica membrane 50/50	Darmawan *et al*., 2015
300	5	1	1.40E-10	418.18	Iron cobalt oxide silica membrane 50/50	Darmawan *et al*., 2015
400	5	1	1.80E-10	537.66	Iron cobalt oxide silica membrane 50/50	Darmawan *et al*., 2015
200	2	1	1.80E-08	53766	α-alumina base support	Lee *et al*., 2011

200	2	1	8.50E-10	2538.95	HCL catalyzed sol	Lee *et al*., 2011
200	2	1	6.00E-09	17922	NH3 catalyzed sol	Lee *et al*., 2011
200	2	1	5.00E-10	1493.5	CH3COOH catalyzed sol	Lee *et al*., 2011
200	2	1	2.90E-10	866.23	TEOS-derived silica	Lee *et al*., 2011
200	2	1	2.10E-09	6272.7	BTESE-derived silica	Lee *et al*., 2011
200	2	1	7.50E-10	2240.25	TEDMDS-derived silica	Lee *et al*., 2011
200	2	1	1.80E-09	5376.6	HEDS-derived silica	Lee *et al*., 2011
200	3	1	3.32E-10	991.684	BTESE hybrid sol at 0.09M	Qureshi *et al*., 2013
200	3	1	3.52E-10	1051.424	BTESE hybrid sol at 0.15M	Qureshi *et al*., 2013
200	3	1	2.52E-10	752.724	BTESE hybrid sol at 0.3M	Qureshi *et al*., 2013
200	3	1	2.05E-10	612.335	BTESE hybrid sol at 0.6M	Qureshi *et al*., 2013
200	3	1	1.80E-10	537.66	BTESE hybrid acid ratio 0.01 and <0.5% humidity	Castricum *et al*., 2015
200	3	1	2.05E-10	612.335	BTESE hybrid acid ratio 0.1 and	Castricum *et al*., 2015

					<0.5% humidity	
200	3	1	5.91E-10	1765.317	Support structure	Castricum *et al*., 2015
200	3	1	1.48E-10	442.076	BTESE hybrid acid ratio 0.01 and 90% humidity	Castricum *et al*., 2015
200	3	1	3.42E-10	1021.554	BTESE hybrid acid ratio 0.1 and 90% humidity	Castricum *et al*., 2015
200	2	1	6.20E-10	1851.94	Pa-Si amine membrane	Yu *et al*., 2017
200	2	1	2.50E-10	746.75	Sa-Si amine membrane	Yu *et al*., 2017
200	2	1	4.50E-10	1344.15	Ta-Si amine membrane	Yu *et al*., 2017

Table A-9: Hydrogen permeances and characteristics from literature

Temperature (ºC)	Feed pressure (Bar)	Permeate pressure (Bar)	Permeance (kmol/Pa s m^2)	Permeance (GPU)	Type of membrane	Source
200	3	1	4.27E-10	1.28E+03	Cobalt silica	Brands *et al.,* 2010.
200	3	1	2.13E-11	63.6231	Cobalt silica after flue gas exposure	Brands *et al.,* 2010.
60	N/a	N/a	1.11148E-11	33.2	Carbon precursor	Favvas *et al*., 2015.
60	N/a	N/a	2.00536E-12	5.99	Carbon 5 minute pyrolysis	Favvas *et al*., 2015.
60	N/a	N/a	1.84131E-12	5.5	Carbon 30 minute pyrolysis	Favvas *et al*., 2015.
60	N/a	N/a	1.47539E-12	4.407	Carbon 60 minute pyrolysis	Favvas *et al*., 2015.
100	2	0.01	2.351E-10	702.2437	Al2O3 fresh	Nitodas *et al*., 2008.
100	2	0.01	9.1E-11	271.817	Al2O3 1h SiO2 deposition	Nitodas *et al*., 2008.
100	2	0.01	4.72E-11	140.9864	Al2O3 9h SiO2 deposition	Nitodas *et al*., 2008.
200	5	1	6.3E-10	1881.81	Pure silica	Boffa *et al.*, 2008.
200	5	1	3.1E-10	925.97	PS at 150C hydrothermal exposure	Boffa *et al.*, 2008.
200	5	1	3E-10	896.1	PS at 200C hydrothermal exposure	Boffa *et al.*, 2008.

200	5	1	3.9E-11	116.493	Niobia-doped silica	Boffa *et al.*, 2008.
200	5	1	3.7E-11	110.519	NS at 150C hydrothermal exposure	Boffa *et al.*, 2008.
200	5	1	2.7E-11	80.649	NS at 200C hydrothermal exposure	Boffa *et al.*, 2008.
300	1	0.01	3E-10	896.1	Silica with sol fired at 550C	Kanezashi *et al.*, 2014.
300	1	0.01	3.9E-11	116.493	Silica with sol fired at 750C	Kanezashi *et al.*, 2014.
400	1	0.01	4.4E-10	1314.28	Silica with sol fired at 550C	Kanezashi *et al.*, 2014.
400	1	0.01	7E-11	209.09	Silica with sol fired at 750C	Kanezashi *et al.*, 2014.
500	1	0.01	5.5E-10	1642.85	Silica with sol fired at 550C	Kanezashi *et al.*, 2014.
500	1	0.01	1.1E-10	328.57	Silica with sol fired at 750C	Kanezashi *et al.*, 2014.
30	1.97	1.01	1.40E-08	4.18E+04	Silica substrate	Gao *et al*., 2013
30	1.97	1.01	1.90E-09	5675.3	Disordered silica 3.7nm pores	Gao *et al*., 2013
300	1.97	1.01	8.50E-09	25389.5	Silica substrate	Gao *et al*., 2013
300	1.97	1.01	1.40E-09	4181.8	Disordered silica 3.7nm pores	Gao *et al*., 2013

200	5	1	6.40E-11	191.168	Iron cobalt oxide silica membrane 10/90	Darmawan *et al*., 2015
300	5	1	1.00E-10	298.7	Iron cobalt oxide silica membrane 10/90	Darmawan *et al*., 2015
400	5	1	1.60E-10	477.92	Iron cobalt oxide silica membrane 10/90	Darmawan *et al*., 2015
200	5	1	3.50E-11	104.545	Iron cobalt oxide silica membrane 25/75	Darmawan *et al*., 2015
300	5	1	4.30E-11	128.441	Iron cobalt oxide silica membrane 25/75	Darmawan *et al*., 2015
400	5	1	6.10E-11	182.207	Iron cobalt oxide silica membrane 25/75	Darmawan *et al*., 2015
200	5	1	6.10E-11	182.207	Iron cobalt oxide silica membrane 50/50	Darmawan *et al*., 2015
300	5	1	7.50E-11	224.025	Iron cobalt oxide silica membrane 50/50	Darmawan *et al*., 2015
400	5	1	9.90E-11	295.713	Iron cobalt oxide silica membrane 50/50	Darmawan *et al*., 2015
200	2	1	2.50E-08	74675	α-alumina base support	Lee *et al*., 2011

200	2	1	8.00E-10	2389.6	HCL catalyzed sol	Lee *et al*., 2011
200	2	1	7.40E-10	2210.38	NH3 catalyzed sol	Lee *et al*., 2011
200	2	1	8.00E-09	23896	CH3COOH catalyzed sol	Lee *et al*., 2011
200	2	1	6.00E-11	179.22	TEOS-derived silica	Lee *et al*., 2011
200	2	1	3.00E-09	8961	BTESE-derived silica	Lee *et al*., 2011
200	2	1	1.00E-09	2987	TEDMDS-derived silica	Lee *et al*., 2011
200	2	1	2.00E-09	5974	HEDS-derived silica	Lee *et al*., 2011
200	3	1	4.62E-10	1379.994	BTESE hybrid sol at 0.09M	Qureshi *et al*., 2013
200	3	1	4.32E-10	1290.384	BTESE hybrid sol at 0.15M	Qureshi *et al*., 2013
200	3	1	3.12E-10	931.944	BTESE hybrid sol at 0.3M	Qureshi *et al*., 2013
200	3	1	2.70E-10	806.49	BTESE hybrid sol at 0.6M	Qureshi *et al*., 2013
200	3	1	2.10E-10	627.27	BTESE hybrid acid ratio 0.01 and <0.5% humidity	Castricum *et al*., 2015
200	3	1	2.70E-10	806.49	BTESE hybrid acid ratio 0.1 and	Castricum *et al*., 2015

					<0.5% humidity	
200	3	1	8.12E-10	2425.444	Support structure	Castricum *et al*., 2015
200	3	1	1.81E-10	540.647	BTESE hybrid acid ratio 0.01 and 90% humidity	Castricum *et al*., 2015
200	3	1	4.52E-10	1350.124	BTESE hybrid acid ratio 0.1 and 90% humidity	Castricum *et al*., 2015
200	2	1	6.20E-10	1851.94	Pa-Si amine membrane	Yu *et al*., 2017
200	2	1	2.75E-10	821.425	Sa-Si amine membrane	Yu *et al*., 2017
200	2	1	5.00E-10	1493.5	Ta-Si amine membrane	Yu *et al*., 2017

Table A-10: Nitrogen permeances and characteristics from literature

Temperature (°C)	Feed pressure (Bar)	Permeate pressure (Bar)	Permeance (kmol/Pa s m^2)	Permeance (GPU)	Type of membrane	Source
200	3	1	7.59E-11	2.27E+02	Cobalt silica	Brands *et al.,* 2010.
200	3	1	3.70E-12	11.0519	Cobalt silica after flue gas exposure	Brands *et al.,* 2010.
60	N/a	N/a	1.77436E-12	5.3	Carbon precursor	Favvas *et al*., 2015.
60	N/a	N/a	3.34784E-15	0.01	Carbon 5 minute pyrolysis	Favvas *et al*., 2015.
60	N/a	N/a	3.01306E-15	0.009	Carbon 30 minute pyrolysis	Favvas *et al*., 2015.
60	N/a	N/a	2.44392E-15	0.0073	Carbon 60 minute pyrolysis	Favvas *et al*., 2015.
100	2	0.01	7.01E-11	209.3887	Al2O3 fresh	Nitodas *et al*., 2008.
100	2	0.01	1.55E-11	46.2985	Al2O3 1h SiO2 deposition	Nitodas *et al*., 2008.
100	2	0.01	2.1E-13	0.62727	Al2O3 9h SiO2 deposition	Nitodas *et al*., 2008.
200	5	1	4.2E-12	12.5454	Pure silica	Boffa *et al.*, 2008.
200	5	1	2.2E-12	6.5714	PS at 150C hydrothermal exposure	Boffa *et al.*, 2008.

200	5	1	2.1E-12	6.2727	PS at 200C hydrothermal exposure	Boffa *et al.*, 2008.
200	5	1	6.2E-12	18.5194	Niobia-doped silica	Boffa *et al.*, 2008.
200	5	1	6.2E-12	18.5194	NS at 150C hydrothermal exposure	Boffa *et al.*, 2008.
200	5	1	6.7E-12	20.0129	NS at 200C hydrothermal exposure	Boffa *et al.*, 2008.
300	1	0.01	7.1E-13	2.12077	Silica with sol fired at 550C	Kanezashi *et al.*, 2014.
300	1	0.01	1.6E-13	0.47792	Silica with sol fired at 750C	Kanezashi *et al.*, 2014.
400	1	0.01	8.1E-13	2.41947	Silica with sol fired at 550C	Kanezashi *et al.*, 2014.
400	1	0.01	1.6E-13	0.47792	Silica with sol fired at 750C	Kanezashi *et al.*, 2014.
500	1	0.01	1.2E-12	3.5844	Silica with sol fired at 550C	Kanezashi *et al.*, 2014.
500	1	0.01	1.6E-13	0.47792	Silica with sol fired at 750C	Kanezashi *et al.*, 2014.
30	1.97	1.01	5.00E-09	14935	Silica substrate	Gao *et al*., 2013
30	1.97	1.01	5.00E-10	1493.5	Disordered silica 3.7nm pores	Gao *et al*., 2013

300	1.97	1.01	2.70E-09	8064.9	Silica substrate	Gao *et al*., 2013
300	1.97	1.01	3.00E-10	896.1	Disordered silica 3.7nm pores	Gao *et al*., 2013
200	5	1	2.10E-12	6.2727	Iron cobalt oxide silica membrane 10/90	Darmawan *et al*., 2015
300	5	1	2.05E-12	6.12335	Iron cobalt oxide silica membrane 10/90	Darmawan *et al*., 2015
400	5	1	2.15E-12	6.42205	Iron cobalt oxide silica membrane 10/90	Darmawan *et al*., 2015
200	5	1	8.00E-12	23.896	Iron cobalt oxide silica membrane 25/75	Darmawan *et al*., 2015
300	5	1	7.20E-12	21.5064	Iron cobalt oxide silica membrane 25/75	Darmawan *et al*., 2015
400	5	1	7.00E-12	20.909	Iron cobalt oxide silica membrane 25/75	Darmawan *et al*., 2015
200	5	1	2.20E-11	65.714	Iron cobalt oxide silica membrane 50/50	Darmawan *et al*., 2015
300	5	1	2.15E-11	64.2205	Iron cobalt oxide silica membrane 50/50	Darmawan *et al*., 2015

400	5	1	2.10E-11	62.727	Iron cobalt oxide silica membrane 50/50	Darmawan *et al*., 2015
200	2	1	7.00E-09	20909	α-alumina base support	Lee *et al*., 2011
200	2	1	4.30E-11	128.441	HCL catalyzed sol	Lee *et al*., 2011
200	2	1	2.50E-09	7467.5	NH3 catalyzed sol	Lee *et al*., 2011
200	2	1	1.00E-10	298.7	CH3COOH catalyzed sol	Lee *et al*., 2011
200	2	1	1.80E-13	0.53766	TEOS-derived silica	Lee *et al*., 2011
200	2	1	4.00E-10	1194.8	BTESE-derived silica	Lee *et al*., 2011
200	2	1	1.70E-10	507.79	TEDMDS-derived silica	Lee *et al*., 2011
200	2	1	1.50E-10	448.05	HEDS-derived silica	Lee *et al*., 2011
200	3	1	4.40E-11	131.428	BTESE hybrid sol at 0.09M	Qureshi *et al*., 2013
200	3	1	3.40E-11	101.558	BTESE hybrid sol at 0.15M	Qureshi *et al*., 2013
200	3	1	2.30E-11	68.701	BTESE hybrid sol at 0.3M	Qureshi *et al*., 2013
200	3	1	1.30E-11	38.831	BTESE hybrid sol at 0.6M	Qureshi *et al*., 2013

200	3	1	3.40E-12	10.1558	BTESE hybrid acid ratio 0.01 and <0.5% humidity	Castricum *et al*., 2015
200	3	1	1.30E-11	38.831	BTESE hybrid acid ratio 0.1 and <0.5% humidity	Castricum *et al*., 2015
200	3	1	2.31E-10	689.997	Support structure	Castricum *et al*., 2015
200	3	1	1.78E-11	53.1686	BTESE hybrid acid ratio 0.01 and 90% humidity	Castricum *et al*., 2015
200	3	1	6.27E-11	187.2849	BTESE hybrid acid ratio 0.1 and 90% humidity	Castricum *et al*., 2015
200	2	1	1.50E-11	44.805	Pa-Si amine membrane	Yu *et al*., 2017
200	2	1	1.00E-11	29.87	Sa-Si amine membrane	Yu *et al*., 2017
200	2	1	3.20E-11	95.584	Ta-Si amine membrane	Yu *et al*., 2017

Table A-11: Carbon dioxide permeances and characteristics from literature

Temperature (°C)	Feed pressure (Bar)	Permeate pressure (Bar)	Permeance (kmol/Pa s m^2)	Permeance (GPU)	Type of membrane	Source
200	3	1	7.69E-11	229.8106306	Cobalt silica	Brands *et al.,* 2010.
200	3	1	4.26E-12	12.72462	Cobalt silica after flue gas exposure	Brands *et al.,* 2010.
60	N/a	N/a	2.04218E-12	6.1	Carbon precursor	Favvas *et al*., 2015.
60	N/a	N/a	1.40609E-13	0.42	Carbon 5 minute pyrolysis	Favvas *et al*., 2015.
60	N/a	N/a	1.03783E-13	0.31	Carbon 30 minute pyrolysis	Favvas *et al*., 2015.
60	N/a	N/a	7.04386E-14	0.2104	Carbon 60 minute pyrolysis	Favvas *et al*., 2015.
100	2	0.01	5.77E-11	172.3499	Al2O3 fresh	Nitodas *et al*., 2008.
100	2	0.01	1.24E-11	37.0388	Al2O3 1h SiO2 deposition	Nitodas *et al*., 2008.
100	2	0.01	1.1E-13	0.32857	Al2O3 9h SiO2 deposition	Nitodas *et al*., 2008.
200	5	1	1.3E-11	38.831	Pure silica	Boffa *et al.*, 2008.
200	5	1	9.5E-12	28.3765	PS at 150C hydrothermal exposure	Boffa *et al.*, 2008.

200	5	1	6.3E-12	18.8181	PS at 200C hydrothermal exposure	Boffa *et al.*, 2008.
200	5	1	8.5E-13	2.53895	Niobia-doped silica	Boffa *et al.*, 2008.
200	5	1	8.2E-13	2.44934	NS at 150C hydrothermal exposure	Boffa *et al.*, 2008.
200	5	1	8.3E-13	2.47921	NS at 200C hydrothermal exposure	Boffa *et al.*, 2008.
300	1	0.01	4.8E-12	14.3376	Silica with sol fired at 550C	Kanezashi *et al.*, 2014.
300	1	0.01	3.3E-13	0.98571	Silica with sol fired at 750C	Kanezashi *et al.*, 2014.
400	1	0.01	3.8E-12	11.3506	Silica with sol fired at 550C	Kanezashi *et al.*, 2014.
400	1	0.01	2.8E-13	0.83636	Silica with sol fired at 750C	Kanezashi *et al.*, 2014.
500	1	0.01	3.8E-12	11.3506	Silica with sol fired at 550C	Kanezashi *et al.*, 2014.
500	1	0.01	2.3E-13	0.68701	Silica with sol fired at 750C	Kanezashi *et al.*, 2014.
30	1.97	1.01	4.90E-09	14636.3	Silica substrate	Gao *et al*., 2013
30	1.97	1.01	8.00E-10	2389.6	Disordered silica 3.7nm pores	Gao *et al*., 2013

300	1.97	1.01	2.30E-09	6870.1	Silica substrate	Gao *et al*., 2013
300	1.97	1.01	2.00E-10	597.4	Disordered silica 3.7nm pores	Gao *et al*., 2013
200	5	1	3.80E-12	11.3506	Iron cobalt oxide silica membrane 10/90	Darmawan *et al*., 2015
300	5	1	3.00E-12	8.961	Iron cobalt oxide silica membrane 10/90	Darmawan *et al*., 2015
400	5	1	2.65E-12	7.91555	Iron cobalt oxide silica membrane 10/90	Darmawan *et al*., 2015
200	5	1	7.20E-12	21.5064	Iron cobalt oxide silica membrane 25/75	Darmawan *et al*., 2015
300	5	1	6.20E-12	18.5194	Iron cobalt oxide silica membrane 25/75	Darmawan *et al*., 2015
400	5	1	6.00E-12	17.922	Iron cobalt oxide silica membrane 25/75	Darmawan *et al*., 2015
200	5	1	2.20E-11	65.714	Iron cobalt oxide silica membrane 50/50	Darmawan *et al*., 2015
300	5	1	2.00E-11	59.74	Iron cobalt oxide silica membrane 50/50	Darmawan *et al*., 2015

400	5	1	1.90E-11	56.753	Iron cobalt oxide silica membrane 50/50	Darmawan *et al*., 2015
200	3	1	1.24E-10	370.388	BTESE hybrid sol at 0.09M	Qureshi *et al*., 2013
200	3	1	1.19E-10	355.453	BTESE hybrid sol at 0.15M	Qureshi *et al*., 2013
200	3	1	8.00E-11	238.96	BTESE hybrid sol at 0.3M	Qureshi *et al*., 2013
200	3	1	4.60E-11	137.402	BTESE hybrid sol at 0.6M	Qureshi *et al*., 2013
200	3	1	4.50E-11	134.415	BTESE hybrid acid ratio 0.01 and <0.5% humidity	Castricum *et al*., 2015
200	3	1	4.60E-11	137.402	BTESE hybrid acid ratio 0.1 and <0.5% humidity	Castricum *et al*., 2015
200	3	1	1.74E-10	519.738	Support structure	Castricum *et al*., 2015
200	3	1	3.66E-11	109.3242	BTESE hybrid acid ratio 0.01 and 90% humidity	Castricum *et al*., 2015
200	3	1	1.23E-10	367.401	BTESE hybrid acid ratio 0.1 and 90% humidity	Castricum *et al*., 2015

200	2	1	9.00E-11	268.83	Pa-Si amine membrane	Yu *et al*., 2017
200	2	1	6.20E-11	185.194	Sa-Si amine membrane	Yu *et al*., 2017
200	2	1	1.80E-10	537.66	Ta-Si amine membrane	Yu *et al*., 2017

Table A-12: Methane permeances and characteristics from literature

Temperature (°C)	Feed pressure (Bar)	Permeate pressure (Bar)	Permeance (kmol/Pa s m^2)	Permeance (GPU)	Type of membrane	Source
60	N/a	N/a	2.24305E-12	6.7	Carbon precursor	Favvas *et al*., 2015.
60	N/a	N/a	2.84566E-15	0.0085	Carbon 5 minute pyrolysis	Favvas *et al*., 2015.
60	N/a	N/a	1.7074E-15	0.0051	Carbon 30 minute pyrolysis	Favvas *et al*., 2015.
60	N/a	N/a	2.67827E-16	0.0008	Carbon 60 minute pyrolysis	Favvas *et al*., 2015.
200	5	1	1.1E-12	3.2857	Pure silica	Boffa *et al.*, 2008.
200	5	1	1.5E-12	4.4805	PS at 150C hydrothermal exposure	Boffa *et al.*, 2008.
200	5	1	1.1E-12	3.2857	PS at 200C hydrothermal exposure	Boffa *et al.*, 2008.
200	5	1	5.4E-12	16.1298	Niobia-doped silica	Boffa *et al.*, 2008.
200	5	1	5.8E-12	17.3246	NS at 150C hydrothermal exposure	Boffa *et al.*, 2008.
200	5	1	5.4E-12	16.1298	NS at 200C hydrothermal exposure	Boffa *et al.*, 2008.
300	1	0.01	3.3E-13	0.98571	Silica with sol fired at 550C	Kanezashi *et al.*, 2014.

300	1	0.01	2.5E-13	0.74675	Silica with sol fired at 750C	Kanezashi *et al.*, 2014.
400	1	0.01	3.2E-13	0.95584	Silica with sol fired at 550C	Kanezashi *et al.*, 2014.
400	1	0.01	2.5E-13	0.74675	Silica with sol fired at 750C	Kanezashi *et al.*, 2014.
500	1	0.01	3.75E-13	1.120125	Silica with sol fired at 550C	Kanezashi *et al.*, 2014.
500	1	0.01	2E-13	0.5974	Silica with sol fired at 750C	Kanezashi *et al.*, 2014.
30	1.97	1.01	7.30E-09	21805.1	Silica substrate	Gao *et al*., 2013
30	1.97	1.01	8.00E-10	2389.6	Disordered silica 3.7nm pores	Gao *et al*., 2013
300	1.97	1.01	3.90E-09	11649.3	Silica substrate	Gao *et al*., 2013
300	1.97	1.01	4.00E-10	1194.8	Disordered silica 3.7nm pores	Gao *et al*., 2013
200	3	1	4.00E-11	119.48	BTESE hybrid sol at 0.09M	Qureshi *et al*., 2013
200	3	1	2.30E-11	68.701	BTESE hybrid sol at 0.15M	Qureshi *et al*., 2013
200	3	1	1.60E-11	47.792	BTESE hybrid sol at 0.3M	Qureshi *et al*., 2013
200	3	1	1.10E-11	32.857	BTESE hybrid sol at 0.6M	Qureshi *et al*., 2013

200	3	1	2.00E-12	5.974	BTESE hybrid acid ratio 0.01 and <0.5% humidity	Castricum *et al*., 2015
200	3	1	1.10E-11	32.857	BTESE hybrid acid ratio 0.1 and <0.5% humidity	Castricum *et al*., 2015
200	3	1	2.94E-10	878.178	Support structure	Castricum *et al*., 2015
200	3	1	1.43E-11	42.7141	BTESE hybrid acid ratio 0.01 and 90% humidity	Castricum *et al*., 2015
200	3	1	7.81E-11	233.2847	BTESE hybrid acid ratio 0.1 and 90% humidity	Castricum *et al*., 2015
200	2	1	1.50E-11	44.805	Pa-Si amine membrane	Yu *et al*., 2017
200	2	1	1.50E-11	44.805	Sa-Si amine membrane	Yu *et al*., 2017
200	2	1	5.00E-11	149.35	Ta-Si amine membrane	Yu *et al*., 2017

Table A-13: SF_6 permeances and characteristics from literature

Temperature (°C)	Feed pressure (Bar)	Permeate pressure (Bar)	Permeance (kmol/Pa s m^2)	Permeance (GPU)	Type of membrane	Source
200	5	1	1E-13	0.2987	Pure silica	Boffa *et al.*, 2008.
200	5	1	1E-13	0.2987	PS at 150C hydrothermal exposure	Boffa *et al.*, 2008.
200	5	1	1E-13	0.2987	PS at 200C hydrothermal exposure	Boffa *et al.*, 2008.
200	5	1	2.9E-12	8.6623	Niobia-doped silica	Boffa *et al.*, 2008.
200	5	1	2.9E-12	8.6623	NS at 150C hydrothermal exposure	Boffa *et al.*, 2008.
200	5	1	3E-12	8.961	NS at 200C hydrothermal exposure	Boffa *et al.*, 2008.
200	2	1	3.80E-09	11350.6	α-alumina base support	Lee *et al*., 2011
200	2	1	6.00E-13	1.7922	HCL catalyzed sol	Lee *et al*., 2011
200	2	1	1.40E-09	4181.8	NH3 catalyzed sol	Lee *et al*., 2011
200	2	1	4.00E-11	119.48	CH3COOH catalyzed sol	Lee *et al*., 2011
200	2	1	0.00E+00	0	TEOS-derived silica	Lee *et al*., 2011

200	2	1	3.00E-12	8.961	BTESE-derived silica	Lee *et al*., 2011
200	2	1	1.70E-12	5.0779	TEDMDS-derived silica	Lee *et al*., 2011
200	2	1	1.00E-12	2.987	HEDS-derived silica	Lee *et al*., 2011
200	2	1	1.60E-14	0.047792	Pa-Si amine membrane	Yu *et al*., 2017
200	2	1	1.50E-13	0.44805	Sa-Si amine membrane	Yu *et al*., 2017
200	2	1	9.00E-14	0.26883	Ta-Si amine membrane	Yu *et al*., 2017

Membrane row,column	Flow in	Permeate flow out	Retentate flow out
membrane 1,1	100	90	10
membrane 1,2	10	9	1
membrane 1,3	1	0.9	0.1
membrane 1,4	0.1	0.09	0.01
membrane 2,1	90	81	9
membrane 2,2	18	16.2	1.8
membrane 2,3	2.7	2.43	0.27
membrane 2,4	0.36	0.324	0.036

Figure A-22: Example of Excel sheet for a 90% stage-cut system

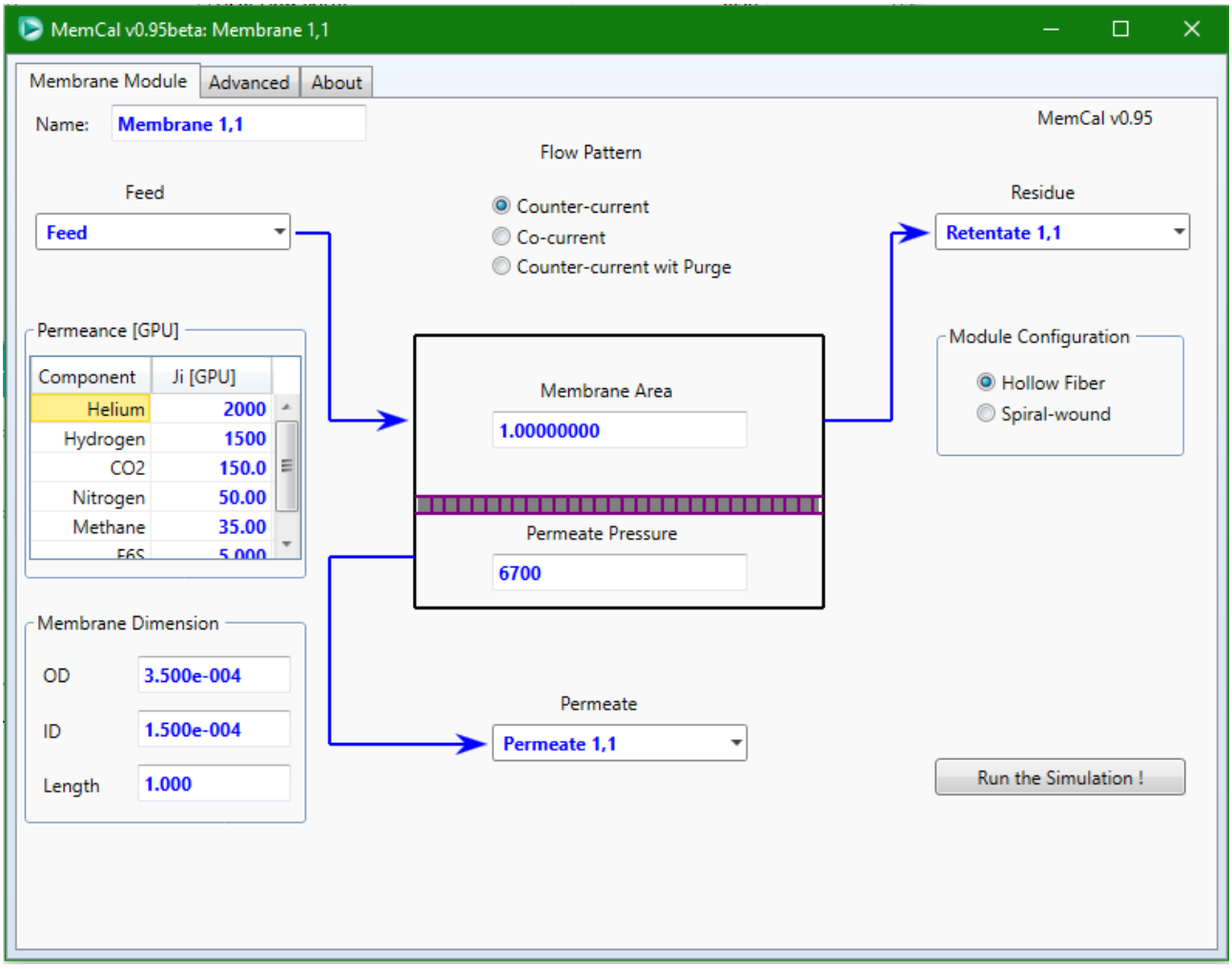

Figure A-23: Example of Memcal unit before the correct area is assigned

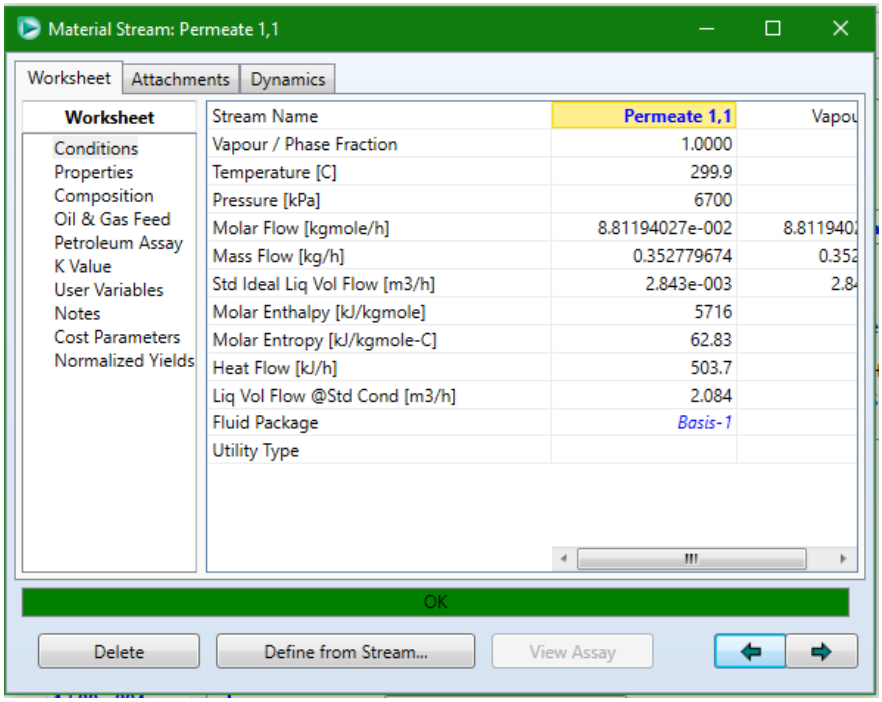

Figure A-24: Example of Memcal unit permeate flow before area is corrected

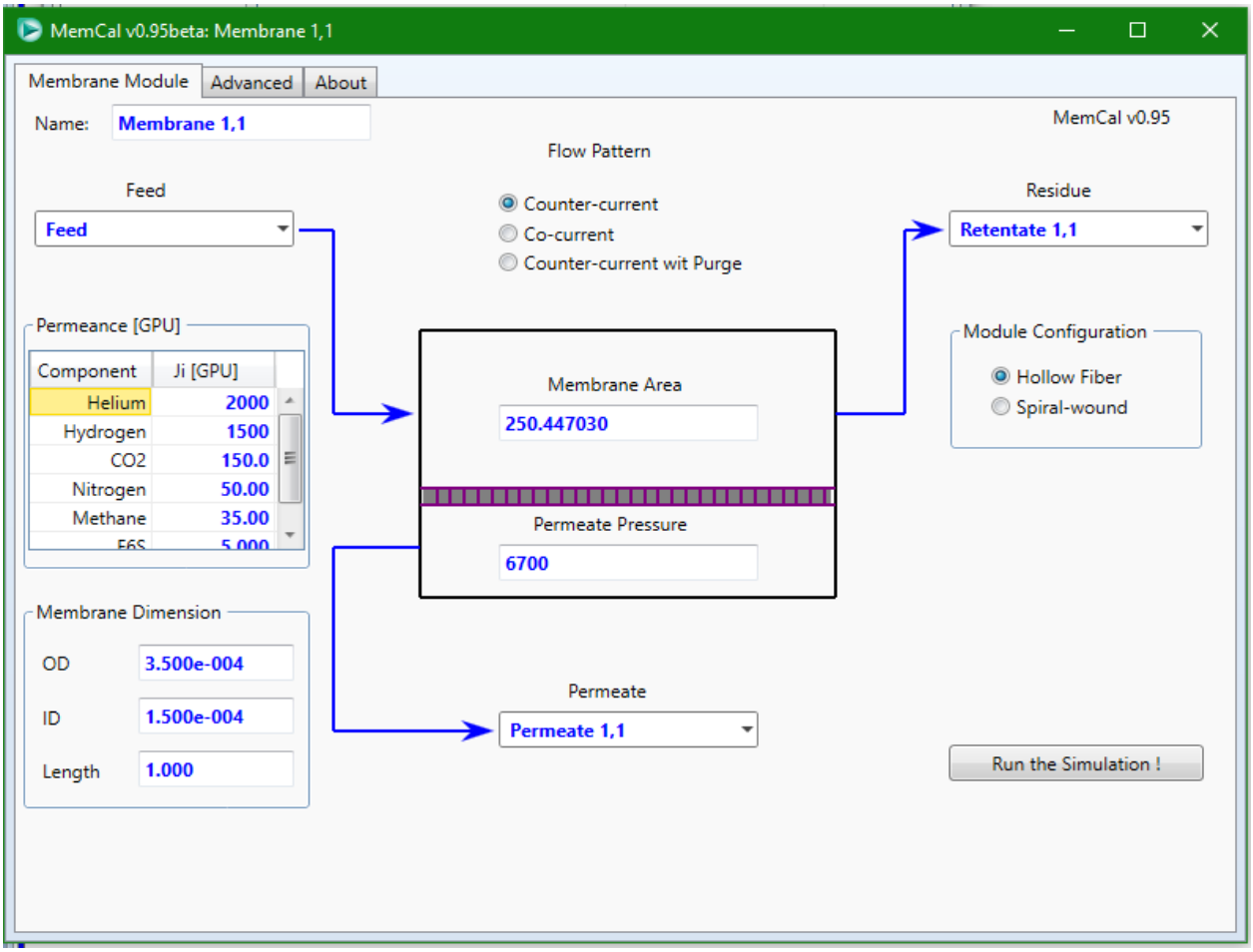

Figure A-25: Example of Memcal unit after area is corrected

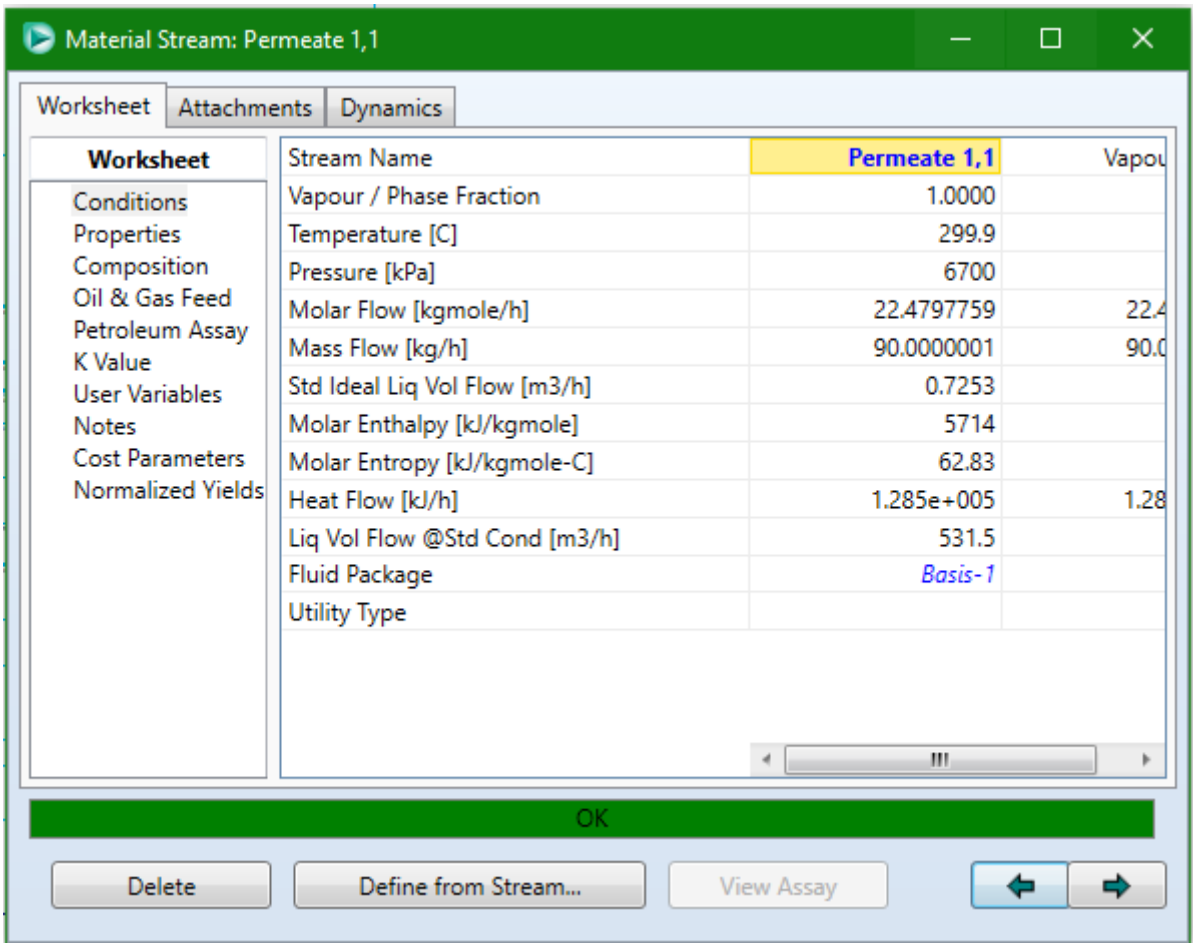

Figure A-26: Example of Memcal unit permeate flow after area is corrected to match Excel sheet

Table A-14: Design 1 membrane flows and areas

Membrane row,column	Flow in (kg/hr)	Permeate flow out (kg/hr)	Retentate flow out (kg/hr)	Membrane area (m^2)
membrane 1,1	100	90	10	250.44705
membrane 1,2	10	9	1	25.017615
membrane 1,3	1	0.9	0.1	2.49812
membrane 1,4	0.1	0.09	0.01	0.249134
membrane 2,1	90	81	9	231.82034
membrane 2,2	18	16.2	1.8	46.32128
membrane 2,3	2.7	2.43	0.27	6.9384
membrane 2,4	0.36	0.324	0.036	0.922743
membrane 3,1	81	72.9	8.1	64.41208
membrane 3,2	24.3	21.9	2.43	64.49807
membrane 3,3	4.86	4.37	0.486	12.852606
membrane 3,4	0.81	0.729	0.081	2.137046
membrane 4,1	72.9	65.61	7.29	199.56385
membrane 4,2	29.2	26.244	2.916	79.75543
membrane 4,3	7.29	6.561	0.729	19.916816
membrane 4,4	1.458	1.3122	0.1458	3.978265
membrane 5,1	65.61	59.049	6.561	185.64384
membrane 5,2	32.805	29.5245	3.2805	92.74081
membrane 5,3	9.8415	8.85735	0.98415	27.794186
membrane 5,4	2.29635	2.066715	0.229635	6.475144
membrane 5,5	0.229635	0.2066715	0.0229635	0.6455993
membrane 6,1	59.049	53.1441	5.9049	173.0669
membrane 6,2	35.4294	31.88646	3.54294	103.749946
membrane 6,3	12.40029	11.160261	1.240029	36.273242
membrane 6,4	3.306744	2.9760696	0.3306744	9.659191
membrane 6,5	0.5373459	0.48361131	0.05373459	1.565795
membrane 6,6	0.05373459	0.048361131	0.005373459	0.1557071
membrane 7,1	53.1441	47.82969	5.31441	161.714504
membrane 7,2	37.20087	33.480783	3.720087	113.101905
membrane 7,3	14.880348	13.3923132	1.4880348	45.19288
membrane 7,4	4.4641044	4.01769396	0.44641044	13.540054
membrane 7,5	0.93002175	0.837019575	0.093002175	2.814879
membrane 7,6	0.141363306	0.127226975	0.014136331	0.4259358
membrane 8,1	47.82969	43.046721	4.782969	151.48542

membrane 8,2	38.263752	34.4373768	3.8263752	121.083126
membrane 8,3	17.2186884	15.49681956	1.72186884	54.436195
membrane 8,4	5.7395628	5.16560652	0.57395628	18.122783
membrane 8,5	1.410975855	1.26987827	0.141097586	4.446953
membrane 8,6	0.268324561	0.241492105	0.026832456	0.842512
membrane 9,1	43.046721	38.7420489	4.3046721	142.34119
membrane 9,2	38.7420489	34.86784401	3.87420489	127.995138
membrane 9,3	19.37102445	17.43392201	1.937102445	63.938125
membrane 9,4	7.102708965	6.392438069	0.710270897	23.415867
membrane 9,5	1.980149166	1.782134249	0.198014917	6.517075
membrane 9,6	0.439507021	0.395556319	0.043950702	1.441918
membrane 10,1	38.7420489	34.86784401	3.87420489	134.20739
membrane 10,2	38.7420489	34.86784401	3.87420489	134.089266
membrane 10,3	21.3081269	19.17731421	2.13081269	73.68143
membrane 10,4	8.523250758	7.670925682	0.852325076	29.438171
membrane 10,5	2.634459325	2.371013393	0.263445933	9.0847443
membrane 10,6	0.659002252	0.593102027	0.065900225	2.26607
membrane 10,7	0.065900225	0.059310203	0.006590023	0.225027
membrane 11,2	34.86784401	31.38105961	3.486784401	126.92947
membrane 11,3	22.66409861	20.39768875	2.266409861	82.42891
membrane 11,4	9.937335543	8.943601989	0.993733554	36.100896
membrane 11,5	3.364746947	3.028272252	0.336474695	12.20579
membrane 11,6	0.929576721	0.836619049	0.092957672	3.3637637
membrane 11,7	0.152267875	0.137041087	0.015226787	0.547833
membrane 12,2	31.38105961	28.24295365	3.138105961	120.72673
membrane 12,3	23.53579471	21.18221524	2.353579471	90.453865
membrane 12,4	11.29718146	10.16746331	1.129718146	43.369914
membrane 12,5	4.157990398	3.742191358	0.41579904	15.940407
membrane 12,6	1.252418089	1.12717628	0.125241809	4.790521
membrane 12,7	0.262282896	0.236054607	0.02622829	0.998255
membrane 13,3	21.18221524	19.06399371	2.118221524	86.514
membrane 13,4	12.28568484	11.05711635	1.228568484	50.12472
membrane 13,5	4.970759842	4.473683858	0.497075984	20.2516
membrane 13,6	1.624252264	1.461827038	0.162425226	6.603697
membrane 13,7	0.398479833	0.35863185	0.039847983	1.61337
membrane 14,3	19.06399371	17.15759434	1.906399371	83.3037
membrane 14,4	12.96351572	11.66716415	1.296351572	56.58283
membrane 14,5	5.77003543	5.193031887	0.577003543	25.15377

membrane 14,6	2.038830581	1.834947523	0.203883058	8.8699565
membrane 14,7	0.562514908	0.506263417	0.056251491	2.438062
membrane 15,4	11.66716415	10.50044774	1.166716415	54.9447
membrane 15,5	6.359748302	5.723773472	0.63597483	29.9133
membrane 15,6	2.470922353	2.223830118	0.247092235	11.60038
membrane 15,7	0.753355652	0.678020087	0.075335565	3.5250705
membrane 16,4	10.50044774	9.450402963	1.050044774	53.90588
membrane 16,5	6.773818246	6.096436421	0.677381825	34.73992
membrane 16,6	2.901211942	2.611090748	0.290121194	14.853747
membrane 16,7	0.968141281	0.871327153	0.096814128	4.941218
membrane 17,5	6.096436421	5.486792779	0.609643642	34.557328
membrane 17,6	3.22073439	2.898660951	0.322073439	18.23
membrane 17,7	1.193400592	1.074060533	0.119340059	6.736437
membrane 18,5	5.486792779	4.938113501	0.548679278	34.99691
membrane 18,6	3.447340229	3.102606206	0.344734023	21.966151
membrane 18,7	1.418794556	1.2769151	0.141879456	9.019574
membrane 19,6	3.102606206	2.792345586	0.310260621	22.82339
membrane 19,7	1.587175721	1.428458149	0.158717572	11.655664
membrane 20,7	1.428458149	1.285612334	0.142845815	12.5778933

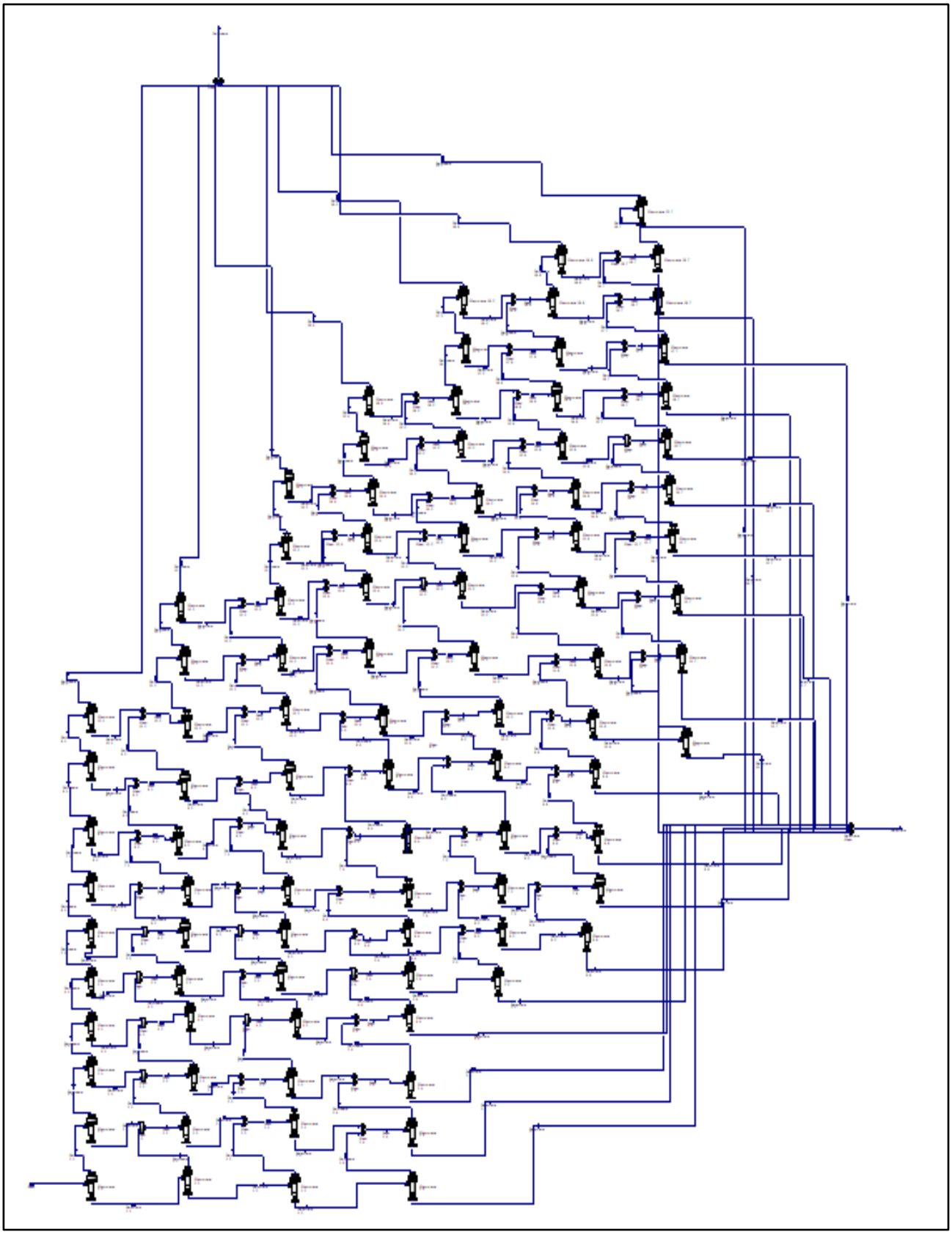

Figure A-27: Design 1 complete Memcal units system

Table A-15: Design 2 membrane flows and areas

Membrane row,column	Flow in (kg/hr)	Permeate flow out (kg/hr)	Retentate flow out (kg/hr)	Membrane area (m^2)
membrane 1,1	100	50	50	142.7122
membrane 1,2	50	32.5	17.5	91.48565
membrane 1,3	17.5	14	3.5	39.0599
membrane 1,4	3.5	3.15	0.35	8.74319
membrane 2,1	50	25	25	73.304
membrane 2,2	57.5	37.375	20.125	108.16061
membrane 2,3	34.125	27.3	6.825	78.3308
membrane 2,4	9.975	8.9775	0.9975	25.62167
membrane 3,1	25	12.5	12.5	37.7356
membrane 3,2	49.875	32.41875	17.45625	96.592635
membrane 3,3	44.75625	35.805	8.95125	105.805
membrane 3,4	17.92875	16.135875	1.792875	47.450896
membrane 3,5	1.792875	1.6135875	0.1792875	4.739401
membrane 4,2	32.41875	21.0721875	11.3465625	64.7233
membrane 4,3	47.1515625	37.72125	9.4303125	114.99016
membrane 4,4	25.5661875	23.00956875	2.55661875	69.812
membrane 4,5	4.17020625	3.753185625	0.417020625	11.373985
membrane 5,2	21.0721875	13.69692188	7.375265625	43.46598
membrane 5,3	45.09651563	36.0772125	9.019303125	113.662373
membrane 5,4	32.02887188	28.82598469	3.202887188	90.40783
membrane 5,5	6.956072813	6.260465531	0.695607281	19.614
membrane 6,3	36.0772125	28.86177	7.2154425	94.17178
membrane 6,4	36.04142719	32.43728447	3.604142719	105.378835
membrane 6,5	9.86460825	8.878147425	0.986460825	28.810494
membrane 7,3	28.86177	23.089416	5.772354	78.20339
membrane 7,4	38.20963847	34.38867462	3.820963847	115.98697
membrane 7,5	12.69911127	11.42920014	1.269911127	38.50761
membrane 8,3	23.089416	18.4715328	4.6178832	65.11246
membrane 8,4	39.00655782	35.10590204	3.900655782	123.25116
membrane 8,5	15.32985593	13.79687033	1.532985593	48.388163
membrane 8,6	1.532985593	1.379687033	0.153298559	4.8325447
membrane 9,4	35.10590204	31.59531184	3.510590204	115.80914
membrane 9,5	17.30746054	15.57671448	1.730746054	57.036083
membrane 9,6	3.110433087	2.799389779	0.311043309	10.237649

membrane 10,4	31.59531184	28.43578065	3.159531184	109.18927
membrane 10,5	18.73624567	16.8626211	1.873624567	64.68434
membrane 10,6	4.673014345	4.205712911	0.467301435	16.113702
membrane 11,4	28.43578065	25.59220259	2.843578065	103.3577
membrane 11,5	19.70619917	17.73557925	1.970619917	71.56294
membrane 11,6	6.176332827	5.558699545	0.617633283	22.4011
membrane 12,4	25.59220259	23.03298233	2.559220259	98.3055
membrane 12,5	20.29479951	18.26531956	2.029479951	77.8791
membrane 12,6	7.588179496	6.829361546	0.75881795	29.08631
membrane 13,4	23.03298233	20.7296841	2.303298233	94.0111
membrane 13,5	20.56861779	18.51175601	2.056861779	83.87013
membrane 13,6	8.886223325	7.997600992	0.888622332	36.19527
membrane 14,4	20.7296841	18.65671569	2.07296841	90.51915
membrane 14,5	20.58472442	18.52625198	2.058472442	89.800095
membrane 14,6	10.05607343	9.050466091	1.005607343	43.8241
membrane 15,4	18.65671569	16.79104412	1.865671569	87.87895
membrane 15,5	20.39192355	18.35273119	2.039192355	95.96415
membrane 15,6	11.08965845	9.980692601	1.108965845	52.13743
membrane 16,4	16.79104412	15.11193971	1.679104412	86.20495
membrane 16,5	20.0318356	18.02865204	2.00318356	102.766
membrane 16,6	11.98387616	10.78548855	1.198387616	61.417663
membrane 17,5	18.02865204	16.22578684	1.802865204	102.17566
membrane 17,6	12.58835375	11.32951837	1.258835375	71.29681
membrane 18,6	11.32951837	10.19656654	1.132951837	72.189
membrane 19,6	10.19656654	9.176909884	1.019656654	74.966
membrane 20,6	9.176909884	8.259218895	0.917690988	80.879264

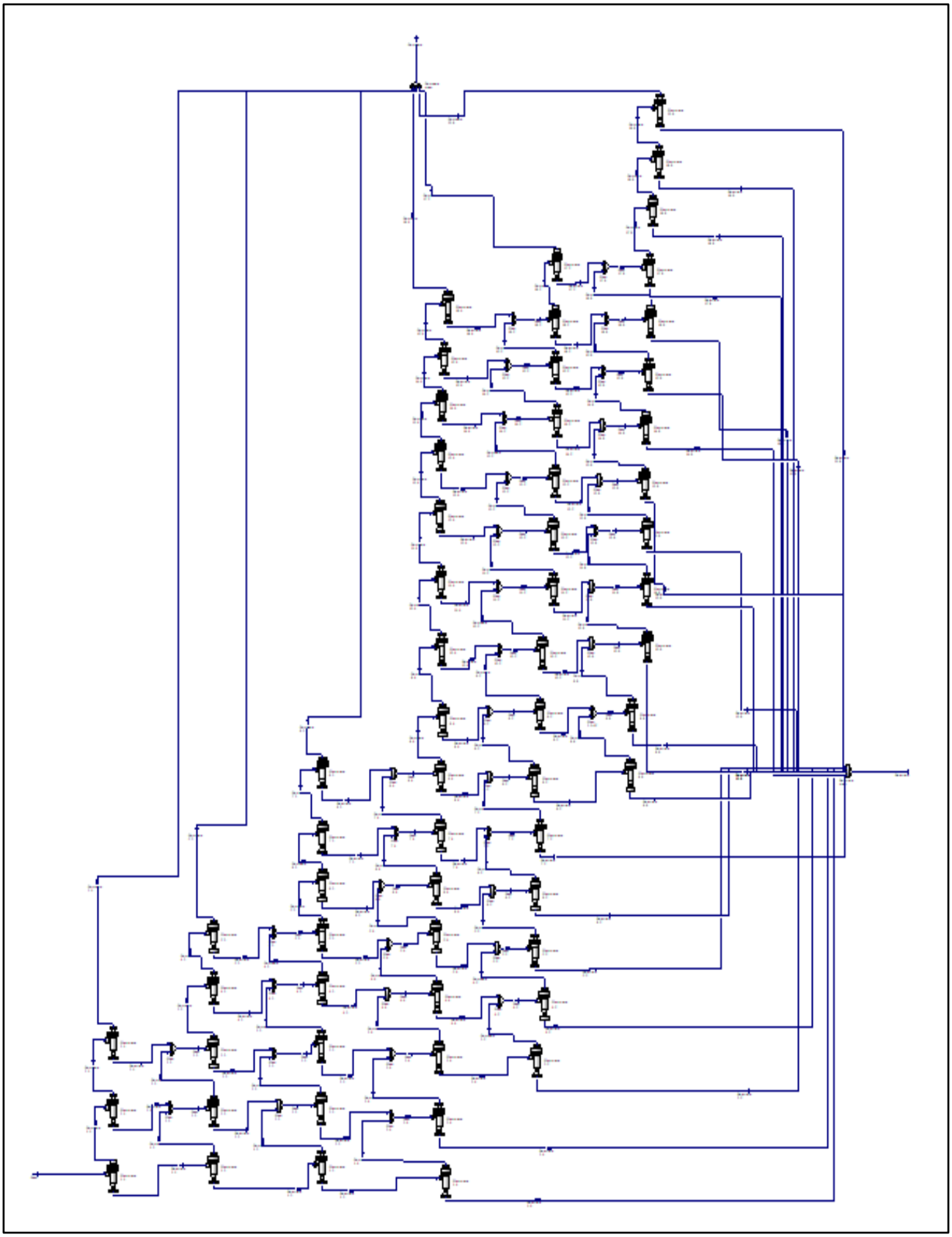

Figure A-28: Design 2 complete Memcal units system

Table A-16: Design 3 membrane flows and areas

Membrane row,column	Flow in (kg/hr)	Permeate flow out (kg/hr)	Retentate flow out (kg/hr)	Area of membrane (m^2)
membrane 1,1	100	90	10	250.44705
membrane 1,2	10	9	1	25.017615
membrane 2,1	90	81	9	231.82034
membrane 2,2	18	16.2	1.8	46.32128
membrane 2,3	1.8	1.62	0.18	4.625796
membrane 3,1	81	72.9	8.1	214.92255
membrane 3,2	24.3	21.9	2.43	64.49807
membrane 3,3	4.05	3.65	0.405	10.73331
membrane 4,1	72.9	65.61	7.29	199.56385
membrane 4,2	29.2	26.244	2.916	79.75436
membrane 4,3	6.561	5.9049	0.6561	17.92675
membrane 5,1	65.61	59.049	6.561	185.64384
membrane 5,2	32.805	29.5245	3.2805	92.74081
membrane 5,3	9.1854	8.26686	0.91854	25.94124
membrane 6,1	59.049	53.1441	5.9049	173.0669
membrane 6,2	35.4294	31.88646	3.54294	103.749946
membrane 6,3	11.8098	10.62882	1.18098	34.54595
membrane 6,4	1.18098	1.062882	0.118098	3.450005
membrane 7,1	53.1441	47.82969	5.31441	161.714504
membrane 7,2	37.20087	33.480783	3.720087	113.101905
membrane 7,3	14.348907	12.9140163	1.4348907	43.57886
membrane 7,4	2.4977727	2.24799543	0.24977727	7.5759
membrane 8,1	47.82969	43.046721	4.782969	151.48542
membrane 8,2	38.263752	34.4373768	3.8263752	121.083126
membrane 8,3	16.7403915	15.06635235	1.67403915	52.9241
membrane 8,4	3.92203458	3.529831122	0.392203458	12.383838
membrane 9,1	43.046721	38.7420489	4.3046721	142.34119
membrane 9,2	38.7420489	34.86784401	3.87420489	127.995138
membrane 9,3	18.94055724	17.04650152	1.894055724	62.517294
membrane 9,4	5.423886846	4.881498161	0.542388685	17.881165
membrane 10,1	38.7420489	34.86784401	3.87420489	134.20739
membrane 10,2	38.7420489	34.86784401	3.87420489	134.089266
membrane 10,3	20.92070641	18.82863577	2.092070641	72.341788

membrane 10,4	6.973568802	6.276211922	0.69735688	24.085745
membrane 11,2	34.86784401	31.38105961	3.486784401	126.92947
membrane 11,3	22.31542017	20.08387815	2.231542017	81.16081
membrane 11,4	8.507753938	7.656978545	0.850775394	30.9074285
membrane 12,2	31.38105961	28.24295365	3.138105961	120.7267
membrane 12,3	23.22198411	20.8997857	2.322198411	89.24787
membrane 12,4	9.979176956	8.98125926	0.997917696	38.310104
membrane 12,5	0.997917696	0.898125926	0.09979177	3.8250138
membrane 13,2	28.24295365	25.41865828	2.824295365	115.45464
membrane 13,3	23.72408106	21.35167296	2.372408106	96.89591
membrane 13,4	11.35366737	10.21830063	1.135366737	46.3221
membrane 13,5	2.033492663	1.830143396	0.203349266	8.283352
membrane 14,3	21.35167296	19.21650566	2.135167296	93.300555
membrane 14,4	12.35346793	11.11812113	1.235346793	53.9203
membrane 14,5	3.065490189	2.75894117	0.306549019	13.361825
membrane 15,3	19.21650566	17.2948551	1.921650566	90.58396
membrane 15,4	13.0397717	11.73579453	1.30397717	61.4024
membrane 15,5	4.06291834	3.656626506	0.406291834	19.10733
membrane 16,3	17.2948551	15.56536959	1.72948551	88.864175
membrane 16,4	13.46528004	12.11875204	1.346528004	69.12708
membrane 16,5	5.00315451	4.502839059	0.500315451	25.655143
membrane 17,4	12.11875204	10.90687683	1.211875204	68.745556
membrane 17,5	4.502839059	4.052555153	0.450283906	25.7695685
membrane 18,4	10.90687683	9.816189148	1.090687683	69.61384
membrane 18,5	5.143242836	4.628918553	0.514324284	32.802674
membrane 19,5	4.628918553	4.166026697	0.462891855	34.06825
membrane 20,5	4.166026697	3.749424028	0.41660267	36.75492

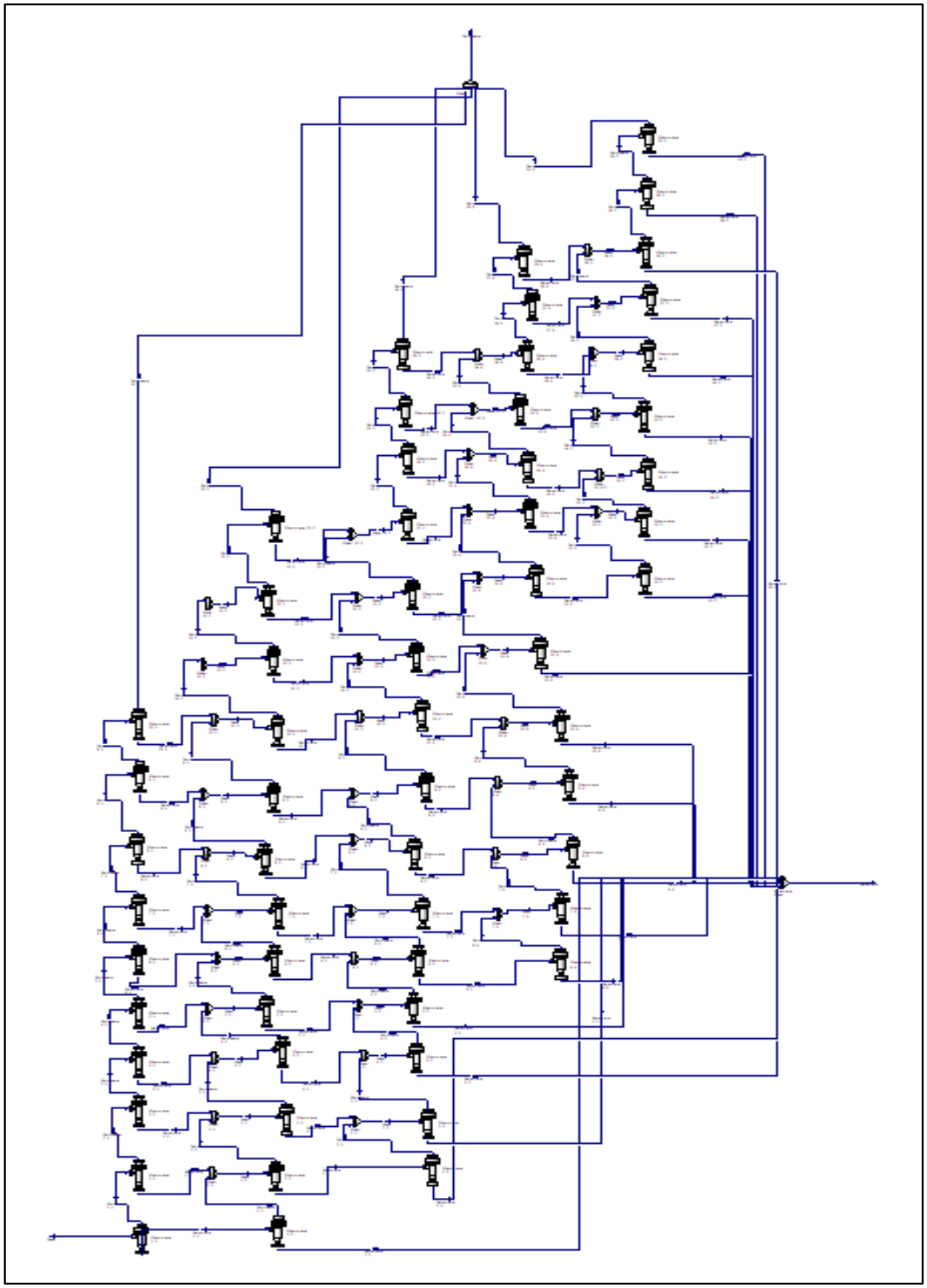

Figure A-29: Design 3 complete Memcal units system

Table A-17: Design 4 membrane areas and flows

Membrane row,column	Flow in	Permeate flow out	Retentate flow out	Membrane area (m^2)
membrane 1,1	100.00000	90.00000	10.00000	151.8741
membrane 1,2	10.00000	9.00000	1.00000	15.169
membrane 1,3	1.00000	0.90000	0.10000	1.513445
membrane 1,4	0.10000	0.09000	0.01000	0.1503012
membrane 2,1	90.00000	81.00000	9.00000	143.6125
membrane 2,2	18.00000	16.20000	1.80000	28.6903
membrane 2,3	2.70000	2.43000	0.27000	4.295202
membrane 2,4	0.36000	0.32400	0.03600	0.570034
membrane 3,1	81.00000	72.90000	8.10000	136.4181
membrane 3,2	24.30000	21.87000	2.43000	40.88178
membrane 3,3	4.86000	4.37400	0.48600	8.163693
membrane 3,4	0.81000	0.72900	0.08100	1.35607943
membrane 4,1	72.90000	65.61000	7.29000	130.32092
membrane 4,2	29.16000	26.24400	2.91600	52.074112
membrane 4,3	7.29000	6.56100	0.72900	13.000528
membrane 4,4	1.45800	1.31220	0.14580	2.5931607
membrane 5,1	65.61000	59.04900	6.56100	125.3404
membrane 5,2	32.80500	29.52450	3.28050	62.60595
membrane 5,3	9.84150	8.85735	0.98415	18.757682
membrane 5,4	2.29635	2.066715	0.229635	4.367009
membrane 5,5	0.229635	0.2066715	0.0229635	0.4343671
membrane 6,1	59.049	53.1441	5.9049	121.56574
membrane 6,2	35.4294	31.88646	3.54294	72.865015
membrane 6,3	12.40029	11.160261	1.240029	25.471665
membrane 6,4	3.306744	2.9760696	0.3306744	6.779086
membrane 6,5	0.5373459	0.48361131	0.05373459	1.0969441
membrane 7,1	53.1441	47.82969	5.31441	119.16818
membrane 7,2	37.20087	33.480783	3.720087	83.332999
membrane 7,3	14.880348	13.3923132	1.4880348	33.29412
membrane 7,4	4.4641044	4.01769396	0.44641044	9.970365
membrane 7,5	0.93002175	0.837019575	0.093002175	2.06977
membrane 8,1	47.82969	43.046721	4.782969	118.46
membrane 8,2	38.263752	34.4373768	3.8263752	94.68282
membrane 8,3	17.2186884	15.49681956	1.72186884	42.5553
membrane 8,4	5.7395628	5.16560652	0.57395628	14.1615785
membrane 8,5	1.410975855	1.26987827	0.141097586	3.46999

membrane 9,1	43.046721	38.7420489	4.3046721	120.028179
membrane 9,2	38.7420489	34.86784401	3.87420489	107.921
membrane 9,3	19.37102445	17.43392201	1.937102445	53.621
membrane 9,4	7.102708965	6.392438069	0.710270897	19.743124
membrane 9,5	1.980149166	1.782134249	0.198014917	5.494005
membrane 10,1	38.7420489	34.86784401	3.87420489	124.969835
membrane 10,2	38.7420489	34.86784401	3.87420489	124.870378
membrane 10,3	21.3081269	19.17731421	2.13081269	68.59645
membrane 10,4	8.523250758	7.670925682	0.852325076	27.387055
membrane 10,5	2.634459325	2.371013393	0.263445933	8.41689
membrane 11,2	34.86784401	31.38105961	3.486784401	135.658912
membrane 11,3	22.66409861	20.39768875	2.266409861	88.116988
membrane 11,4	9.937335543	8.943601989	0.993733554	38.58515
membrane 11,5	3.364746947	3.028272252	0.336474695	13.01605
membrane 12,2	31.38105961	28.24295365	3.138105961	158.75384
membrane 12,3	23.53579471	21.18221524	2.353579471	118.933501
membrane 12,4	11.29718146	10.16746331	1.129718146	57.01365
membrane 12,5	4.157990398	3.742191358	0.41579904	20.882004

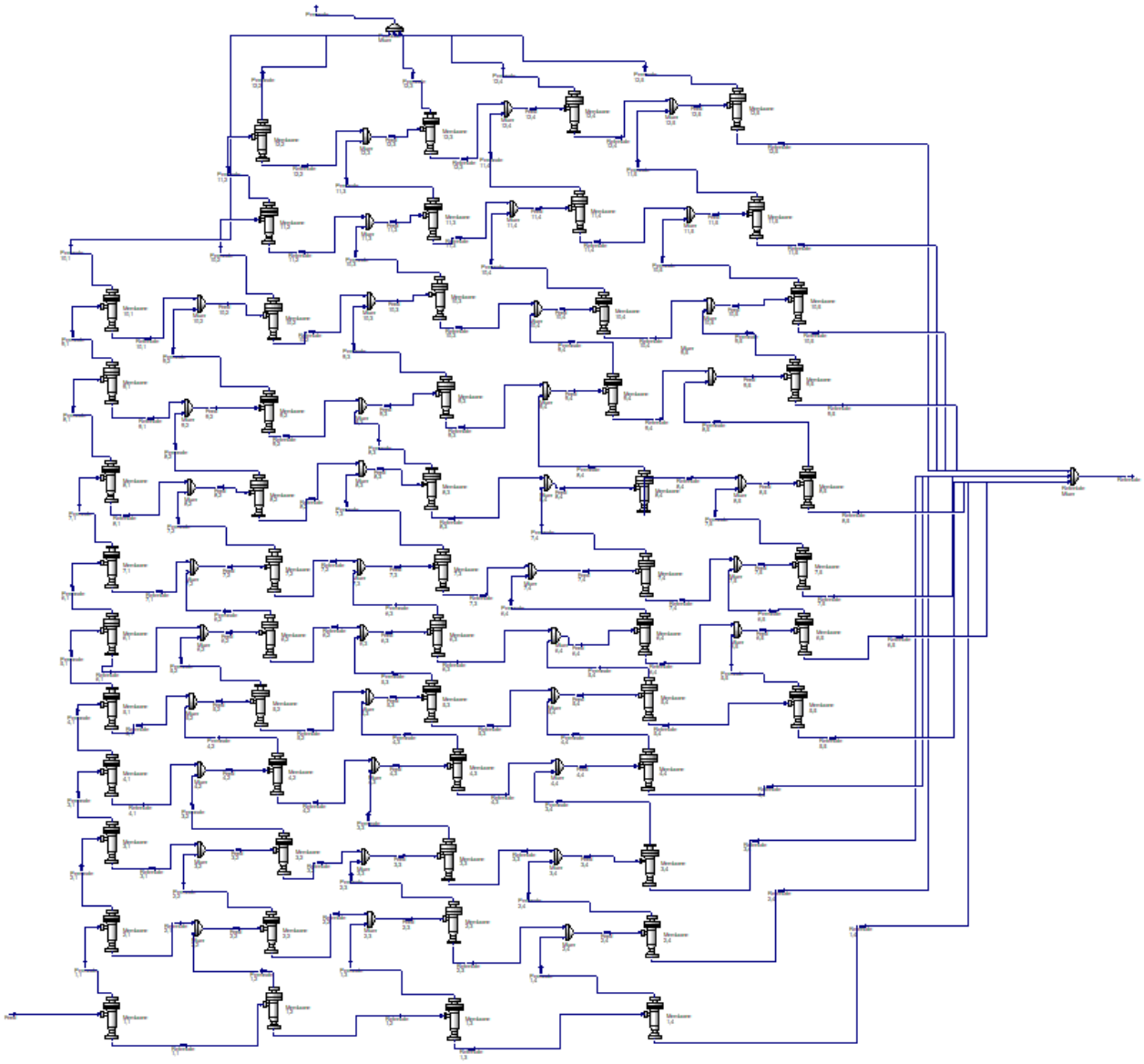

Figure A-30: Design 4 complete Memcal units system

Table A-18: Design 5 membrane flows and areas

Membrane row,column	Flow in	Permeate flow out	Retentate flow out	Membrane area (m^2)
membrane 1,1	100.00000	90.00000	10.00000	250.44705
membrane 1,2	10.00000	9.00000	1.00000	25.017615
membrane 1,3	1.00000	0.90000	0.10000	2.49812
membrane 1,4	0.10000	0.09000	0.01000	0.249134
membrane 2,1	90.00000	81.00000	9.00000	231.82034
membrane 2,2	18.00000	16.20000	1.80000	46.32128
membrane 2,3	2.70000	2.43000	0.27000	6.9384
membrane 2,4	0.36000	0.32400	0.03600	0.922743
membrane 3,1	81.00000	72.90000	8.10000	64.41208
membrane 3,2	24.30000	21.87000	2.43000	64.49807
membrane 3,3	4.86000	4.37400	0.48600	12.852606
membrane 3,4	0.81000	0.72900	0.08100	2.137046
membrane 4,1	72.90000	65.61000	7.29000	199.56385
membrane 4,2	29.16000	26.24400	2.91600	79.75543
membrane 4,3	7.29000	6.56100	0.72900	19.916816
membrane 4,4	1.45800	1.31220	0.14580	3.978265
membrane 5,1	65.61000	59.04900	6.56100	185.64384
membrane 5,2	32.80500	29.52450	3.28050	92.74081
membrane 5,3	9.84150	8.85735	0.98415	27.794186
membrane 5,4	2.29635	2.066715	0.229635	6.475144
membrane 5,5	0.229635	0.2066715	0.0229635	0.6455993
membrane 6,1	59.049	53.1441	5.9049	173.0669
membrane 6,2	35.4294	31.88646	3.54294	103.749946
membrane 6,3	12.40029	11.160261	1.240029	36.273242
membrane 6,4	3.306744	2.9760696	0.3306744	9.659191
membrane 6,5	0.5373459	0.48361131	0.05373459	1.565795
membrane 7,1	53.1441	47.82969	5.31441	161.714504
membrane 7,2	37.20087	33.480783	3.720087	113.101905
membrane 7,3	14.880348	13.3923132	1.4880348	45.19288
membrane 7,4	4.4641044	4.01769396	0.44641044	13.540054
membrane 7,5	0.93002175	0.837019575	0.093002175	2.814879
membrane 8,1	47.82969	43.046721	4.782969	151.48542
membrane 8,2	38.263752	34.4373768	3.8263752	121.083126
membrane 8,3	17.2186884	15.49681956	1.72186884	54.436195
membrane 8,4	5.7395628	5.16560652	0.57395628	18.122783

membrane 8,5	1.410975855	1.26987827	0.141097586	4.446953
membrane 9,1	43.046721	38.7420489	4.3046721	142.34119
membrane 9,2	38.7420489	34.86784401	3.87420489	127.995138
membrane 9,3	19.37102445	17.43392201	1.937102445	63.938125
membrane 9,4	7.102708965	6.392438069	0.710270897	23.415867
membrane 9,5	1.980149166	1.782134249	0.198014917	6.517075
membrane 10,1	38.7420489	34.86784401	3.87420489	134.20739
membrane 10,2	38.7420489	34.86784401	3.87420489	134.089266
membrane 10,3	21.3081269	19.17731421	2.13081269	73.68143
membrane 10,4	8.523250758	7.670925682	0.852325076	29.438171
membrane 10,5	2.634459325	2.371013393	0.263445933	9.0847443
membrane 11,2	34.86784401	31.38105961	3.486784401	126.92947
membrane 11,3	22.66409861	20.39768875	2.266409861	82.42891
membrane 11,4	9.937335543	8.943601989	0.993733554	36.100896
membrane 11,5	3.364746947	3.028272252	0.336474695	12.20579
membrane 12,2	31.38105961	28.24295365	3.138105961	120.72673
membrane 12,3	23.53579471	21.18221524	2.353579471	90.453865
membrane 12,4	11.29718146	10.16746331	1.129718146	43.369914
membrane 12,5	4.157990398	3.742191358	0.41579904	15.940407

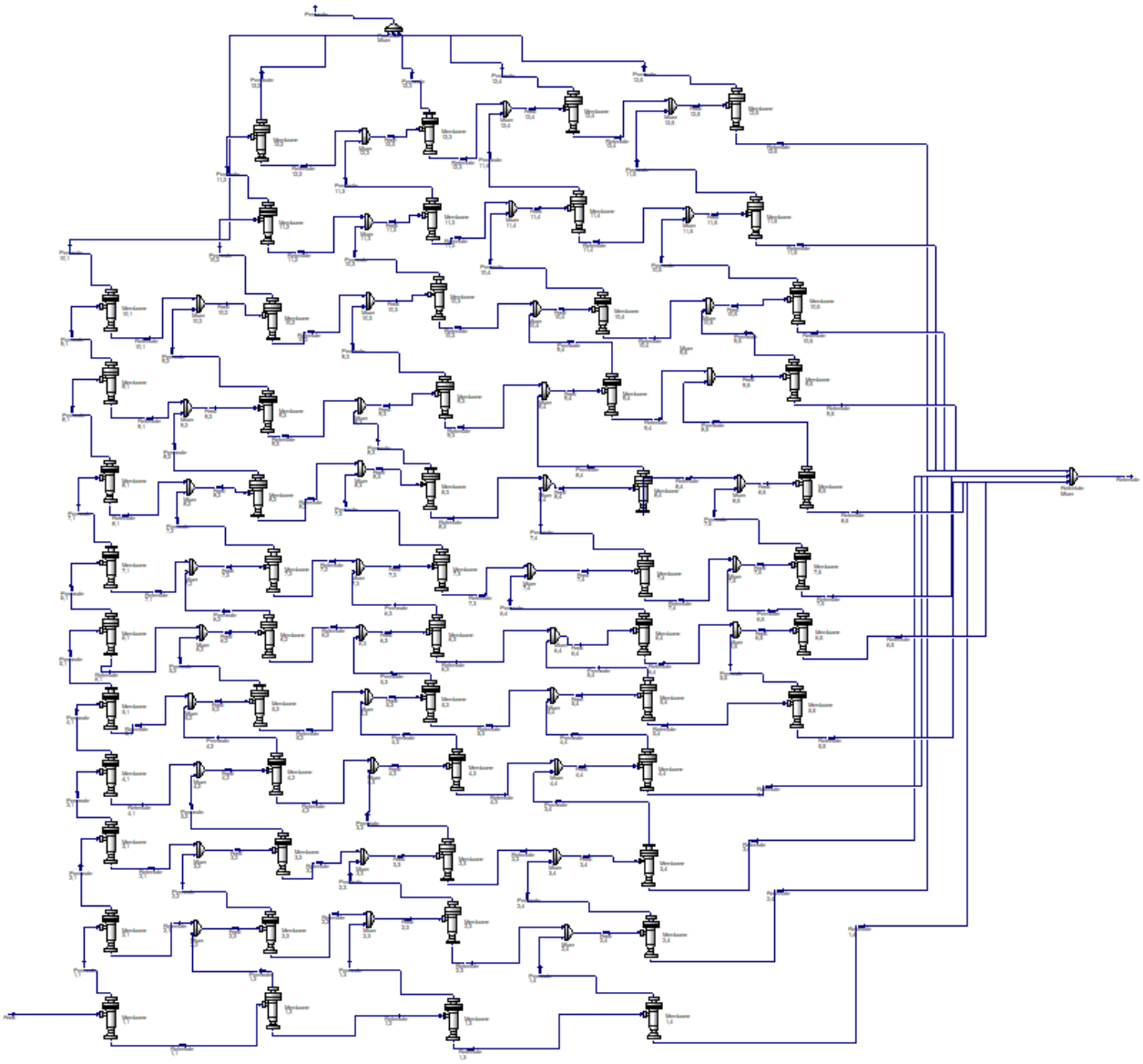

Figure A-31: Design 5 complete Memcal units system